Influence of miR-221/222 on GIRK1/4 channel function and LTCC-dependent calcium handling in cardiomyocytes

Dissertation

for obtaining the

Doctoral degree in natural sciences (Dr. rer. nat.)

at the

Faculty of Natural Sciences I - Biosciences -
Martin Luther University
Halle-Wittenberg

submitted by

Maria Knyrim

born on 31.03.1990 in Erfurt

Reviewers:

Prof. Dr. Stefan Hüttelmaier
Prof. Dr. Michael Gekle
Prof. Dr. Henning Morawietz

Date of public defense: 21.10.2021

Contents

2

1. Introduction

Cardiovascular diseases are the leading cause of death worldwide. Cardiac remodeling comprises all changes in molecular, cellular and interstitial composition of the heart and can lead to cardiac dysfunction, malignant arrhythmias, sudden cardiac arrest or heart failure (Azevedo et al., 2016). Electrical remodeling including altered ion channel expression and imbalance of calcium homeostasis can have detrimental effects on cardiac function (Aiba & Tomaselli, 2010). MicroRNAs have been implicated in cardiac remodeling and disease. This study is about the role of miR-221/222 in electrical remodeling in cardiomyocytes.

1.1 Pacemaking and propagation of excitation

The mammalian heart is an autorhythmic pump that maintains blood flow throughout the vascular system. The timely and spatially tightly regulated flux of ions across the cardiomyocyte cell membrane forms the basis of each heartbeat. Thus, ion channels are the basis of heart function. Cardiac pacemaking is enabled by the complex interaction of different ion channels, Calcium cycling and other mechanisms (Mesirca et al., 2014). Pacemaker cardiomyocytes do not show a stable resting membrane potential and therefore are able to rhythmically generate action potentials (APs). Two possible mechanisms for pacemaking are proposed: voltage clock (funny current) and calcium clock (SR calcium cycling) (Carmeliet, 2019). Until now it is not clear which one contributes the most to pacemaker potential. Both mechanisms may probably work in combination (coupled clock system) (Bartos et al., 2015). APs generated by the sinoatrial node are propagated throughout right and left atria and then merge in the atrioventricular node before spreading through the His bundle branches and Purkinje fibers into the ventricles. Adjacent cardiomyocytes within the ventricles are activated via gap junctions. This leads to fast excitation and contraction of the whole myocardium in a coordinated and synchronous manner.

1.2 Action potential

As atrial and ventricular cardiomyocytes do not show autorhythmic properties, APs are triggered only by supra-threshold depolarization. In general, the AP is determined by ion channel expression, kinetics of activation and inactivation, voltage-dependence etc. Due to regionally diverse expression of ion channels AP phases take very different shapes in distinct regions of the heart. For instance, APs generated by pacemaker cells look very different from APs in working myocardium. Figure 1 depicts human atrial vs. ventricular APs. In contrast to pacemaker cells, atrial and ventricular cardiomyocytes show a stable resting membrane potential (atria: -65 to -80 mV (Pandit, 2018), ventricles: ~ -90 mV; phase 4) which is mediated by inwardly rectifying K^+ currents such as I_{K1} and $I_{K,ATP}$. In addition, atrial cells also express GIRK1/4 which mediates $I_{K,ACh}$.

Upon excitation the membrane is depolarized and an AP is initiated. The prominent upstroke phase (0) in both atria and ventricles is mediated by voltage-gated Na^+ channels (Nav1.5). These channels are activated at about -55 mV (Nerbonne & Kass, 2005). The upstroke phase is very short because Nav1.5 channels inactivate rapidly (Nass et al., 2008; Nerbonne & Kass, 2005). Membrane depolarization provides the trigger for activation of voltage-gated Ca^{2+} and K^+ channels. Voltage-gated Kv4.x channels mediate a transient outward K^+ current (I_{to}) leading to an early transient repolarization (phase 1). While human I_{to} seems to be formed by Kv4.3 together with KChIP2 as auxiliary subunit, mouse I_{to} is comprised of Kv4.2, Kv4.3 and KChIP2 (J. Liu et al., 2015). The initial membrane depolarization also activates voltage gated L-type Ca^{2+}channels (LTCC, pore-forming subunit Cav1.2, long-lasting current $I_{Ca,L}$). Phase 2 is characterized by a balance between inward ($I_{Ca,L}$) and outward currents (transient outward current I_{to}; delayed rectifying currents I_{Kr} and I_{Ks}; inwardly rectifying current I_{K1}) leading to a plateau in the AP curve. Atrial cells additionally express Kv1.5 channels (I_{Kur}, ultra-rapid delayed rectifying current) which are activated at the same time/potential as Kv4.x but I_{Kur} lasts longer than I_{to} so the plateau phase is very short in these cells in contrast to ventricular cells. Beside its depolarizing properties, LTCC-mediated Ca^{2+} influx is the trigger for excitation contraction coupling (see next chapter). LTCCs inactivate in a voltage- and calcium-dependent way. Then the repolarizing currents predominate (phase 3) and repolarization is continued until the membrane reaches again the resting potential.
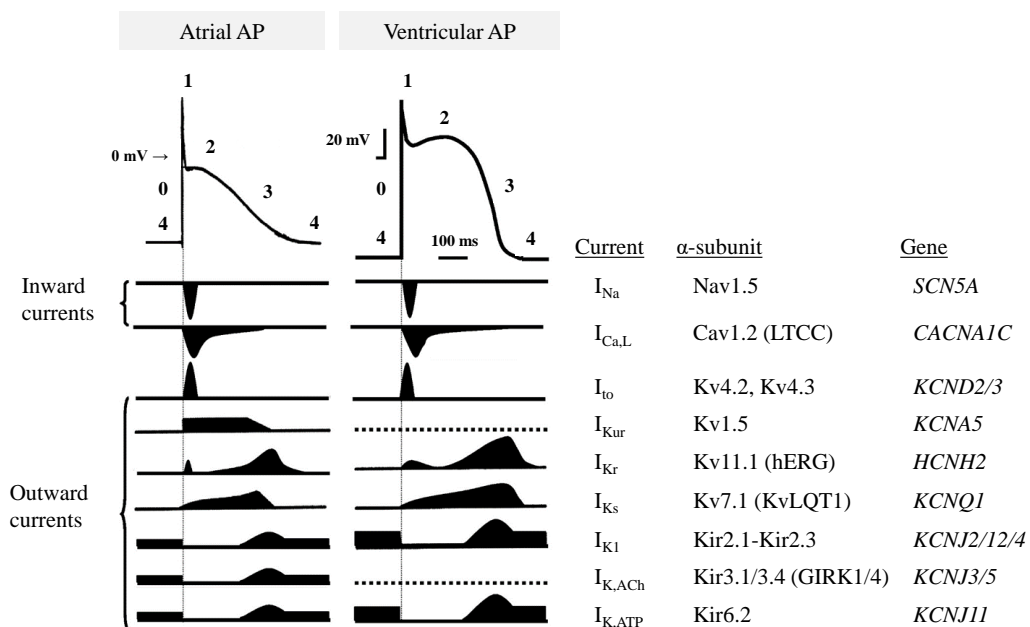
Figure 1. Atrial and ventricular action potentials and underlying ion currents. Shown are action potentials from human atrial trabeculum (left) and ventricular papillary muscle (right). Numbers indicate AP phases. Contributing currents are depicted below the AP curves. Subunits are shown for human and mouse. AP: action potential, $I_{Ca,L}$: L-type Ca^{2+} current, I_{to}: transient outward K^+ current, I_{Kur}: ultra-rapid delayed rectifying K^+ current, I_{Kr}: rapidly activating delayed rectifying K^+ current, I_{Ks}: slowly activating delayed rectifying K^+ current, I_{K1}: inwardly rectifying K^+ current, $I_{K,ACh}$: ACh-mediated inwardly rectifying K^+ current through GIRK1/4, $I_{K,ATP}$: ATP-sensitive inwardly rectifying K^+ current. Figure modified from (Ravens, 2010).

1.3 Cardiomyocyte calcium signaling and excitation-contraction coupling

Calcium is involved in many cellular processes as a universal second messenger. In cardiomyocytes calcium is crucial for action potential generation and conduction (LTCC, gap junctions, intercellular communication), excitation-contraction coupling, activation and relaxation kinetics of contractile filaments, energy consumption and production, excitation-transcription coupling and cell death regulation (apoptosis, necrosis) (Bers, 2008).

Tightly regulating calcium concentrations within the cytosol or organelles like the nucleus or mitochondria is the main requirement to use it as a second messenger. For this purpose, the calcium signaling system comprises components for calcium entry (LTCC), decay of intracellular calcium (SERCA, PMCA, NCX) and Ca^{2+} buffering (Ca^{2+} binding proteins) as well as Ca^{2+} storage (SR, mitochondria, nuclear envelope) (Bootman et al., 2009; Smith & Eisner, 2019; Uhlén & Fritz, 2010). Ca^{2+} signals consist of a transient increase in calcium concentration followed by a decay of calcium to baseline levels. Cytosolic Ca^{2+} changes can be transient, sustained or oscillating (Uhlén & Fritz, 2010). The cell is able to distinguish and thus decode several different Ca^{2+} signals according to the signal amplitude, duration, oscillation frequency and spatial extent (cellular sublocalization in microdomains) (Bootman et al., 2006). Decoding occurs when Ca^{2+}-sensitive proteins (e.g. CaMKII, troponin C) sense altered intracellular Ca^{2+} concentration and change their conformation and/or activity accordingly (Smedler & Uhlén, 2014).

Figure 2 shows the mechanism how cardiomyocytes link the electrical excitation of the plasma membrane to the mechanical action of the myofilaments leading to sarcomere shortening and contraction of the cell (excitation contraction coupling, ECC). At each cardiomyocyte the action potential triggers cell membrane depolarization and thereby activates voltage-gated LTCCs. LTCC channel density is especially high in the t-tubules. ECC is mediated in the dyadic cleft, where membranes of t-tubules and SR are very close (Eisner et al., 2017). The calcium influx through LTCC activates RyR2 on the membrane of the SR which open to release calcium into the cytosol thereby greatly amplifying the calcium signal (calcium-induced calcium release, CICR). Contraction is initiated by calcium binding to troponin c (Bootman et al., 2006). This binding induces a conformational change of tropomyosin, uncovering the binding site of myosin on actin filaments. With this the sliding filament mechanism of sarcomeric actin and myosin filaments can be initiated, leading to shortening of sarcomeres and contraction of the cell. Relaxation is achieved by reducing cytosolic Ca^{2+} levels via SERCA or NCX/PMCA (Nass et al., 2008).

The autonomic nervous system influences cardiac action by modulating calcium dynamics in cardiomyocytes. This influences chronotropy, inotropy, dromotropy and lusitropy of the whole heart. Sympathetic stimulation via β-adrenergic receptors and G_s activates AC leading to increased cAMP levels which then activates PKA. PKA has multiple effects on calcium

dynamics: Phosphorylation of LTCC and RyR promotes their activity whereas phosphorylation of PLB releases SERCA from inhibition. PKA also increases sarcomeric Ca^{2+}-sensitivity. All these effects lead to a faster Ca^{2+} transient with increased amplitude and shorter duration. This enables cardiomyocytes to contract faster and with higher force.

In pacemaker cells sympathetic input also activates HCN channels, leading to increased heart rate. Parasympathic nerve endings release ACh which binds to the muscarinic ACh receptor type 2 (M2R). This leads to G_i-mediated inhibition of AC and therefore counteracts sympathetic effects on calcium handling. Additionally, GIRK1/4 is activated leading to K^+ outflux and cell membrane hyperpolarization. This prolongs the diastolic phase of the pacemaker AP, stabilizes resting membrane potential and leads to reduced heart rate. Apart from the autonomic nervous system hormones influence cardiac action as well, e.g. angiotensin II (AngII). Its effects on cardiac tissue are mainly mediated by AT1R and induce SR Ca^{2+} release via PKC/IP3-mediated activation of IP3R (Egger & Domenighetti, 2010).
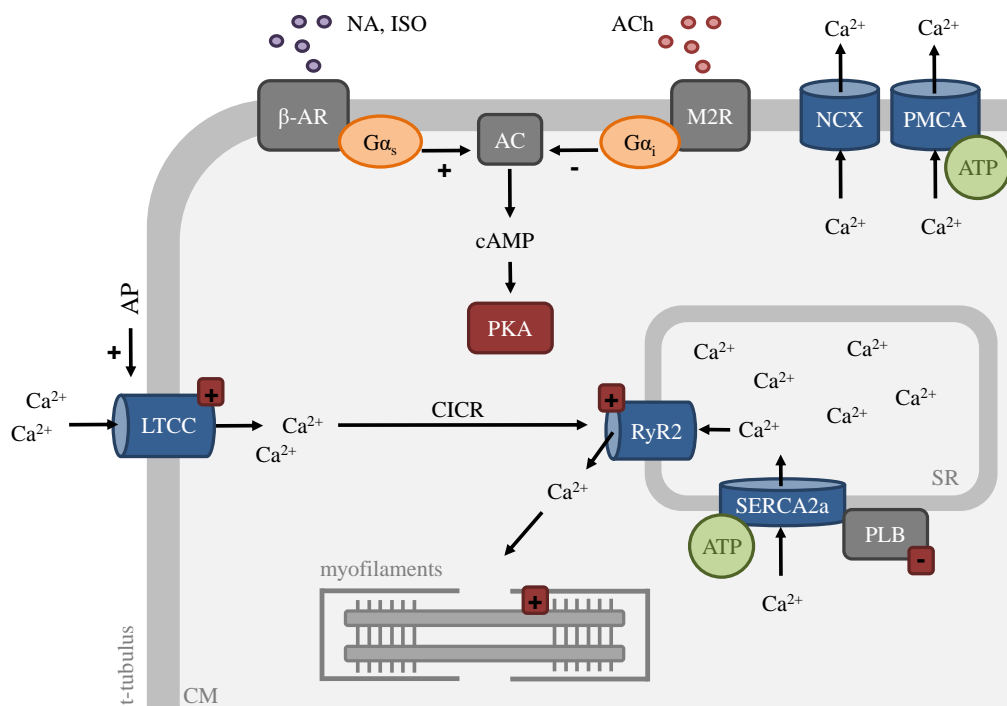
Figure 2. Modulation of calcium cycling in cardiomyocytes. The scheme gives a simplified overview over excitation-contraction coupling and modulation of calcium dynamics by the autonomic nervous system in CM form working myocardium. PKA phosphorylation targets are indicated by small red boxes: + indicates activation, – indicates inhibition. Abbreviations: AC: adenylyl cyclase, ACh: acetylcholine, AP: action potential, CICR: Ca^{2+}-induced Ca^{2+} release, CM: cardiomyocyte (intracellular space), Gα: G protein α subunit (s: stimulating, i: inhibiting), ISO: isoprenaline, M2R: muscarinergic acetylcholine receptor type 2, NA: noradrenaline, NCX: Na^+/Ca^{2+} exchanger, PKA: protein kinase A, PLB: phospholamban, PMCA: plasma membrane Ca^{2+} ATPase, RyR2: ryanodine recptor type 2, SERCA2a: sarco/endoplasmic reticulum Ca^{2+} ATPase, β-AR: β-adrenergic receptor. Scheme modified from (Bers, 2002).

1.4 L-type Ca^{2+} channel (LTCC)

L-type Calcium channels belong to the family of voltage-gated Ca^{2+} channels that are involved in many important processes of excitable cells like excitation-transcription coupling, excitation-contraction coupling, hormone secretion or transmitter release (Zamponi et al., 2015). There are three subgroups of voltage-gated Ca^{2+} channels derived from their differing pore forming α1 subunits: Cav1-Cav3. Cardiac I$_{Ca}$ is mediated by Cav1.2, Cav1.3 as well as Cav3.1 and Cav3.2 (Dolphin, 2006; Gandini et al., 2014). While Cav1-containing channels produce a long-lasting inward Ca^{2+} current (I$_{Ca,L}$) upon depolarization (Zamponi et al., 2015) and are therefore named L-type channels, Cav3 channels activate at lower membrane potentials and show a shorter lasting, transient inward Ca^{2+} current (T-type, I$_{Ca,T}$). In the heart I$_{Ca,T}$ is mainly observed in cells of pacemaker and conduction system while I$_{Ca,L}$ is expressed throughout the different cardiac cell types, especially in ventricular cardiomyocytes (Bers, 2008). Cav1.2 (α1 pore subunit: Cacna1c gene) is the predominantly expressed form of LTCCs in cardiomyocytes and contributes most to overall cardiac I$_{Ca}$. In contrast, Cav1.3 (α1 pore subunit: Cacna1d gene) is only expressed in pacemaker cells (Bers, 2008) and to a minor extent also in atrial CM (Striessnig et al., 2014). Figure 3 shows a schematic view of the LTCC with the α1 pore subunit as well as the accessory subunits that are co-expressed in the heart. The α1 subunit is composed of four repeats of six transmembrane helices each (Striessnig et al., 2014). Segments S5 and S6 together with their linker build the channel pore and helix S4 (Fig. 3 A, yellow) serves as the voltage sensor. The α1 subunit also provides binding sites for α1 subunit-specific toxins or drugs (Striessnig et al., 2014). Subunit α2δ enhances α1 subunit trafficking to the cell membrane and increases channel inactivation (Davies et al., 2007). In contrast to the other subunits the β auxiliary subunit remains completely on the intracellular side of the channel and interacts with the cytosolic domains of α1 (Gandini et al., 2014). The β subunit enhances channel trafficking due to increased ER export and protects against proteasomal degradation by antagonizing ubiquitylation of α1 (Gandini et al., 2014; Striessnig et al., 2014). It also alters the voltage dependence of LTCC activation or inactivation towards more negative potentials (Gandini et al., 2014) and enhances channel open probability (Striessnig et al., 2014). The function of γ subunits is not entirely clear, although an inhibitory effect on LTCC activity has been repeatedly shown (Gandini et al., 2014; L. Yang et al., 2011).

To adapt I$_{Ca,L}$ to current needs, a high variety of signaling pathways and mechanisms converge at modulating LTCC function. The most important modulators include β-adrenergic signaling, intracellular Ca^{2+} concentration and membrane voltage (Striessnig et al., 2014). LTCCs form signaling complexes with β-adrenergic receptors and other signaling molecules (Fig. 3 B) to enable localized regulation of LTCC function (Striessnig et al., 2014).
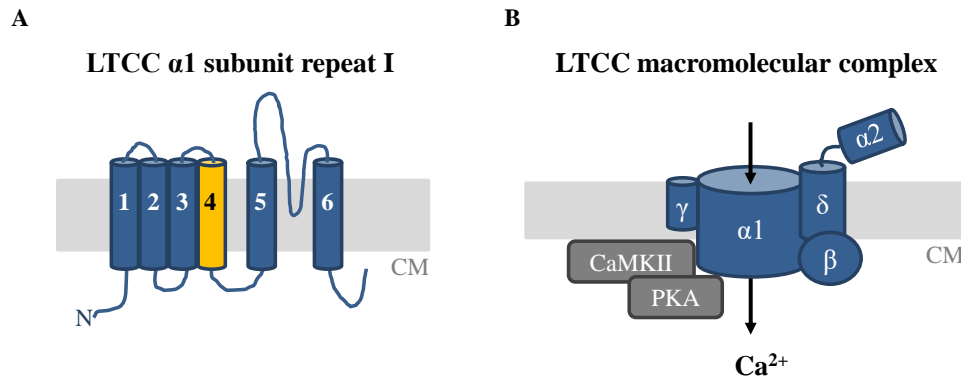
Figure 3. LTCC subunits and macromolecular complex. LTCCs consist of Cav1.2 pore-forming α1 subunit with auxiliary α2δ, β and γ subunits. **A** LTCC α1 subunit with voltage sensing (4, yellow) and pore-forming transmembrane domains (5-6). Shown is one of four repeats, C-terminus is located at repeat IV. **B** Simplified scheme of the LTCC macromolecular complex including the most important modulators of channel function. CM: cardiomyocyte (intracellular space); CaMKII, Ca^{2+}/calmodulin-dependent protein kinase II; PKA, protein kinase A. Modified from (Landstrom et al., 2017; Zamponi et al., 2015).

1.5 Cardiac G-protein activated K$^+$ channel (GIRK1/4)

The family of G protein-activated, inwardly rectifying potassium channels (GIRK1-4 or Kir3.1-3.4) is involved in regulation of cellular excitability in the brain and heart (Zylbergold et al., 2010). GIRKs consist of two transmembrane-spanning helices, combined by a pore loop, and large hydrophilic N- and C-terminal cytosolic domains. These intracellular domains provide binding sites for numerous regulatory factors and are the basis for voltage-dependence of inward rectification (Zylbergold et al., 2010). At hyperpolarized potentials GIRK channels mediate large inward currents, whereas there are only small outward currents upon depolarization, thus they are termed inwardly rectifying. The reason for this discrepancy between inward and outward currents is blockade by intracellular magnesium and positively charged polyamines (spermine, spermidine) which bind to the cytosolic pore region (Zylbergold et al., 2010).

In the heart GIRK1/4 is involved in parasympathetic modulation of heart rate and stabilization of resting membrane potential due to hyperpolarization by mediating $I_{K,ACh}$ (Liang et al., 2014). Cardiac GIRK channels are usually expressed as heterotetramers consisting of two GIRK1 and two GIRK4 subunits. However, homotetramers of GIRK4 have also been shown in atrial tissue (Corey & Clapham, 1998).

GIRK1 cannot form homotetramers because it lacks an ER export signal and reaches the cell membrane only when coexpressed with GIRK4 (Kennedy et al., 1999; Zylbergold et al., 2010). Activation of GIRK1/4 channels mediates negative chronotropic and dromotropic effects in sinoatrial node, atria and cardiac conduction system (Liang et al., 2014).

Classically, GIRK1/4 is activated by acetylcholine or adenosine via $G_{i/o}$-coupled GPCRs (Dascal & Kahanovitch, 2015; Soattin et al., 2020; X. Wang et al., 2013). In cardiomyocytes GIRK1/4 is activated via acetylcholine-mediated activation of M2R (Fig. 4) (Dascal & Kahanovitch, 2015).

Agonist binding at the GPCR induces GDP-GTP exchange at the associated Gα leading dissociation of Gα and Gβγ (Lambert, 2008). Binding of Gβγ to GIRK1/4 induces conformational changes, enhanced interaction with PIP$_2$ which is necessary for channel pre-activation, opening of the channel and current activation. Gating is mainly dependent on available Gβγ if PIP$_2$ is present in physiological concentrations. GIRK channels have four Gβγ binding sites and it has been shown that each bound Gβγ contributes to enhanced open probability of the channel in a cooperative way (Dascal & Kahanovitch, 2015). When the agonist is removed from the GPCR, GTP is hydrolysed by Gα and the trimeric G protein is reassembled leading to GIRK channel closure and current deactivation. This process is highly regulated by RGS proteins. GIRK currents show relatively slow desensitization, meaning a decay of the current in presence of the agonist (Dascal & Kahanovitch, 2015).
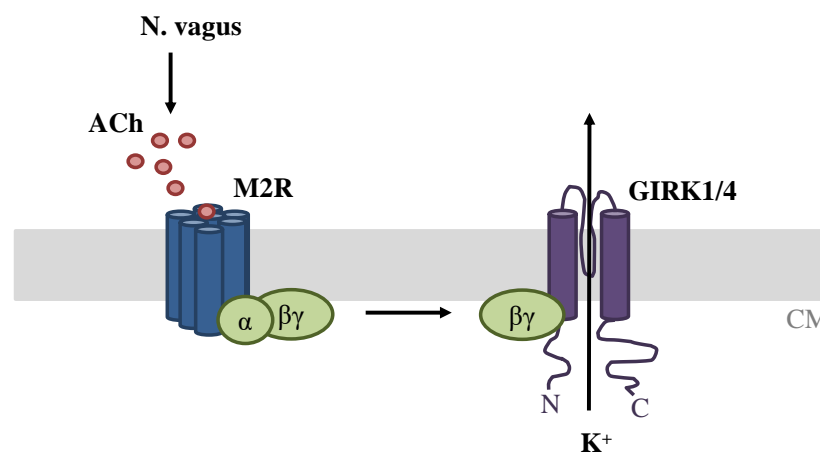
Figure 4. Canonical activation of GIRK1/4. For clarity, only one subunit of the GIRK1/4 heterotetramer is depicted here. ACh binding to M2R activates associated G proteins leading to dissociation of Gβγ from Gα. Gβγ activates GIRK1/4. Abbreviations: ACh: acetylcholine, CM: cardiomyocyte (intracellular side), GIRK1/4: G-protein-coupled inwardly rectifying K$^+$ channel, M2R: muscarinergic acetylcholine receptor type 2, N. vagus: vagal nerve. Modified from (Touhara & Mackinnon, 2018; Voigt et al., 2014; Zheng & Kruse, 2019).

In GIRK4 KO mice there was no effect on resting heart rate, but a difference in heart rate variability (Wickman et al., 1998). Thus, GIRK4 is important for heart rate regulation even at baseline. Furthermore, Mesirca et al. reported that GIRK1/4 current is important for recovery of resting heart rate after sympathetic stimulation (Mesirca et al., 2013). Additionally, it was proposed that GIRK1/4 may even belong to the voltage clock in pacemaking, although its role is more passive as I$_{K,ACh}$ inhibition by RGS6 is required to maintain normal pacemaking rhythm (Posokhova et al., 2013).

In contrast to earlier data suggesting that GIRK1/4 is only activated by neurotransmitters or ligands via GPCRs and therefore confers an agonist-evoked current, evidence amounts that this channel possesses also a substantial basal activity (Dascal & Kahanovitch, 2015). This has been

implicated in regulation of cardiac pacemaker activity. While basal activity may be low under physiological conditions in the adult mammalian heart, it is increased in atrial fibrillation where it is associated with AP shortening (Dascal & Kahanovitch, 2015). Mintert and colleagues showed that simply overexpressing GIRK4 leads to a constitutively active inward-rectifier current in adult rat cardiomyocytes (Mintert et al., 2007).

In contrast to the classical view that GIRK1/4 is only expressed in atria and the conduction system, there is evidence that GIRK1/4 may play a role in ventricular repolarization (Liang et al., 2014). Several studies found ventricular GIRK1/4 expression using western blot or immunofluorescence (Dobrzynski et al., 2001), in t-tubules or intercalated discs (Dobrzynski et al., 2001; Liang et al., 2014). Additionally, there is a growing body of literature suggesting widespread parasympathetic innervation in the ventricles (Coote, 2013; Liang et al., 2014) and relevance of GIRK1/4 or $I_{K,ACh}$ in ventricular myocardium (Takahashi et al., 2003; Y. Yang et al., 2010). This suggests that GIRK1/4 is important in the whole heart.

1.6 Cardiac remodeling

Cardiac remodeling comprises all molecular, cellular and interstitial alterations of the heart in response to physiological or pathological stimuli, e.g. endurance training, ischemic injury or chronically increased afterload (Azevedo et al., 2016). While physiological remodeling leads to reversible cardiac hypertrophy (e.g. pregnancy, physical exercise), pathological remodeling is mostly irreversible (Shimizu & Minamino, 2016). Pathological remodeling of the heart involves both structural and electrical remodeling. Structural remodeling includes cardiomyocyte hypertrophy and fibrosis (Tham et al., 2015), while alterations in ion channel expression, contribution and function lead to electrical remodeling (Aiba & Tomaselli, 2010).

Although cardiac remodeling is a compensatory mechanism at first, continued pathological stimulation eventually leads to decompensated remodeling combined with further adverse events like cardiac dysfunction, arrhythmias and can progress to heart failure (Tham et al., 2015).

Aberrant calcium handling contributes to pathological electrical remodeling. The failing myocardium is characterized by systolic and diastolic dysfunction (Davlouros et al., 2016). Systolic dysfunction can be caused by reduced calcium entry due to reduced expression or activity of LTCC and SR calcium depletion (Davlouros et al., 2016). Combined with reduced dyadic coupling of LTCC and RyR2 this can lead to reduced effectiveness of CICR, reduced calcium transient amplitude and reduced contractility. Furthermore, prolongation of the duration of calcium transients due to reduced SERCA2a activity impairs proper relaxation of the myocardium. Together with leaky RYR2 this can cause diastolic depolarizations, rendering the heart highly susceptible for malignant arrhythmias (Davlouros et al., 2016). This can lead to sudden cardiac death or progress further towards chronic heart failure and death.

1.7 Electrical remodeling in mice with cardiac hypertrophy

Our group has previously studied a mouse model with epidermal growth factor receptor (EGFR) knockout in vascular smooth muscle cells (VSMC) and cardiomyocytes. These mice show profound cardiac hypertrophy and changes in the electrocardiogram (ECG) that might stand for prolonged AP conduction within the heart (Fig. 5) (Schreier et al., 2013, 2014). Survival was significantly reduced in EGFR KO mice. However, no signs for heart failure were observed as there were no signs of ischemia and lung weight/tibia length was not increased in KO mice. Increased lung wet weight induced by lung congestion due to reduced left ventricular systolic function would be a sign for cardiac decompensation and heart failure. Furthermore, left ventricular ejection fraction was preserved and fibrosis was not increased. Our hypothesis is that these mice died from sudden cardiac arrest due to continued remodeling processes.

To analyse possible mechanisms responsible for cardiac remodeling in EGFR KO mice, NGS transcriptome and microRNA analysis of hearts from EGFR KO and WT mice was performed. Among others, the miR-221/222 cluster was found to be about 2-fold increased in EGFR KO hearts compared to WT (Binas et al., 2020). Subsequent enrichment analysis identified differentially regulated ion channels associated to the t-tubule cluster in EGFR KO mice which were also predicted targets of miR-221/222 (Binas et al., 2020). This implicates a possible role of dysregulated miR-221/222 levels in cardiac electrical remodeling.

Increased miR-221/222 expression was validated in cardiomyocytes from KO animals. Additionally, pri-miR-221/222 levels were also elevated, suggesting transcriptional regulation of miR-221/222 (Binas et al., 2020). Intriguingly, further in vitro studies showed that transient transfection of HL-1 cells with miR-221/222 mimics led to downregulation of the calcium and potassium ion channel mRNAs Cacna1c, Cacnb2, Cacna2d1, Kcnd2 and Girk4 (Kcnj5) (Binas et al., 2020).

A heart hypertrophy

WT   KO

1.5 mm

B changes in ECG
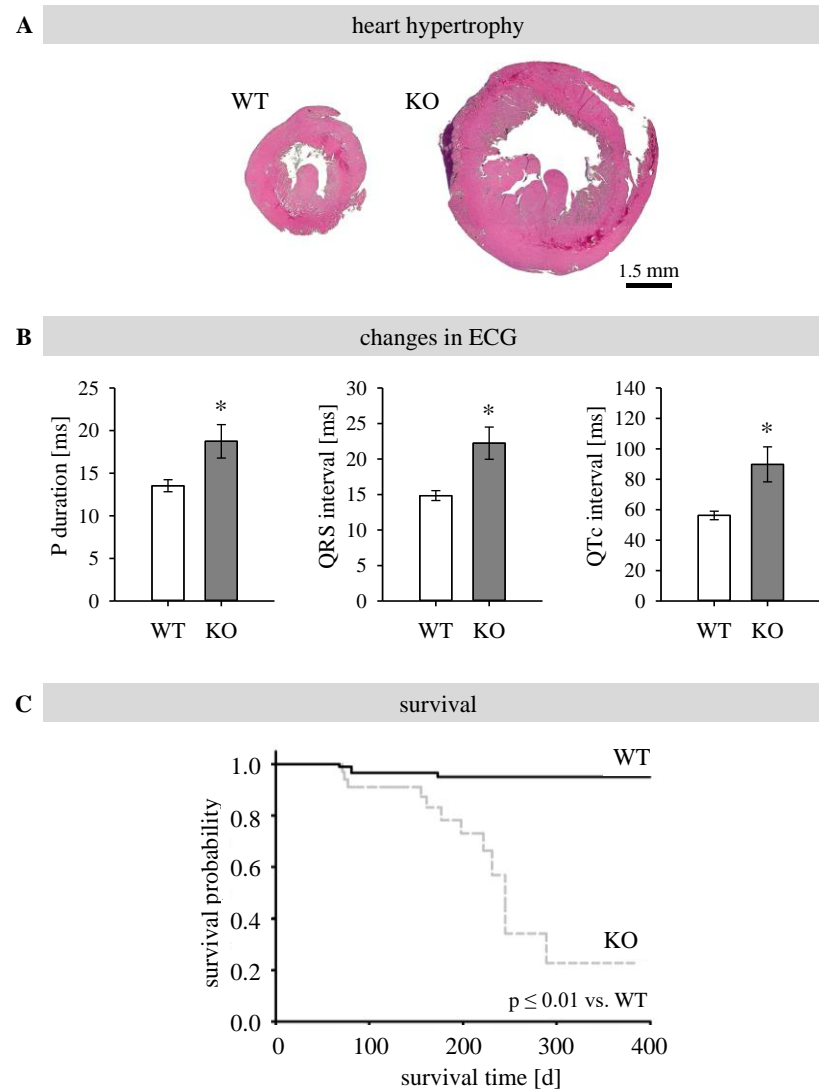
C survival

Figure 5. Cardiac hypertrophy, electrocardiogram and survival rate of EGFR KO mice. A Cross-sections of left ventricles show profound heart enlargement in knockout (KO) mice compared to wild type (WT) (scale bar 1.5 mm). **B** Electrocardiogram (ECG) parameters were altered in male EGFR KO mice. The P duration indicates the duration of atrial excitation during one heart beat. The QRS interval indicates the duration of ventricle excitation. The QTc interval comprises both depolarization and repolarization of the ventricles and is corrected (c) for heart rate. Data are displayed as mean $\pm$ sem, N=3-5 animals/group. **C** Survival was significantly reduced in EGFR KO mice (n=34–92 animals per genotype). Figures modified from (Schreier et al., 2013, 2014).

1.8 Implications of miR-221/222 in cardiac health and disease

1.8.1 MicroRNAs

MicroRNAs are short (~22 nucleotides) non-coding RNAs involved in posttranscriptional regulation of mRNAs (Ha & Kim, 2014). They bind to target mRNAs via complementary base pairing. Partial complementarity is supposed to lead to direct inhibition of translation while perfect complementarity enables incorporation of mRNA-miR-duplex into the RNA-induced silencing complex (RISC) and subsequent RNA degradation (Amini et al., 2019; Harada et al., 2014). MiRNA binding sites can occur in an mRNA's 3'-UTR, 5'-UTR or coding region (Kabekkodu et al., 2018). The most important part of mRNA binding are the 5'-nucleotide positions 2-7 which determine the seed sequence (Ha & Kim, 2014).

MiRs are involved in the regulation of all cellular processes, many miRs are conserved across species and aberrant miR expression has been linked to pathogenesis (Harada et al., 2014). Since one miR has many targets and has mostly moderate effects on expression, miRs are thought to be involved more in the fine-tuning of posttranscriptional regulation (Ravegnini et al., 2019). MiRs can also be involved in communication between cells of the same or different cell type, e.g. via miR-containing exosomes (Bang et al., 2014; Lai et al., 2020).

The general importance of miRNAs for heart development and function was established by a series of dicer knockout experiments. Conditional or inducible cardiac-specific knockout of dicer led to severe phenotypes with the precise manifestation depending on the developmental stage of the mice (Bauersachs & Thum, 2011). While cardiac dicer knockout is embryonically lethal, it is accompanied with sudden cardiac arrest in young mice and heart failure in adult mice (Da Costa Martins et al., 2008; Saxena & Tabin, 2010; Zhao et al., 2007).

1.8.2 MiR-221/222

Although miR-221/222 do not belong to cardiac-enriched miRs like miR-1, miR-133, miR-208 and miR-499, they are also involved in cardiac pathology (Tang et al., 2020). MiR-221/222 are clustered miRNAs located on chromosome Xp11.3 (human) that share the same seed sequence (Song et al., 2019). They are ubiquitously expressed and conserved between e.g. mouse and human (Tang et al., 2020).

Expression of miR-221/222 has been widely analysed in cancer research. A meta-analysis of 50 studies revealed that high miR-221/222 expression in tumor tissue is correlated with poor overall survival in cancer patients (Ravegnini et al., 2019). The oncogenic potential of miR-221/222 is associated with drug resistance, apoptosis, pro-angiogenic effects, invasion and metastasis (Amini et al., 2019). Most studies describe miR-221/222 as oncomiRs, however, tumour-suppressive functions have also been shown (Amini et al., 2019).

The role of miR-221/222 in cardiac remodeling is discussed highly controversial. In the last decade our understanding of miR-221/222 in remodeling has deepened but whether these miRs mediate mainly detrimental or beneficial effects in the heart is still unclear.

Several studies show that miR-221/222 are linked to hypertrophy. Wang et al. showed that miR-221 is upregulated in patients with hypertrophic cardiomyopathy (C. Wang et al., 2012). They also induced cardiac hypertrophy in mice by pressure-overload due to transverse aortic constriction (TAC). In these mice miR-221/222 were also upregulated. In line with this, miR-221 or miR-222 overexpression in rat neonatal cardiomyocytes (neoCMs) led to increased myocyte size (C. Wang et al., 2012) and proliferation as well as reduced apoptosis (X. Liu et al., 2015). Additionally, p27, a suppressor of cardiac hypertrophy, was shown to be a direct target of miR-221 (C. Wang et al., 2012). In another study analysing cardiac tissue from deceased patients with cardiac hypertrophy, miR-221 was significantly increased in patients with cardiac hypertrophy who died from sudden cardiac arrest in comparison to patients with compensated cardiac hypertrophy who died from other causes (Kakimoto et al., 2018). Furthermore, circulating miR-221/222 have been reported to be elevated after acute physical exercise (Baggish et al., 2011), especially after endurance training (Ramos et al., 2018; Wardle et al., 2015), thus suggesting a role not only in pathological but also in physiological heart hypertrophy.

MiR-221/222 have also been studied as potential biomarkers for cardiovascular disease, e.g. for early prediction of acute myocardial infarction (Coskunpinar et al., 2016). Further evidence for a potential prognostic role of miR-221/222 came from a study of heart failure patients receiving left ventricular assist devices (LVADs). Here, myocardial miR-221/222 expression was inversely correlated with cardiac function and decreased during LVAD treatment as cardiac function was improved (Lok et al., 2015). These studies suggest that miR-221/222 expression levels are associated with disease state.

In line with this, cardiac-specific overexpression of either miR-221 or miR-222 led to cardiac hypertrophy, cardiac fibrosis, apoptosis, reduced autophagy and development of heart failure in mice (Su et al., 2015, 2016). In these two studies, miR-221 or -222 overexpression seems to lead to remodeling processes in the heart that impair cardiac function.

However, there are other studies attributing a more cardioprotective role to miR-221/222 (Schmitz & Brand, 2018). For example, cardiomyocyte-specific inducible overexpression of miR-222 protected against adverse cardiac remodeling in mice subjected to ischemia-reperfusion injury (X. Liu et al., 2015). Similarly, miR-221 had a protective effect after hypoxia and reoxygenation in H9c2 cells and rat neoCMs by reducing autophagy and apoptosis and increasing metabolic activity (Q. Chen et al., 2016). Furthermore, in patients with viral myocarditis, miR-221/222 were upregulated in myocardial biopsies and inhibition of miR-221/222 in a mouse

model of viral myocarditis led to increased viral load, injury and inflammation in the heart (Corsten et al., 2015). Downregulation of miR-221/222 was positively correlated with severity of interstitial fibrosis in myocardial biopsies from patients with dilated cardiomyopathy or aortic stenosis (Verjans et al., 2018).

Additionally, there are studies suggesting that the protective effect may be mediated by physical exercise-induced miR-221/222 expression. For example, Tian et al. showed that physical exercise or miR-221/222 lead to downregulation of angiopoietin-like protein 2 (ANGPTL2), thereby reducing pathological cardiac remodeling (Tian et al., 2016). They showed that miR-221/222 levels were increased in a pressure overload model (TAC) and heart failure development was more likely in mice with a cardiomyocyte-specific knockout of miR-221/222 than in control mice (Tian et al., 2016). Vujic et al. showed that exercise induced cardiomyogenesis after myocardial infarction in the border zone of the affected area and that miR-222 inhibition blocks this effect (Vujic et al., 2018).

Some studies even suggest miR-221/222 as promising therapy in cardiac diseases. For example, uptake of microvesicular miR-221 from mesenchymal stem cells into co-cultured cardiomyocytes induced an anti-apoptotic and therefore protective effect during hypoxia by reducing PUMA expression (p53 upregulated modulator of apoptosis) (Yu et al., 2013). In another study, exosomal miR-221 improved regeneration in rat hearts after myocardial infarction in vivo. It also had a protective effect on cardiomyocytes in vitro by reducing fibrosis and apoptosis and promoting survival (L. Sun et al., 2020). However, the clear downside is the unspecific targeting of vesicles containing miRs and also the possibility of tumorigenic side effects since miR-221/222 are frequently found to be upregulated in cancer (Uchida & Dimmeler, 2015). To overcome these side effects, cardiomyocyte-specific upregulation of miR-221/222 by the use of adeno-associated virus-vectors could be a promising strategy (Uchida & Dimmeler, 2015).

In conclusion, miR-221/222 have been implicated in cardiac remodeling, in both structural and electrical remodeling. However, the mechanisms leading to the reported detrimental or protective effects remain largely unknown. This includes both the regulation of miR-221/222 expression and their effects on target genes in cardiomyocytes.

1.9 Aims of this study

While it is established that miR-221/222 are associated with cardiac remodeling and disease the precise role remains unclear. Upregulated miR-221/222 expression in hearts from EGFR KO mice was correlated to downregulated cardiac ion channel genes which are predicted targets of both miRs (Binas et al., 2020). Thus, miR-221/222 could be involved in electrical remodeling in the heart by targeting ion channel mRNAs. Therefore, the goal of this study was to analyse the possible role of miR-221/222 in electrical remodeling in cardiomyocytes.

The first aim was to detect and validate direct targets of miR-221/222 in cardiomyocytes using dual luciferase assays in HEK-293 cells. From the ion channel genes that were downregulated in EGFR KO hearts (NGS analysis) and also predicted targets for miR-221/222, only those with a fragments per million (FPM) value >10 in wild type mice were chosen for dual luciferase assays: LTCC subunits Cacna1c, Cacnb2 and Cacna2d1 as well as K$^+$ channel genes Kcnd2 and Girk4. Subsequently, mutagenesis of the predicted miR binding sites within the 3'-UTRs should be performed to validate these binding sites in dual luciferase assays.

The second aim was to investigate the biological relevance of the miR-target interaction using functional measurements (patch clamp analysis or fluorescent Tl$^+$ flux assays in HEK-293 cells and HL-1 cardiomyocytes for regulated K$^+$ channels, ratiometric fluorescent calcium imaging in HL-1 cells for regulated LTCC subunits).

The third aim was to study the impact of miR-221/222 on spontaneous calcium transients. For this, ratiometric fluorescent calcium measurements in neonatal cardiomyocytes (neoCMs) under control conditions and with β-adrenergic stimulation should be established in our lab. Stimulation of β-adrenergic receptors helps to characterize cardiomyocyte function regarding their ability to adapt to differing cardiac demands and also has relevance in cardiac disease.

The fourth aim was to link the calcium results with functional consequences for the cardiomyocytes. For this purpose, the impact of miR-221/222 on spontaneous contractility in neoCMs should be studied under control conditions and with β-adrenergic stimulation.

The fifth aim was to investigate a possible mechanism of transcriptional regulation of miR-221/222 expression, also in the context of the different cardiac cell types, e.g. by using co-culture settings with cardiomyocytes and fibroblasts. Since miR-221/222 expression was elevated in AngII-treated mice and miR-222 was increased in ISO-treated mice (Binas et al., 2020), cells should be incubated with AngII and ISO to test if these substances influence miR-221/222 expression in vitro.

2. Materials

All materials, chemicals and reagents were purchased from Sigma Aldrich (Munich, Germany) unless stated otherwise in the text. If not mentioned otherwise, sterile nuclease-free water for molecular biology from Sigma Aldrich was used as water. Buffers were made with ultrapure water (Werner).

2.1 List of manufacturers and distributors

Abcam	Cambridge, UK
Agilent Technologies	Santa Clara, USA
Alomone Labs	Jerusalem, Israel
Amersham	Freiburg, Germany
Applied Biosystems via Life Technologies	Darmstadt, Germany
Axon Instruments, now Molecular Devices	San Jose, California, USA
Berthold Technologies	Bad Wildbad, Germany
Biochrom	Berlin, Germany
BioRad	Munich, Germany
Capricorn Scientific	Ebsdorfergrund, Germany
Carl Zeiss	Oberkochen, Germany
Cell Signaling Technology	Danvers, USA
Clontech, now Takara Bio	Kyoto, Japan
Dunn	Asbach, Germany
Falcon via Corning	Corning, New York, USA
GE Healthcare	Berlin Germany
GeneCopoeia	Rockville, USA
Hielscher	Teltow, Germany
Hilgenberg	Malsfeld, Germany
Ibidi	Gräfelfing, Germany
Invitrogen via Life Technologies	Darmstadt, Germany
IonOptix	Westwood, Massachusetts, USA
Keyence	Osaka, Japan
LI-COR	Lincoln, Nebraska, USA
Life Technologies	Darmstadt, Germany
Merck	Billerica, Massachusetts, USA
Microsoft	Redmond, Washington, USA
MFK	Niedernhausen, Germany
New England Biolabs	Frankfurt, Germany
Origene	Herford, Germany
Perkin Elmer	Krakow, Poland
Promega	Mannheim, Germany
Qiagen	Venlo, Netherlands
Ratiopharm	Ulm, Germany
Rockland	Limerick, USA
Sigma Aldrich	Munich, Germany
Stratagene	La Jolla, CA USA
Systat Software	Chicago, Illinois, USA

Tecan   Männedorf, Schweiz
Thermo Fisher Scientific   Waltham, Massachusetts, USA
Visitron Systems   Puchheim, Germany
Werner   Leverkusen, Germany
Whitehead Institute for Biomedical Research   Cambridge, Massachusetts, USA
Zeiss   Oberkochen, Germany

2.2 Plasmids

Plasmid maps are provided in the appendix.

pCMV6-Girk1   Origene
pCMV6-Girk4   Origene
pCMV6-Chrm2   Origene
pRFP-N1   Clontech
pEZX-MT06   GeneCopoeia
pAT1R   Origene
pGL3-basic   Promega
pcDNA3.1-His_lacZ   Invitrogen
pMiR-221, pMiR-222   Applied Biosystems
pSEAP-basic   Clontech
pGL4.74-hRLuc   Promega

2.3 Software

Harmony 4.8 software   Perkin Elmer
Image J v1.53f   https://imagej.nih.gov/ij/ (10.02.2021)
IonWizard   IonOptix
ISO2   MFK
Microsoft Office 2016   Microsoft
Myocyter plugin for Image J v1.3   Tobias Jung (Grune et al., 2019)
QuikChange Primer Design   Agilent Technologies
SigmaPlot 12.5   Systat Software
TargetScanMouse 7.1   Whitehead Institute for Biomedical Research
VisiVIEW Imaging Software   Visitron Systems

3. Methods

3.1 Isolation of murine cardiomyocytes

3.1.1 Ethics statement

All mouse experiments described in this manuscript were performed according to the guidelines of the directive 2010/63/EU of the European Parliament on the protection of animals used for scientific purposes and, if applicable, were approved by the local government (Landesverwaltungsamt Sachsen-Anhalt, Germany, permit numbers: 42502-2-1124 and -1201 MLU).

3.1.2 Mouse models

Wildtype C57BL/6 and EGFR KO (Schreier et al., 2013, 2014) mice were kept in the facilities of the University of Halle-Wittenberg at a room temperature of 20 ± 1°C, with a 12 h/12 h light/dark cycle and were fed *ad libitum* with standard chow.

3.1.3 Isolation of adult cardiomyocytes and cardiac fibroblasts

Adult cardiomyocytes and fibroblasts from hearts of EGFR KO or WT mice were isolated as described in a very detailed protocol by Liao and Jain (R. Liao & Jain, 2007). In the context of this study only fibroblasts from these animals were used, cardiomyocytes were used in a different project. In short, mice were injected i.p. with 50 µl 1250 units/ml heparin (Ratiopharm) and anaesthetized with 100 µl 50 mg/ml pentobarbital. Hearts were removed from fully anaesthetized animals and immediately attached to the perfusion cannula through the aorta. Hearts were retrogradely perfused (Langendorff-preparation) with perfusion buffer for 3 min (for buffer composition, see appendix). Then perfusion was switched to digestion buffer. After 7-10 min the heart was pale and flaccid and the digestion was completed. Subsequently, the hearts were removed from the cannula, atria and great vessels were removed and the ventricles were cut into smaller pieces and further dissociated into single cells by pipetting the suspension using a Pasteur pipette. The solution was strained through a 250 µm filter and transferred to a 50 ml tube where cells were allowed to settle for 15 min by gravity. The supernatant contained cardiac fibroblasts which are much smaller than adult CM and therefore do not settle as fast. After the CM pellet was carefully removed using a Pasteur pipette, the fibroblast solution was centrifuged at 1000 rpm for 5 min at room temperature. The supernatant was discarded and fibroblasts were resuspended in DMEM containing 10% FCS. Fibroblasts were subcultured only to expand the culture and then were subjected to the incubation experiments described below. Cardiomyocytes were placed in buffers with successively increasing calcium concentrations (0.06 mM to 1.2 mM) and always allowed to settle by gravity before transferring into the next buffer. At last, the CM pellet was transferred to plating buffer and cardiomyocytes were resuspended. Cardiomyocytes were plated

on laminin-coated culture dishes and after one h the calcium transfer buffer was replaced with culture medium.

3.1.4 NeoCMs and cardiac fibroblasts

NeoCMs were isolated from wild type C57BL/6 newborn mice on postnatal day 0-2. Mice were sacrificed by decapitation and hearts were removed and placed in cold 0.9% NaCl solution. Hearts from all littermates were pooled. Connective tissue was removed from the hearts. Whole hearts were transferred into 5 ml digestion buffer and minced into small pieces. Digestion was performed in 6-8 successive 10 min steps in 25 ml beakers at room temperature and constant stirring at 300 rpm. The total number of digestion steps depends on the number of hearts. Generally, digestion steps were performed until all tissue pieces were digested. After 10 min of digestion the undigested tissue was allowed to settle down to the bottom of the beaker and the supernatant containing single cells was transferred to a 15 ml falcon tube with 6 ml FCS (for trypsin inactivation). New digestion buffer was added to the still undigested tissue and stirred again for 10 min. This was repeated until all tissue pieces were digested. After each digestion step the supernatant/FCS mixture was centrifuged at 1000 rpm for 5 min at room temperature. The supernatant was removed and the cell pellet resuspended in neoCM medium (5% FCS, buffer and medium composition see appendix) supplemented with 25 µl/ml penicillin/streptomycin. To remove most of the non-cardiomyocytes (mainly fibroblasts) from the cardiomyocyte culture, a pre-plating step was included. For this, cells were incubated for 1-2 h on untreated 5 mm Petri dishes at 37°C. In contrast to the cardiomyocytes, fibroblasts adhered to the untreated surface and the medium containing mainly cardiomyocytes could be removed and was centrifuged again. The cell pellet was then resuspended in neoCM medium (5% FCS) without antibiotics and the cells were plated onto fibronectin-1-coated glass cover slides in 5 mm Petri dishes (about two hearts per Petri dish). The next day the medium was changed to remove dead cells. After the initial seeding the FCS content was reduced to 1% to minimize fibroblast growth.

If needed, neonatal fibroblasts were further cultured in DMEM containing 4.5 g/l glucose supplemented with 10% FCS.

3.2 Cell culture

3.2.1 Culture of cell lines

All cells were maintained at 37°C and 5% CO_2 and routinely tested for mycoplasma contamination.

HL-1 cells were maintained in Claycomb medium with the following supplements: 10% FCS (Biochrom) 2 mM L-glutamine, 100 µM noradrenaline, 100 U/ml penicillin and 100 µg/ml streptomycin. Cells were subcultured at confluency (once a week; 1/10) and medium was changed twice a week.

Mouse fibroblast NIH-3T3 cells were cultured in DMEM (4.5 g/l glucose) supplemented with 10% FCS. They were subcultured before reaching confluency and splitted 1/10, generally twice a week. Medium was changed only when cells were splitted.

HEK-293 cells were cultured in DMEM Ham's F12 medium (Merck) supplemented with 10% FCS (Biochrom). Cells were splitted once a week 1/20 and medium was changed twice per week.

3.2.2 Incubation of HEK-293 and HL-1 cells

HEK-293 cells or HL-1 cells were transfected on 10 cm Petri dishes with 2 µg pAT1R (human angiotensin II receptor type 1) or empty vector control for 24 h using polyfect (Qiagen) or lipofectamine 2000 (Invitrogen), respectively. After transfection cells were splitted (to three 3.5 cm Petri dishes each) and 24 h later incubated with 100 nM angiotensin II or control for further 48 h. MiR expression was analysed by qRT-PCR using Taqman microRNA Assays as described above.

3.2.3 Incubation of adult cardiac fibroblasts

Cells were serum-starved for 24 h and incubated on the following day with 100 nM AngII, 10 µM ISO or 10 ng/ml TGFβ in DMEM without FCS for 48 h. MiR expression was analysed by qRT-PCR using Taqman microRNA Assays as described above.

3.2.4 Co-culture of cardiomyocytes and fibroblasts

Co-culture experiments were performed with HL-1 cells (cardiomyocytes) in combination with NIH-3T3 cells (fibroblasts) in a transwell setting (Fig. 6). HL-1 cells were seeded onto 6 well plates and NIH-3T3 were seeded onto cell culture inserts with PET membranes (Falcon, 0.4 µm pore size) in their respective cell culture medium. At this point each cell type remained in a separate well in mono-culture. The next day the co-culture was started by placing the inserts (HL-1) into the 6 well plates (NIH-3T3) and both cell types were serum starved for 24 h in DMEM medium. After that, cells were incubated for 48 h with 100 nM AngII, 10 µM ISO or 10 ng/ml TGFβ in DMEM without FCS. RNA was isolated as described above. MiR expression was analysed by qRT-PCR using Taqman microRNA Assays as described above.
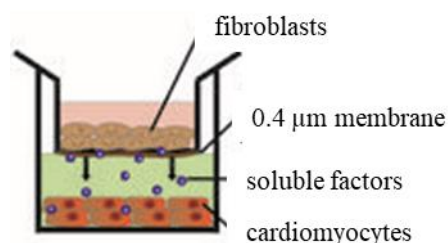
Figure 6. Scheme of the transwell co-culture system. Shown is the side view of one well within a 6-well plate. Description see text. Scheme modified from (Bang et al., 2014).

3.3 Molecular biology

3.3.1 Transformation and plasmid DNA preparation

One Shot™ TOP10 Chemically Competent *E. coli* 50 µl vials (Invitrogen) were thawed on ice. 1-5 µl (10 pg – 100 ng) of plasmid solution were pipetted directly into the bacteria suspension, mixed carefully and kept on ice for 30 min. After that, bacteria were heat-shocked for 30 s in the water bath at 42°C and then placed on ice for 2 min. 250 µl S.O.C. medium was added to each vial and the vials were incubated for 1 h at 37°C with shaking at 225 rpm. Of each reaction 20 µl or 200 µl solution was plated onto LB agar plates containing the appropriate antibiotics (ampicillin: 60 µg/ml, kanamycin: 50 µg/ml). LB agar plates were inverted and incubated over night at 37°C and 5% CO_2.

On the following day 6 bacterial colonies were selected and cultured in 5 ml LB medium containing the appropriate antibiotics at 37°C and 225 rpm overnight. On the subsequent day 4 ml of bacteria suspension were harvested for plasmid preparation (Qiagen plasmid mini kit), DNA was resuspended in water and measured with NanoVue Plus spectrophotometer (GE Healthcare). The remaining bacteria were used for cryo stock preparation (15% glycerine).

For plasmid preparation from bacterial stocks frozen bacteria were added to 5 ml LB medium containing the appropriate antibiotics using a pipette tip and cultured over night at 37°C and 225 rpm. The following day the culture was used for plasmid preparation (Qiagen plasmid mini kit; resuspended in water). For larger plasmid amounts 200 ml overnight cultures generated from 5 ml pre-cultures were used and plasmid DNA was isolated with the Qiagen plasmid maxi kit following manufacturer's instructions. DNA was resuspended in water.

3.3.2 Mutagenesis

Putative miR-221/222 binding sites in the 3'-UTR of pEZX-Cacna1c_b and pEZX-Kncj5 were mutated using the QuikChange II XL site-directed mutagenesis kit (Agilent Technologies) following the manufacturer's instructions.

In silico analysis of miR-221/222 binding sites

Putative miR-221/222 binding sites in the above mentioned 3'-UTRs were determined using TargetScanMouse 7.1 (http://www.targetscan.org/mmu_71/; (Agarwal et al., 2015)) (Table 1).

Design of mutagenic primers

To design the primers for mutagenesis the QuikChange Primer Design tool was used (Agilent Technologies; https://www.chem.agilent.com/store/primerDesignProgram.jsp) (Table 2).

Table 1. Predicted pairing of 3'-UTR target region and miR-221/222 by TargetScan. Underlined: putative binding site of the respective miRNA, gray-shaded: seed sequence (defined as nucleotides 2-8 from 5' direction), vertical lines: predicted nucleotide pairing between miR and 3'-UTR.

Sequence position	Predicted consequential pairing of target region (top) and miRNA (bottom)
Position 2524-2530 of Cacna1c 3'-UTR mmu-miR-221-3p	5' ...CAUUUAUGCAGCCUU<u>UGUAGCAC</u>... |||| |||||| 3' CUUUGGGUCGUCUGUUACAUCGA
Position 2524-2530 of Cacna1c 3'-UTR mmu-miR-222-3p	5' ...CAUUUAUGCAGCCUU - <u>UGUAGCAC</u>... |||| |||||| 3' UGGGUCAUCGGUCUACAUCGA
Position 2062-2069 of Girk4 3'-UTR mmu-miR-221-3p	5' ...CGUGUGGCAUGUAUG<u>AUGUAGCA</u>... ||| ||||||| 3' CUUUGGGUCGUCUGU - - UACAUCGA
Position 2062-2069 of Girk4 3'-UTR mmu-miR-222-3p	5' ...CGUGUGGCAUGUAUG<u>AUGUAGCA</u>... ||||||| 3' UGGGUCAUCGGUCUACAUCGA

Mutated miR-221/222 binding sites

miR-221/222 binding site in Cacna1c 3'-UTR:

wild type: 5'-…CATTTATGCAGCCTT<u>TGTAGCAC</u>…-3'

mutated: 5'-…CATTTATGCAGCCTT**GACTATT**C…-3'

miR-221/222 binding site in Girk4 3'-UTR:

wild type: 5'-…CGTGTGGCATGTATG<u>ATGTAGCA</u>…-3'

mutated: 5'-…CGTGTGGCATGTATG**CATGCTA**A…-3'

Principle of site-directed mutagenesis

The aim of this method is to introduce mutations into double-stranded plasmid DNA *in vitro* using two synthetic oligonucleotide primers that are complementary to both strands of the plasmid, both carrying the desired mutation. This is achieved in a 3-step protocol (Fig. 7).

During the first step the primers are annealed to the plasmid and extended by *PfuUltra* high-fidelity DNA polymerase to generate plasmids containing the desired mutation. In the second step the parental DNA is digested by the methylation-specific restriction enzyme Dpn I, thereby keeping only the mutated plasmid DNA. The third step involves transformation of XL10-Gold ultracompetent *E.coli* and subsequent preparation of mutated plasmid DNA.

Figure 7. Overview of the QuikChange II XL site-directed mutagenesis method. Modified from (Walquist & El-Gewely, 2018).

mutant stand synthesis

Dpn I digestion of template

transformation

Table 2. Primers containing the mutated version of the miR binding site in Cacna1c_b and Girk4 3'-UTR.

Primer name	Primer sequence (5' to 3')
Cacna1c_b_mut_R	TATCTCTAGAAGCCCTTATGGGAATAGTCAAGGCTGCATAAATGCTCGGTCAACCACATATGGAAATCCA
Cacna1c_b_mut_F	TGGATTTCCATATGTGGTTGACCGAGCATTTATGCAGCCTTGACTATTCCCATAAGGGCTTCTAGAGATA
Girk4_mut_R	CACAAAGACATACACACCACAGCATACACATTAGCATGCATACATGCCACACGCATGTACACAAACACC
Girk4_mut_F	GGTGTTTGTGTACATGCGTGTGGCATGTATGCATGCTAATGTGTATGCTGTGGTGTGTATGTCTTTGTG

Step 1: mutant strand synthesis

Sample reaction mix and cycling program were performed following manufacturer's instructions. 50 ng of plasmid DNA (pEZX-Cacna1c_b or pEZX-Girk4, respectively) were added. Thermal cycling was as follows: initial 95°C for 1 min, then 18 cycles of 95°C for 50 s, 60°C for 50 s and elongation at 68°C for 9 min, followed by final extension at 68°C for 7 min.

Step 2: *Dpn* I digestion of template DNA

1 µl 10 U/µl *Dpn* I restriction enzyme was added to each amplification reaction and samples were incubated for 1 h at 37°C.

Step 3: transformation and preparation of plasmid DNA

XL10-Gold ultracompetent *E. coli* were thawn on ice. To each 45 µl of bacteria 2 µl β-ME mix were added, swirled gently to mix and incubated on ice for 10 min. Then 2 µl of Dpn I-treated DNA was transferred to the bacterial suspension, mixed gently and incubated on ice for 30 min. After a heat pulse in a 42°C water bath for 30 s the tubes were placed on ice for 2 min. After 500

µl NZY+ broth was added to each vial they were incubated for 1 h at 37°C with shaking at 225-250 rpm. Plating, colony selection, culture and plasmid preparation was performed as described above.

Sequencing of mutated plasmid DNA

To confirm successful mutagenesis, plasmid DNA was subjected to sequencing.

Table 3. Primer for sequencing after mutagenesis.

Primer name	Primer sequence (5' to 3')
Cacna1c_b_mut_F_sequ	TCCAGTCCCAGTGACCTACC
Girk4_mut_R_sequ	TCACTGTGGACTCCCTTTCC

3.3.3 Transient transfection with miR-221/222 mimics

For transient transfection of cells with miR-221/222 miRCURY LNA microRNA mimics (Qiagen) were used. These mimics are made out of three RNA molecules: one miRNA strand and a complementary strand that is divided into two smaller LNA-modified strands. While the two passenger strands are degraded rapidly, only the miRNA strand is loaded into the RNA-induced silencing complex (RISC), thus minimizing off-target effects. Negative miRCURY LNA miRNA mimic controls (Qiagen) that show no homology to known sequences in mouse were used as mimic controls.

Table 4. Overview over the used miR mimics.

Short name	Name	Modification
mimic control	Negative Control 5 miRCURY LNA miRNA Mimic	no label
miR-221	hsa-miR-221-3p miRCURY LNA miRNA Mimic	no label
miR-222	hsa-miR-222-3p miRCURY LNA miRNA Mimic	no label

HL-1 cells were transiently transfected with 30 nM of miRCURY LNA miR-221/222 mimics or mimic negative control using 5 µl lipofectamine 2000 (Thermo Fisher Scientific) in 1.5 ml DMEM (Biochrom; without FCS) following manufacturer's instructions. After 24 h the medium was changed and cells were kept on Claycomb medium with supplements for further 48 h.

NeoCMs were transiently transfected with 30 nM of miRCURY LNA miR-221/222 mimics or mimic negative control using 5 µl lipofectamine 2000 (Thermo Fisher Scientific) in 1.5 ml DMEM (Biochrom) with 4.5 g/l glucose following manufacturer's instructions. After 24 h the medium was changed and cells were kept on DMEM with 4.5 g/l glucose, 20 µg/ml vitamin B_{12} and 5% FCS medium for further 48 h.

3.3.4 RNA isolation

Total RNA was isolated using Trizol (Invitrogen). After removing the medium and washing the cells with cold PBS, cells were lysed in 1 ml Trizol. To each sample 200 µl chloroform was added and the samples were shaken vigorously. After a 3 min incubation at room temperature samples were centrifuged at 12000 g for 15 min at 4°C. Afterwards, the upper watery phase was transferred to a new reaction tube. To precipitate RNA 500 µl isopropanol was added, mixed well and incubated for at least 30 min or overnight at -20°C. Samples were centrifuged at 12000 g for 10 min at 4°C and the supernatant was discarded. The remaining pellet was washed 1-2 times with 75% ethanol and centrifuged at 12000 g for 10 min at 4°C. The pellets were dried at 37°C for 10 min and then resuspended in 30 µl sterile RNase free water. RNA concentration was measured by NanoVue Plus spectrophotometer (GE Healthcare).

To extract RNA from mouse organ samples, Trizol-treated tissue was additionally ground in a tissue mill (TissueLyser LT, Qiagen) for 5 min at 50 Hz using two steel balls. Afterwards RNA was isolated as described above.

3.3.5 cDNA synthesis

To remove genomic DNA contamination, one µg of total RNA was treated with 2 units of DNase I (RNase-free; New England Biolabs) at 37°C for 10 min, followed by enzyme inactivation at 75°C for 10 min. Reverse transcription (RT) reaction of DNase I-treated total RNA was performed with random primers using SuperScript II reverse transcriptase (Invitrogen) with the following program: 5 min 25°C, 30 min 42°C and 5 min 95°C.

3.3.6 Droplet digital PCR

To determine the absolute amount of RNA, droplet digital PCR (ddPCR) was performed using the QX200 system from BioRad. cDNA was prepared as described above and used in ddPCR at the same conditions as in realtime qPCR using either EvaGreen supermix (for AT1R) or Taqman probes (miRs). The threshold between negative and positive droplets was manually set to optimally distinguish signal from noise (in this case to 18433 for all samples). Positive droplets per µl were extrapolated to ng of input RNA by taking into account all diluting steps.

Table 5. Primer for ddPCR.

Primer	Sequence 5'-3'	Annealing	Cycles
hAT1R_F	GGCGCGGGTTTGATATTTGA	60°C, 45 s	40
hAT1R_R	CAAATACACCTGGTGCCGAC		
mAT1R_F	AAGGGCCATTTTGCTTTTCT	60°C, 45 s	40
mAT1R_R	AATGGCTGGCATTTTGTCTG		

### 3.3.7 TaqMan RT and qPCR assay for miR detection

The principle of the 2-step RT and qPCR of TaqMan miRNA assays is depicted in Figure 8. Isolated RNA was diluted to 10 ng/µl in water. Reverse transcription was performed using miR-specific stemloop RT primers (TaqMan, Applied Biosystems). In RT reactions multiplexed for miR-221, miR-222 and U6 snRNA 12.5 ng RNA were used per miR. Thermal conditions were as follows: 30 min 16°C, 30 min 42°C, 5 min 85°C.

qPCR was performed using miR-specific Taqman small RNA assays as well as TaqMan™ Universal PCR Master Mix, no AmpErase™ UNG (Applied Biosystems). Thermal conditions: initial 95°C for 10 min followed by 40 cycles of 95°C for 15 s and 60°C for 60 s. The list of TaqMan™ assays is given in table 6. Fold change of miR-221/222 expression was calculated using the formula below. U6 was used as reference RNA.

$$fold\ change = 2^{control[Ct(target)-Ct(reference)]-treatment[Ct(target)-Ct(reference)]}$$

Table 6. Taqman assays for miR detection.

Taqman Assay	Order ID	miRBase Accession Nr
hsa-miR-221	000524	MIMAT0000278
hsa-miR-222	002276	MIMAT0000670
U6 snRNA	001973	-
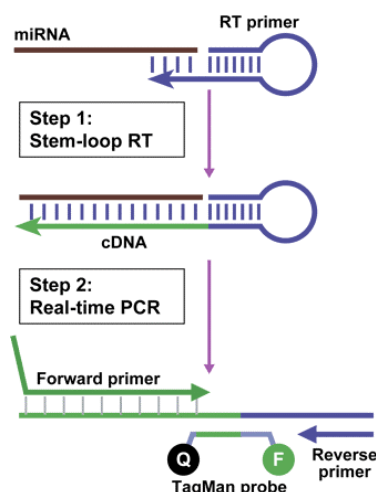
Figure 8. Scheme showing the principle of the 2-step RT-PCR of TaqMan miRNA assay. Step 1: Reverse transcription (RT) of mature miRs is performed using miR-specific stem-loop RT primers. Step 2: Real-time PCR follows with a miR-specific forward primer, a stem-loop-specific reverse primer and TaqMan probe. The tail on the forward primer is used to increase the melting temperature. Modified from (C. Chen et al., 2005).

3.3.8 Protein isolation and Western blot

For Western Blot analysis miR-221-transfected HL-1 cells were washed with PBS and lysed in RIPA buffer and sonicated (UP100H; Hielscher). Protein concentration was measured with BCA assay (Pierce BCA Protein Assay Reagent A, Thermo Fisher) and $CuSO_4$. Afterwards, cell lysates were matched for protein content, Redmix was added and proteins were denatured at 95°C for 5 min. After separation via SDS-PAGE (5% stacking gel, 10% separating gel) the proteins were transferred to a nitrocellulose membrane (GE Healthcare).

For GIRK1/4 detection, the membrane was incubated with primary antibodies (GIRK1: 1:1000, ab129182, Abcam; GIRK4: 1:750, ab113699, Abcam; HSP90: 1:1000, 4874, Cell Signaling Technology) at 4°C overnight. The bound primary antibody was visualized using horseradish peroxidase-conjugated secondary IgG (anti-rabbit, 1:20000, Rockland) and the ECL system (Amersham).

For pERK1/2/ERK1/2 and pAKT/AKT detection, the membrane was incubated with primary antibodies (ERK1/2: 1:1000, #4696; pERK1/2: 1:1000, #9101; AKT: 1:2000, #2920 40D4; pAKT: 1:2000, #4060 D9E, all from Cell Signaling) at 4°C overnight. The bound primary antibody was visualized using fluorescently labelled secondary antibodies (Anti-Rabbit IRDye 800CW green and Anti-Mouse IRDye 680RD red, both 1:40000, both from LI-COR), Clarity Western enhanced chemiluminescence (ECL) Substrate (BioRad) and the Odyssey imaging system (LI-COR).

Densitometry analysis was performed with Quantity One software (BioRad) for GIRK1/4 or Image Studio Lite Ver 5.2 (LI-COR) for pERK1/2/ERK1/2 and pAKT/AKT.

3.3.9 Dual luciferase reporter assay

Reporter constructs (pEZX-MT06 dual luciferase reporter; GeneCopoeia, Rockville, USA) containing the 3'-UTRs of murine ion channel mRNAs downstream of the firefly luciferase are listed in table 7. The backbone of pEZX-MT06 is shown in Figure 9. As the 3'-UTRs of mice for Cacna1c and Cacna2d1 were longer than 3.5 kb, the 3'-UTRs were splitted into three or two fragments, respectively. HEK-293 cells were seeded onto 24 well plates and transfected with each 10 ng of reporter construct or empty vector control as well as 30 nM of miRCURY LNA miR-221 mimics, miR-222 mimics or mimic negative control (Exiqon) using 1.5 µl Polyfect (Qiagen) in 350 µl DMEM/Ham's F12 (Merck; without FCS). After 24 h the medium was changed and cells were cultured in DMEM/Ham's F12 (without FCS). After further 48 h cells were lysed and the luciferase activity in the lysate was measured using the Dual Luciferase Assay System (Promega) following the manufacturer's instructions and the TriStar LB 941 Multimode Microplate Reader (Berthold Technologies). Firefly luciferase activity was normalized to Renilla luciferase activity of the same sample. After that, values were normalized to mimic negative control as well as empty vector.
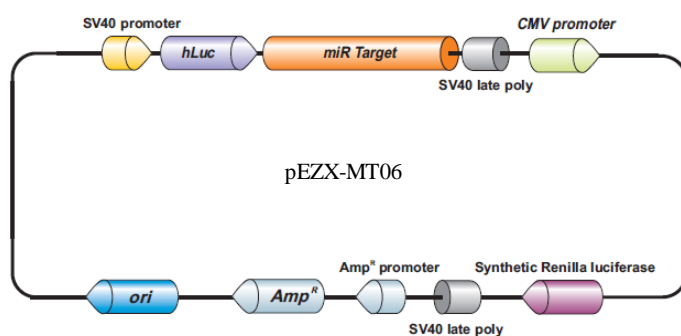
Figure 9. Backbone structure of pEZX-MT06 reporter plasmid. The 3'-UTR of a putative miR target gene is cloned downstream of the hLuc (human firefly luciferase) gene. Thus, firefly luciferase activity depends on the regulation of the target 3'-UTR by the miR, while renilla luciferase is not regulated. Image modified from manufacturer's data sheet (GeneCopoeia).

As a positive control for miR-221/222 activity pMiR-221 or pMiR-222 vectors that contain the respective mature miR sequence in the 3'-UTR of the firefly luciferase gene were used. HEK-293 cells were co-transfected with 40 ng pMiR-221 or pMiR-222 (firefly luciferase) and 10 ng pGL4.74-hRLuc (renilla luciferase) plus 30 nM of miRCURY LNA mimics for miR-221, miR-222 or control as described above. After 24 h the medium was changed and cells were cultured in DMEM/Ham's F12 (without FCS). After further 48 h cells were lysed and the luciferase activity in the lysate measured as described above.

Table 7. Overview over used dual luciferase reporter constructs.

Reporter construct	Catalog name (GeneCopoeia)	Length 3'-UTR (position of fragment within 3'-UTR)	RefSeq
pEZX-EV (empty vector)	CmiT000001-MT06	-	-
pEZX-Cacnb2	MmiT076945-MT06	1832 bp	NM_001252533.1
pEZX-Cacna1c_a	MmiT073710a-MT06	2228 bp (-16 - 2211 bp)	NM_001159533.2
pEZX-Cacna1c_b	MmiT073710b-MT06	2322 bp (2143 - 4464 bp)	NM_001159533.2
pEZX-Cacna1c_c	MmiT073710c-MT06	2299 bp (4393 - 6691 bp)	NM_001159533.2
pEZX-Cacna2d1_a	MmiT054931a-MT06	1894 bp (-1 - 1892 bp)	NM_001110843.1
pEZX-Cacna2d1_b	MmiT054931b-MT06	2000 bp (1844 - 3843 bp)	NM_001110843.1
pEZX-Kcnd2	MmiT032013-MT06	2462 bp	NM_019697.3
pEZX-Girk4	MmiT029508-MT06	2797 bp	NM_010605.4

3.3.10 MiR-221/222 promoter studies

HEK-293 cells were seeded on a 24 well plate and transiently transfected with 50 ng/well pGL3-hmiR-221 (containing a 2000 bp human miR-221/222 promoter fragment) or pGL3-basic as empty vector control (EV) and either 40 ng/well pAT1R or pSEAP basic as EV. Samples were also transfected with 20 ng/well pcDNA3.1-His_lacZ to normalize firefly luciferase activity to β-galactosidase activity. After 24 h medium was changed to different test media (10% FCS, 100 nM AngII, 1 µM losartan, 5 µM IKK inhibitor IV, 1 µM EGFR inhibitor AG1478) and cells were incubated for further 48 h. Firefly luciferase activity was measured using the Dual Luciferase Assay System (Promega) following the manufacturer's instructions and the TriStar LB 941

multimode microplate reader (Berthold Technologies). β-galactosidase activity was determined with 2-Nitrophenyl β-D-galactopyranoside (ONPG, 4 mg/ml). 10 µl of each lysate were pipetted to a 96 well plate, 50 µl of 1x cleavage buffer and 20 µl ONPG were added and incubated at 37°C for 30 min. The reaction was stopped with 125 µl stop buffer (1 M Na_2CO_3). Absorption was measured at 405 nm using the Sunrise absorbance microplate reader (Tecan).

10x cleavage buffer was composed as follwos (in M): 0.6 Na_2HPO_4 x 7 H_2O, 0.4 NaH_2PO_4 x H_2O, 0.1 KCl and 0.01 $MgSO_4$ x 7 H_2O, pH 7.

3.3.11 Immunofluorescence

Freshly isolated ventricular neoCMs were plated on fibronectin-1-coated Multitest slides (Dunn) and incubated for 24 h. Cells were fixated with 4% paraformaldehyde for 15 min at room temperature. After three washing steps with 1xPBS for 5 min each, cells were permeabilized using 1xPBS with 1% TritonX-100 for 30 min at room temperature. This was followed by two washing steps: 10 min with 1xPBS with 1%SDS and 100 mM glycine and 10 min with 1xPBS with 100 mM glycine at room temperature. Cells were incubated with 1xPBS containing 10% goat serum, 10% donkey serum, 1% BSA for 30 min to block unspecific antibody binding sites and washed once with 1xPBS. Then primary antibody solution was added and incubated overnight at 4°C. The next day, after three 5 min washing steps with 1xPBS, cells were incubated with secondary antibody solution for 45 min at room temperature in the dark. Then cells were again washed three times with 1xPBS for 5 min. To stain nuclei, DAPI working solution was added and cells were incubated for 2-15 min. After three further washing steps with 1xPBS slides were mounted with Dako fluorescence mounting medium (Agilent) and coverslips were added. The slides were incubated at 4°C overnight to dry.

Background fluorescence was checked in samples treated with only secondary antibodies. Immunofluorescence was analysed using the fluorescence microscope BioZero BZ-8100 (Keyence).

Primary antibodies: mouse anti-cTnT: dilution 1:300 (ab10214, Abcam); rabbit anti-vimentin: 1:100 (#5741, Cell Signaling Technology) in PBS/1% goat serum/1% donkey serum/1% BSA

Secondary antibodies: donkey anti-mouse Alexa Fluor 594, 1:1000 (A21203, Invitrogen); goat anti-rabbit Oregon Green 488, 1:1000 (O-6381, Invitrogen) in PBS/1% goat serum/1% donkey serum/1% BSA

4 % paraformaldehyde: For 250 ml stock solution 10 g paraformaldehyde are dissolved in 250 ml 1xPBS and the pH is adjusted to 7.4. The solution is heated to 65°C and NaOH is added until the paraformaldehyde is completely dissolved.

Glycine solution: 100 mM in 1xPBS; pH is adjusted to 7.4

Blocking solution: 10% goat serum, 10% donkey serum, 1% BSA (Capricorn Scientific) in 1xPBS

DAPI: DAPI stock solution: 10 mg/ml in water, DAPI working solution: 1 µg/ml (dilute 1 µl DAPI stock solution in 10 ml PBS)

3.4 Patch clamp $I_{K,ACh}$

HL-1 cells were plated for 24 h on 3.5 cm Petri dishes in 2 ml of Claycomb medium plus supplements. On the day of the measurement, they were trypsinized to obtain single cells. After 1-2 h cells reattached to the plate surface but were still rounded and therefore easier to patch. Current recordings were performed in the whole-cell configuration of the patch-clamp technique using an Axopatch 200A patch-clamp amplifier (Axon Instruments). Patch pipettes were fabricated from thick wall (2 mm outside diameter) borosilicate glass capillaries (Hilgenberg) and filled with an internal solution of the following composition (in mM): 20 KCl, 110 potassium aspartate, 6 $MgCl_2$ x 6 H_2O, 5 Na_2ATP, 10 EGTA, 10 HEPES, pH was adjusted to 7.2 with KOH (and HCl); 100 µM GTP was freshly added to pipette solution. Electrical resistances of the fire polished electrodes were 3-4 MΩ when filled with internal solution. Cells were measured in a bath solution of the following composition (in mM): 136 NaCl, 5.4 KCl, 10 $CaCl_2$ x 2 H_2O, 0.8 $MgCl_2$ x 6 H_2O, 10 HEPES, 10 glucose, pH was adjusted to 7.4 with NaOH. $I_{K,ACh}$ was induced after application of the test solution (20 µM ACh) at a holding potential of -90 mV. For control measurements water was applied. Current signals were sampled at 16 to 40 kHz and low pass filtered at 5 kHz with a four-pole Bessel filter and stored for off-line analysis (ISO2, MFK). Series resistance was partially compensated (>70%). By integrating the capacitive current at the end of 10 ms long voltage step (-80 mV to -70 mV) the input capacitance of the cells was obtained. All experiments were carried out at room temperature (20-24°C).

3.5 Thallium flux assay

Principle

This assay is based on two concepts: 1) the ability of Thallium ions (Tl^+) to flow through K^+ channels (Hille, 1973; Park, 1994) and 2) the absence of Tl^+ in cardiomyocytes under physiological conditions. The principle of this assay is depicted in Figure 10. First, cells are pre-loaded with a non-fluorescent, Tl^+-specific dye. Cells are then stimulated with a solution that contains the channel activator and also Tl^+. In this setting, GIRK1/4 is activated by carbachol (CCH) binding to the muscarinic acetylcholine receptor type 2 (M2R). GIRK1/4 activation leads to an inward flux of Tl^+ following its concentration gradient. Inside the cell, Tl^+ binds to the specific dye and a fluorescence signal is generated which is proportional to channel activity.
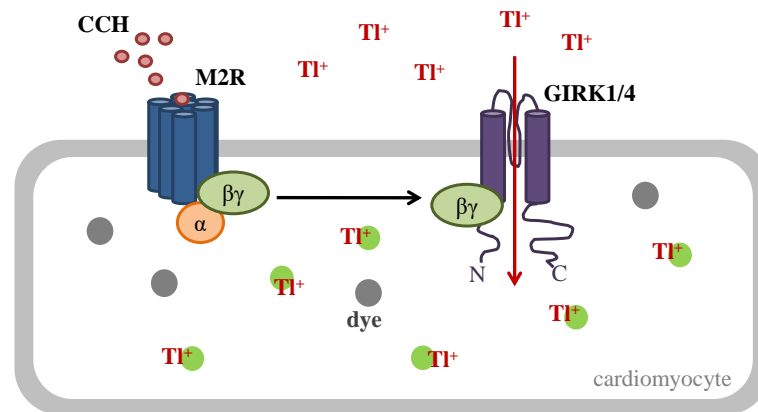
Figure 10. Principle of Tl$^+$ flux assay for GIRK1/4. HL-1 cells that express both the muscarinic acetylcholine receptor type 2 (M2R) and GIRK1/4 channel are pre-loaded with a non-fluorescent, Tl$^+$-specific dye (gray filled circles). Cells are then stimulated with a solution that contains the channel activator and also Tl$^+$. In this setting, GIRK1/4 is activated by carbachol (CCH, acetylcholine analog). Stimulation with CCH leads to activation of the M2R, dissociation of G$\beta\gamma$ from Gα and activation of GIRK1/4 by G$\beta\gamma$. GIRK1/4 activation evokes an inward flux of Tl$^+$ following its concentration gradient. Inside the cell, Tl$^+$ binds to the specific dye and a fluorescence signal is generated (green filled circles) which is proportional to channel activity.

Thallium ion concentration series and carbachol effect

Initially, HEK-293 or HL-1 cells seeded in 5 cm petri dishes were transfected with 1 µg of pCMV6-Girk1, pCMV6-Girk4, pCMV6-Chrm2 and RFP-N1 in different combinations as indicated in the results. For transfection 10 µl polyfect per 1 µg DNA were mixed in 250 µl DMEM. 24 h after transfection cells were split to a 96 well plate and kept in DMEM Ham's F12 with 10% FCS for another 48 h until the measurement. Fluxor II Green Potassium Ion Channel Assay (Invitrogen) was performed according to manufacturer's instructions using the Operetta CLS High-Content Analysis System (Perkin Elmer). Cells were measured at 37°C. Images were acquired with the following parameters: 20x objective; binning 2; FITC channel: exposure time 10 ms, power 100%, height 4.5 µm; brightfield channel: exposure time 10 ms, power 20%, height -3.5 µm; TagRFP channel: exposure time 10 ms, power 100%, height 2 µm; one field per well.

First, to obtain the optimal thallium ion (Tl$^+$) concentration, different [Tl$^+$] varying between 0 and 1 mM were applied. After obtaining the baseline fluorescence (F$_0$), a buffer containing Tl$^+$ was added and the fluorescence was measured every 100 s. All following Fluxor experiments were carried out with 1 mM Tl$^+$.

For testing the carbachol (CCH, 10 µM final concentration) effect, CCH was added simultaneously with Tl$^+$ to the cells. The time interval was 53 s for HEK-293 cells and 60 s for HL-1 cells. For calculation of the CCH effect, the fluorescence signal of control and CCH wells was paired a priori, e.g. the first well of the control group was always paired with the first well of the CCH group.

100 µM CCH were also tested, but did not result in higher Tl$^+$ flux (Fig. 26). According to Posokhova et al., 10 µM are enough to saturate the channels (Posokhova et al., 2010).

Tertiapin q

To confirm that carbachol-induced thallium ion flux was indeed carried by GIRK1/4, experiments with tertiapin q (TQ, 100 nM final concentration, Alomone Labs), an inhibitor of GIRK1/4, were performed in HL-1 cells.

Tertiapin is a 21-residue peptide isolated from honey bee venom that has been shown to specifically inhibit GIRK1/4 channels by blocking the channel pore (Kitamura et al., 2000). In this experiment the more stable tertiapin analog TQ was used. In TQ a methionine residue is replaced by glutamine thereby rendering the peptide inert to oxidation by air (Jin et al., 1999).

After obtaining the baseline fluorescence (F_0), a buffer containing Tl^+ alone (control) or additionally CCH with or without TQ was added and the fluorescence was measured every 15 s.

MiR transfection

HL-1 cells seeded on a 35 mm or 60 mm petri dishes were transiently transfected with miR-221/222 mimics for 24 h as described above. 48 h after start of transfection cells were seeded onto a 96 well plate and incubated for another 24 h in Claycomb medium with supplements. After obtaining the baseline fluorescence (F_0), a buffer containing Tl^+ alone (control) or additionally CCH was added and the fluorescence was measured every 15 s.

Data acquisition and analysis

Image acquisition and analysis was performed using Harmony 4.8 software (Perkin Elmer) with the following parameters: exposure time FITC 10 ms, RFP 20 ms, brightfield 10 ms; power FITC 100%, RFP 100%, brightfield 20%; binning 2; sampling interval depended on the number of included wells and was between 15 and 100 s for different measurements. Fluxor dye-loaded (FITC+) cells were detected using the FIND CELLS option (method C). The time course of fluorescence intensity of FITC+ cells was obtained with the TRACK OBJECTS option (standard method) (Fig. 11). To include only transfected cells in the analysis, detected FITC+ cells were additionally checked for RFP fluorescence. Correspondingly, only double positive cells (FITC+, RFP+) cells were tracked over time. In HEK-293 cells, both RFP-positive cells (see Figure) and all FITC+ cells were analyzed.
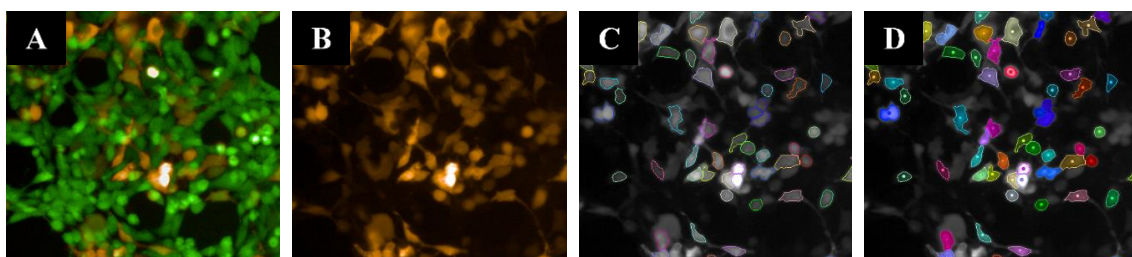
Figure 11. Exemplary and represensative images of RFP-transfected, Fluxor dye-loaded HEK-293 cells and their analysis. A Image of HEK cells with two active channels: FITC (green) indicates Fluxor dye-loaded cells and RFP (red) shows transfected cells. **B**-**D** RFP-positive cells (**B**) are subjected to further analysis: the operetta analysis software functions FIND CELLS (**C**) and TRACK CELLS (**D**) are used to distinguish single cells and track them over the time course of the experiment.

As Tl[+] flux in HL-1 cells was also measured in untransfected cells, results in all measurements were obtained from all FITC+ cells instead of FITC+/RFP+ cells only.

Fluorescence data were normalized to baseline fluorescence (F/F_0). The time course of F/F_0 was integrated to obtain the area under the curve (AUC). The CCH effect was calculated as AUC (CCH) - AUC (control) of a priori paired wells for each individual experiment.

3.6 Calcium measurements

3.6.1 Calcium imaging in HL-1 cells

Principle

Calcium homeostasis in HL-1 cells was measured by ratiometric fluorescence microscopy using fura-2 AM. Changes in intracellular (cytosolic) calcium were measured at single-cell level using the VisiChrome High Speed Polychromator System (with High Speed Random Access Monochromator; Visitron Systems) and the Observer A.1 Axio inverse fluorescence microscope (Zeiss) connected to a CoolSNAP EZ CCD camera (Visitron Systems).

Protocol transfection

HL-1 cells were plated on FCS-coated custom-made glass coverslips for 24 h in Claycomb medium with supplements. To enhance coating and adherence the glass coverslips were pre-treated with 1 M HCl. The next day, the cells transfected with miRCURY LNA miR-221/222 mimics or mimic negative control in DMEM as described above. After 24 h of transfection, cells were allowed to grow in Claycomb medium including supplements for further 24 h. After that, they were serum-starved for 24 h prior to calcium measurement.
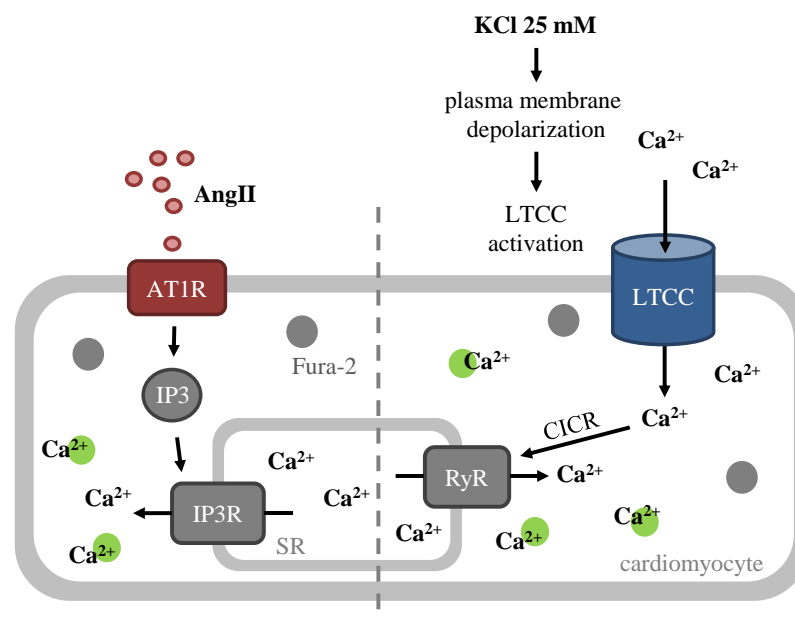
Calcium imaging

HL-1 cells were loaded with 4 µM fura-2 AM (stock solution: 1 mM in DMSO) at 37°C for 30 min. Then, cells were superfused with pre-warmed control and test solutions (temperature when reaching the cells: 37°C). Before beginning the measurement, cells were allowed to acclimatize to the superfusion with Ringer solution for 200 s. The measurement started with control Ringer solution for 200-300 s to get a stable baseline signal, followed by superfusion with 100 nM AngII for 150 s to observe a transient $[Ca^{2+}]_i$ increase. After this, control Ringer solution was applied for 150 s to wash out AngII. To depolarize the cell membrane and activate LTCCs, the next step included Ringer solution with 25 mM KCl (instead of 5 mM in control solution) for 300 s. In the last step, cells were superfused with 1 µM ionomycin which is a calcium ionophore (C. M. Liu & Hermann, 1978) and serves as a positive control to discriminate between non-responding and dead cells. Living cells that do not respond to AngII and/or KCl still react to ionomycin with an increase in cytosolic Ca^{2+} concentrations. Dead cells on the other hand no longer have an intact plasma membrane, leading to an early accumulation of calcium in the cytosol and therefore no pronounced response upon ionomycin application.

To test whether AngII and 25 mM KCl elicit the expected specific effects, inhibitors of AT1R (losartan, 10 µM) and LTCC (verapamil, 20 µM) were also applied.

Images of fura-2 fluorescence intensity at excitation wavelengths of 340 nm and 380 nm were obtained with VisiVIEW Imaging Software (Visitron Systems; exposure: 40 ms, bin: 2, sampling interval: 2 s, emission: 510 nm).

Analysis

Analysis was performed on single cell level by defining one region of interest per cell. Background fluorescence was subtracted. The reaction of a cell to a substance was defined as a response if the maximum value was higher than the mean plus three times the standard deviation of the control solution before substance application (e.g. maximum value (AngII) > mean (Ringer) + 3x standard deviation (Ringer)). First, dead cells were eliminated due to lack of response to ionomycin. Then, responding and non-responding cells were defined. Response parameters, e.g. baseline shift, peak height, AUC (AngII: 150 s, KCl: first 150 s), were only obtained from responding cells.

Figure 12. Principle of calcium imaging in HL-1 cells. Cells are pre-loaded with the Ca^{2+}-specific dye fura-2 (gray filled circles). **Left side:** angiotensin II (AngII) activates the AngII receptor type 1 (AT1R) which leads to inositol 1,4,5-trisphosphate (IP3) generation and IP3 receptor (IP3R) activation. IP3R releases calcium from the sarcoplasmic reticulum (SR). Ca^{2+} binds to fura-2 (green filled circles) and the increased cytosolic Ca^{2+} concentration leads to increased fura-2 fluorescence signal. **Right side:** External application of Ringer buffer containing 25 mM KCl leads to cell membrane depolarization and therefore to activation of the L-type Ca^{2+} channel (LTCC). Ca^{2+} enters the cells through LTCC and binds to fura-2, thus increasing the fluorescence (green filled circles). Ca^{2+} also directly activates to ryanodine receptors (RyR) on the SR membrane inducing release of Ca^{2+} from the SR (Ca^{2+}-induced Ca^{2+} release, CICR). This further increases cytosolic Ca^{2+} concentration and fura-2 fluorescence signals.
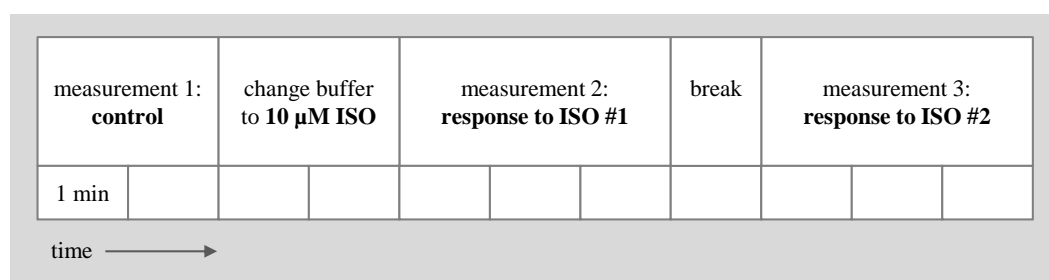
3.6.2 Calcium measurement in neoCMs

Principle

Calcium transients from spontaneous or electrically evoked activity in fura-2-loaded neoCMs were obtained with the Myocyte Calcium and Contractility System (IonOptix). This system provides a Galvanometer-driven mirror to switch between two wavelengths (340 nm, 380 nm) at a frequency of up to 250 Hz, allowing for very high sampling rates up to 250 Hz.

Calcium measurement

NeoCMs were measured after 6-9 days after isolation. NeoCM monolayers were transiently transfected with miR mimics for 24 h as described above. Then they were kept on 1% FCS for further 48 h until the measurement. Cells were loaded with 4 µM fura-2 AM (stock solution: 1 mM in DMSO) at 37°C for 30 min. After washing the cells once with medium, cells were incubated with medium for 15 min at 37°C to allow complete de-esterification of internalized fura-2. Then cells were washed in Ringer solution (pH 7.4 at room temperature) and measured or stored at room temperature until the measurement. Each sample was measured three times: after recording control signals for 2 min the buffer was changed to 10 µM isoprenaline (ISO) and response to ISO was measured after 2-5 min and 6-9 min after ISO addition (Fig. 13). If possible, spontaneous calcium transients were recorded. Otherwise, cells were paced at 1 Hz to evoke calcium transients (MyoPacer, 5-10V per pulse, pulse duration max. 4 ms). IonWizard 6.6 was used for data acquisition at sampling frequencies of 100 Hz (average 4: 4 collected data points are averaged into one raw data point) or 250 Hz (average 1).

measurement 1: **control**	change buffer to **10 µM ISO**	measurement 2: **response to ISO #1**	break	measurement 3: **response to ISO #2**
1 min				

time ⟶

Figure 13. Scheme of the timeline of calcium measurements. One small rectangle indicates an interval of 1 min. ISO: isoprenaline.

Monotonic transient analysis

Monotonic transient analysis was performed using IonWizard 6.6 (IonOptix). Prior to analysis, raw data were filtered with the lowpass Butterworth filter (cut-off frequency: 5 Hz, number of poles: 2). Transient marks were converted from event marks of the MyoPacer (transient values: offset: -0.05 s, duration: 0.9 s). T_0 is defined as the time of the event mark for paced cells. For spontaneous transients, transient marks were added manually and the time of departure was chosen as T_0. Every transient was manually checked to assure appropriate detection and recognition of peaks and fitting of transient parameter functions. An overview of the applied

transient parameters is given in Figure 14. Average calcium transients were obtained with IonWizard to visualize differential effects of ISO on miR-transfected monolayers.
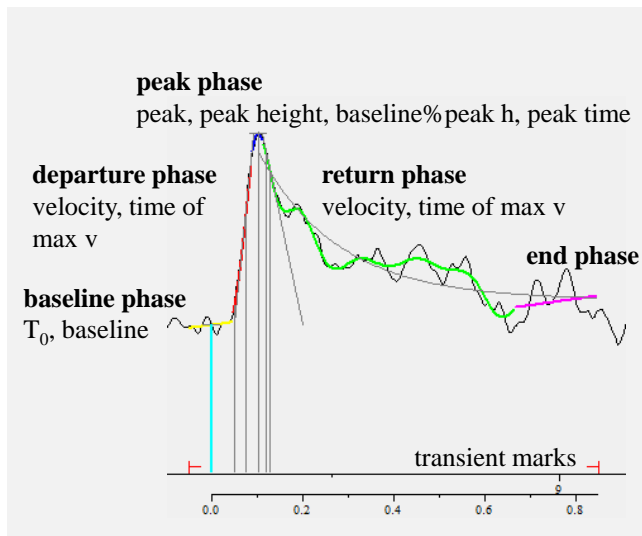
Figure 14. Scheme showing parameters of monotonic transient analysis associated with different phases of the calcium transient. Screenshot from a typical calcium transient of neoCMs, analysed with IonWizard software. Transients are divided into different phases: baseline, departure, peak, return and end phase, indicated by different colours on the transient. Corresponding parameters are written below the respective phase.

3.7 Contraction analysis in neoCMs

Contractions with verapamil

NeoCMs were isolated and cultured as described above. Spontaneous contractions of neoCM clusters were recorded at room temperature using the fluorescence microscope BioZero BZ-8100 (Keyence) (brightfield, 4x objective, 8 fps). After about 1 min the medium was changed to medium containing 10 µM verapamil. Reaction of clusters to verapamil was recorded at two successive periods of about 1 min each.

Contractions with isoprenaline

NeoCMs were isolated as described above and cells from about one heart were plated onto one 35 mm petri dish. Monolayers were transfected with mimic control or miR-222 as described above and measured after about 7-8 days in culture. Before the recording cells were washed with Ringer buffer once. Cells were then placed into a pre-heated Ibidi chamber (Ibidi heating system 1; plate temperature: 38°C, lid: 42°C) and allowed to acclimatize for 1 min. Contraction recordings were performed as listed below (10x objective, Observer A.1 Axio inverse fluorescence microscope (Zeiss) connected to a CoolSNAP EZ CCD camera (Visitron Systems); sampling rate: 10 fps; VisiView Software). All three movies from the same petri dish recorded the same section of cells. Movies (.avi) were generated without compression and with a frame rate of 10 fps.

Timeline for contraction recordings:

Acclimatization of the cells (Ringer)	1 min
Movie 1 (control)	0.5 min
Buffer change to 10 µM isoprenaline & acclimatization	2.5 min
Movie 2 (ISO 1)	0.5 min
Break	1.5 min
Movie 3 (ISO 2)	0.5 min

Analysis with Image J plugin Myocyter

Movies were analyzed using Myocyter with the following parameters: "detection": 10, "% of max recognized as beat": 20. Manual ROIs were carefully placed to analyze the same regions in all three movies from one petri dish. Number of ROIs varied between 8-37 depending on confluency and synchronicity of the monolayer and cluster size within the monolayer. The number of spontaneous contractions for each ROI within each 30 s movie was extracted using the parameter "beats counted", always excluding the first and last event.

3.8 Statistical analysis

Data are presented as mean ± standard error of mean. Student's t-test, Mann-Whitney rank sum test or Wilcoxon signed rank test were used as applicable according to pre-test data analysis by SigmaPlot 12.5. Tests were unpaired and two-tailed unless stated otherwise in the text. Grubbs tests were performed to identify outliers. A p-value <0.05 was considered statistically significant.

4. Results

4.1 Cacna1c and Girk4 are targets of miR-221/222

4.1.1 Differential interaction of miR-221/222 with ion channel 3'-UTRs

MiR-221/222 expression is increased in two mouse models with heart hypertrophy (epidermal growth factor receptor (EGFR) knockout (KO); chronic angiotensin II infusion) but without significant signs of heart failure. RNA-Seq and gene enrichment analyses identified differentially regulated ion channels associated to the t-tubule cluster in EGFR KO mice, which were also predicted targets of miR-221/222 (Binas et al., 2020). This implicates a possible role of dysregulated miR-221/222 levels in cardiac electrical remodeling.

To evaluate direct interactions of miR-221/222 with ion channel transcripts dual luciferase reporter assays were performed in HEK-293 cells. Figure 15 shows the effects of both miR-221 and -222 on ion channel 3'-UTRs. Ion channel 3'-UTRs longer than 2.5 kb were divided into two or three plasmids with overlapping fragments (Cacna1c, Cacna2d1). To estimate the maximum possible effect of the miRNAs, a positive control was added. This control is a luciferase reporter plasmid with the complementary sequence of the respective miRNA in the 3'-UTR of the firefly gene.

Interestingly, despite having exactly the same seed sequence miR-221/222 display differential targeting in transfected HEK-293 cells. Both miRNAs show different levels of luciferase repression in their respective positive controls: about 35% downregulation for miR-221 and 64% for miR-222 (Fig. 15; miR-221: 0.65 ± 0.02 vs. miR-222: 0.36 ± 0.02 relative luciferase activity). However, it seems that not only the seed sequence but also the surrounding sequences determine the miR effect on luciferase activity. In contrast to the results mentioned above (Fig. 15), the miR effect is decreased when miR-221 was combined with pMiR-222 and miR-222 with pMiR-221. Here, miR-222 only led to an 18% and miR-221 to a 12% reduction in luciferase activity (Fig. 16).

MiR-221/222 also seem to regulate the tested ion channel 3'-UTRs differently. While miR-221 represses luciferase expression of the 3'-UTRs of Cacna1c_b, Cacna1c_c and Girk4, miR-222 additionally regulates Cacnb2, Cacna1c_a, Cacna2d1_b and Kcnd2 3'-UTRs. Apart from the difference in regulated targets, the level of repression also varies. For instance, miR-221 has a higher inhibitory effect on Canca1c_b than miR-222 (miR-221: 0.47 ± 0.07 vs. miR-222: 0.62 ± 0.08 relative luciferase activity), whereas its effect on Girk4 is much smaller compared to miR-222 (miR-221: 0.81 ± 0.02 vs. miR-222: 0.28 ± 0.03 relative luciferase activity). Overall, the most prominently regulated targets of both miRNAs seem to be Cacna1c and Girk4.
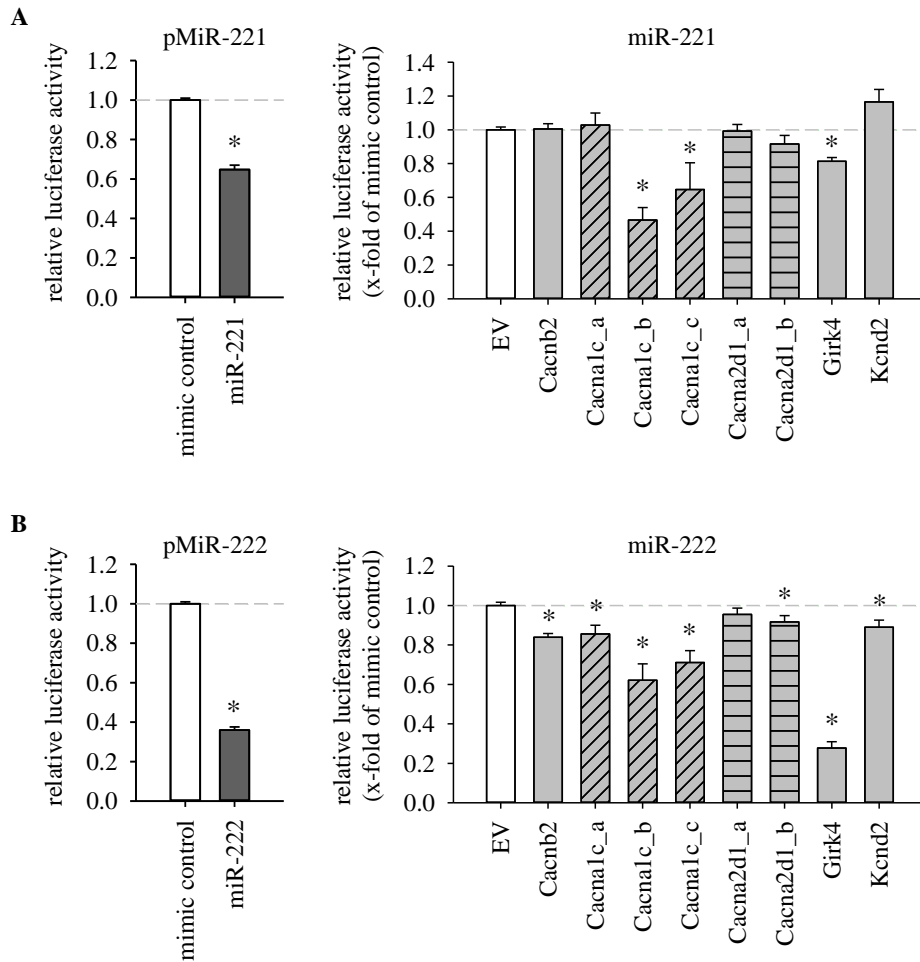
Figure 15. Dual luciferase reporter assays show differential regulation of ion channel 3'-UTRs for miR-221 (A) and miR-222 (B). The left side shows the effect of miR-221 or miR-222 mimics on the respective positive control plasmid (pMiR-221 or pMiR-222). On the right side their effect on ion channel 3'-UTRs is depicted. 3'-UTRs longer than 2.5 kb were divided into two or three plasmids with overlapping fragments. For ion channel 3'-UTRs the miR-effect is normalized to the respective mimic control and then normalized to the corresponding empty vector control (EV). Data are shown as mean ± sem; * indicates p < 0.05. MiR-221: N=4-5, n=12-15; miR-222: N=3-5, n=9-15.
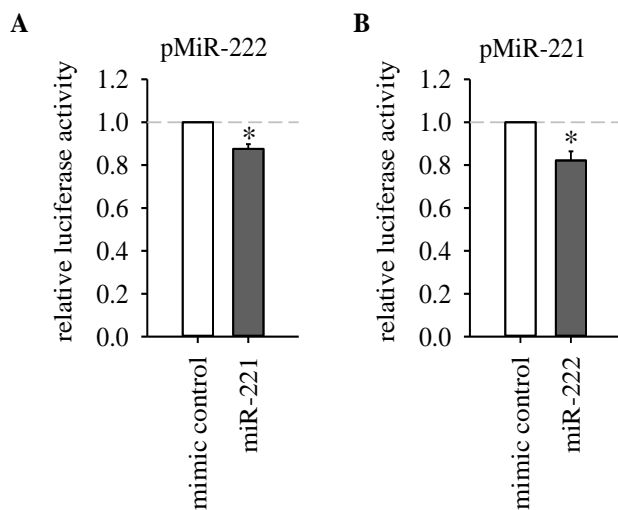
Figure 16. Not only the seed sequence but also the surrounding sequences determine the miR effect on luciferase activity. HEK-293 cells were transfected with either pMiR-221 or pMiR-222 plus the non-corresponding miR. Data are displayed as mean ± sem, * indicates p < 0.05 respective to mimic control, N=2-3, n=6-8.

4.1.2 Mutation of predicted miR-221/222 binding sites

To further verify the miRNA targets from the previous dual luciferase experiments, putative miR binding sites were mutated in the dual luciferase reporter plasmids. The two most prominent targets were chosen for further investigation: Cacna1c and Girk4. Regarding Cacna1c 3'-UTR, there was a predicted miR-221/222 binding site in Cacna1c_b only. Therefore, from the three Cacna1c plasmids only Cacna1c_b was chosen for mutation. The mutations in both plasmids reduce the effect of miR-221 on relative luciferase activity compared to wild type controls (Fig. 17 A; Cacna1c_b WT vs. M: 0.66 ± 0.02 vs. 0.85 ± 0.02; Girk4 WT vs M: 0.85 ± 0.02 vs. 1.05 ± 0.04). However, mutated Cacna1c_b still shows some downregulation of firefly activity due to miR-221 (Girk4 M: 1.05 ± 0.04 vs. Cacna1c_b M: 0.85 ± 0.02). Thus, in this Cacna1c 3'-UTR fragment there seems to be at least one more binding site for miR-221. Regarding Girk4, the analysed binding site seems to be the only relevant binding site for miR-221, as the miR effect is completely abolished in the mutated form. In contrast to miR-221, miR-222 shows less downregulation of Cacna1c_b WT in this experiment compared to the previous data and there is no significant difference between WT and M (Fig. 17 B). Furthermore, the effect on Girk4 is completely gone, even in the wild type form.
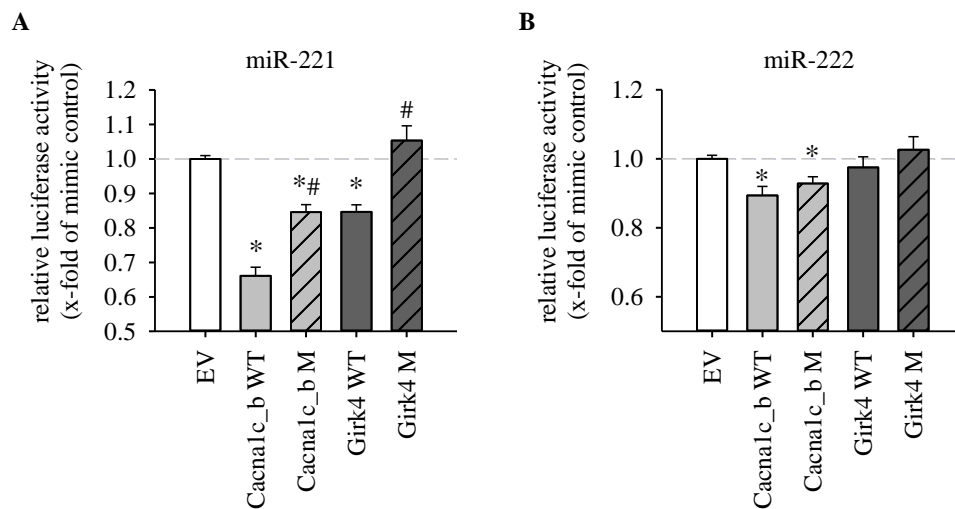

Figure 17. Mutagenesis of putative miR binding sites in Cacna1c_b and Girk4 3'-UTR leads to reduction or loss of the miR effect in HEK-293 cells transfected either with miR-221 (A) or miR-222 (B). The miR effect is normalized to the respective mimic control and then normalized to empty vector control. Abbreviations: EV: empty vector control, WT: wild type miR binding site; M: mutated miR binding site. Data are shown as mean ± sem; symbols indicate significant difference to EV (*) or corresponding WT (#); N=7-8, n=21-24.

4.1.3 Control experiments for dual luciferase assays

Using this artificial system of dual luciferase assays there are several aspects to consider. For example, the miR-to-plasmid ratio should be appropriate to get conclusive results. Furthermore, there is the possibility of endogenous miR expression interfering with the effects of miR transfection. These questions were addressed in the following control experiments.

Figure 18 shows that the maximal miR effect with the pMiR positive control is a reduction of luciferase activity of about 40% (miR-221) or 60% (miR-222). Even with only 1 ng pMiR, there is no stronger effect on luciferase activity, probably because the signal to noise ratio is too low. Overall, miR-222 seems to be more effective than miR-221 at 30 nM.
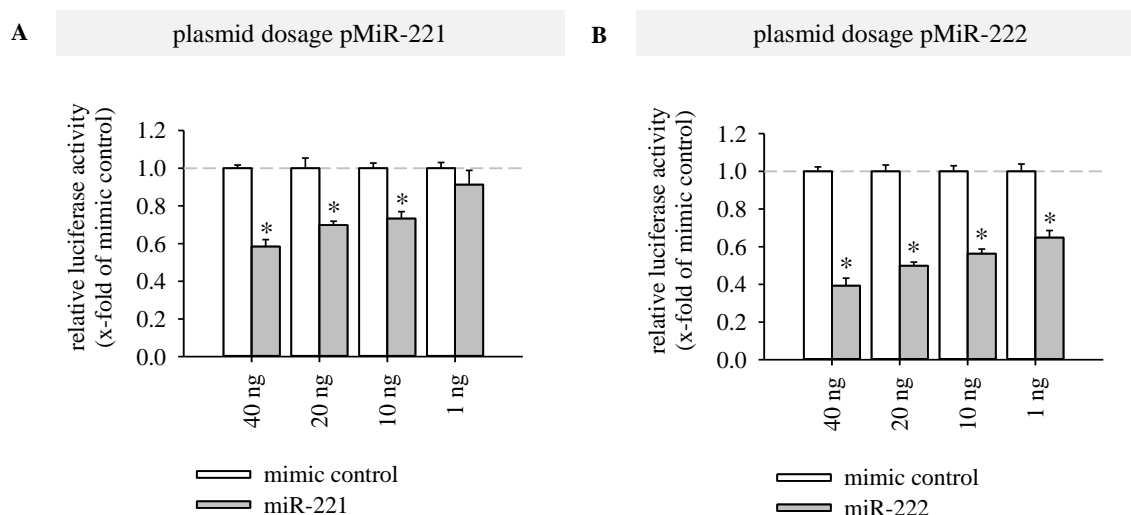
Figure 18. Extent of luciferase activity reduction depends on plasmid concentration. HEK-293 cells were transfected with differing amounts of pMiR and same amounts of corresponding miR mimics (30 nM). All cells were also transfected with 10 ng of renilla luciferase reporter vector (pGL4.74-hRLuc). **A** Effect of pMiR-221 dosage on miR-221 effect. **B** Effect of pMiR-222 dosage on miR-222 effect. Firefly luciferase activity is normalized to renilla luciferase activity. Data are displayed as mean ± sem. Paired t test, * indicates $p < 0.05$ respective to mimic control, N=1, n=3.

Plasmid dosage was also analysed for the 3'-UTR reporter construct pEZX. Figure 19 clearly shows that the maximum miR effect on Girk4 3'-UTR expression can be reached at 10 ng plasmid amount. Furthermore, the fact that a higher amount of Girk4 plasmids (40 ng) does not enhance the luciferase signal accordingly indicates that the transfected miRs are still in excess inside the cell compared to plasmid amount.

In conclusion, the dosage of miRs and plasmids used in the experiments shown above was appropriate for pMiR controls as well as for pEZX vectors.

plasmid dosage Girk4
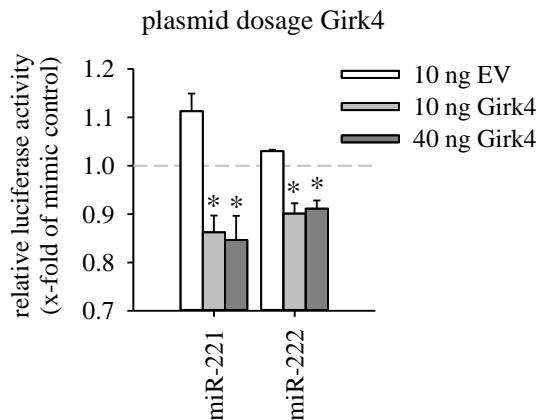
Figure 19. Increasing the plasmid concentration does not change the effect of miR-221/222 on Girk4 3'-UTR reporter vector. HEK-293 cells were transfected with either 10 ng or 40 ng pEZX-Girk4 or EV plus miR-221/222 mimics. Data are not normalized to EV, only to the corresponding mimic control. Data are displayed as mean ± sem, * indicates $p < 0.05$ respective to mimic control, N=3, n=9.

Regarding the question of interference by endogenous miRs, inhibitors for miR-221/222 were used in the next experiment. Since HEK-293 cells express miR-221/222 endogenously (Cheng et al., 2013), we would expect to see a difference between inhibitor control (where miRs may bind to the 3'-UTR and therefore reduce luciferase activity) and inhibitor (where miRs are prevented from binding the 3'-UTR). However, there is no significant difference between both groups (Fig. 20). Additionally, enhancing the plasmid/miR ratio does not lead to a significantly altered effect. These data imply that the observed miR effect in the dual luciferase experiments is not significantly diluted by endogenous miR-221/222 and that externally applied miR-221/222 are still in excess.

inhibition of endogenous miRs
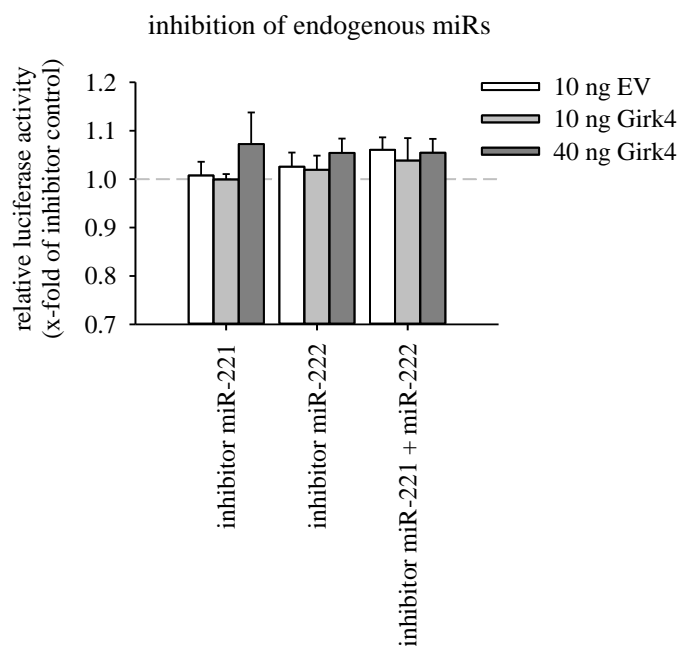
Figure 20. Inhibition of endogenous miR-221/222 does not alter luciferase activity. HEK-293 cells were transfected with either 10 ng or 40 ng pEZX-Girk4 or EV plus miR-221/222 inhibitors or inhibitor controls (30 nM each, except for combination: 15 nM each). Data are not normalized to EV, only to the corresponding inhibitor control. Data are displayed as mean ± sem, * indicates $p < 0.05$ respective to mimic control, N=3, n=9.

4.1.4 Combinatorial effect of miR-221 and miR-222

As both miR-221 and miR-222 are processed from the same transcript (pri-miR), an interesting question is whether there is any combinatorial effect of those miRNAs. This was tested in dual luciferase reporter assays in HEK-293 cells. The combination of miR-221 and miR-222 at 30 nM each does not amplify the effect of both miRNAs alone (Fig. 21; relative luciferase activity for miR combination: 0.49 ± 0.01 vs. miR-221: 0.50 ± 0.05 and miR-222: 0.81 ± 0.03). Moreover, the effect of miR combination is not even additive, as it is in the same range as the effect of miR-221 alone. Regarding miR-221, enhancing the dose to 60 nM does not strengthen the downregulation of luciferase activity (relative luciferase activity: 0.48 ± 0.03). Thus, the maximum effect is already reached at 30 nM. The different expression levels of miR-221 to miR-222 observed in cardiomyocytes (Binas et al., 2020) were not applied in this experiment. In cardiomyocytes, miR-221 seems to be higher expressed than miR-222. In this context, it seems possible that a very high concentration of miR-222 (60 nM) could even have an inhibitory effect on target binding.
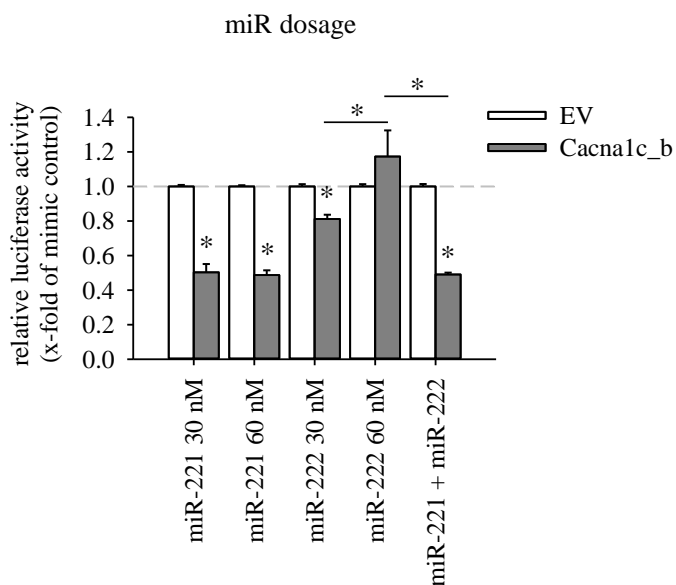
Figure 21. Combination of miR-221 and miR-222 does not lead to a synergistic effect on 3'-UTR regulation. Data are displayed as mean $\pm$ sem, * indicates $p < 0.05$ respective to mimic control, N=2, n=6.

Since separate transfection of miR-221 and miR-222 revealed differential targeting of ion channel 3'-UTRs and combination of miR-221 and -222 had no additional effect on Cacna1c_b, the following experiments were also performed with separate miR transfection to further elucidate possible differences between both miRs.

4.2 GIRK1/4 expression and function are reduced by miR-221/222

It was previously shown that while miR-221/222 are upregulated in the hearts of EGFR KO mice, Girk4 mRNA is downregulated (Binas et al., 2020). Girk4 mRNA was confirmed as a target of miR-221/222 in dual luciferase reporter assays and mutation of predicted miR binding sites added evidence for a direct interaction at least for miR-221. However, whether this interaction may also lead to altered GIRK1/4 protein expression or function of the channel remained unclear. To answer this question, western blot and thallium ion flux measurements were performed.

4.2.1 MiR-221 leads to reduced GIRK4 protein expression

The influence of miR-221/222 on GIRK1/4 protein expression was analysed in the cardiomyocyte cell line HL-1. HL-1 cells are derived from mouse atria and show some characteristics of atrial cardiomyocytes like ion channel expression and spontaneous beating (Claycomb et al., 1998). Transfection of HL-1 cells with miR-221 leads to significantly reduced protein expression of GIRK4, but not GIRK1 (Fig. 22; 0.64 ± 0.02 vs. 0.92 ± 0.09).
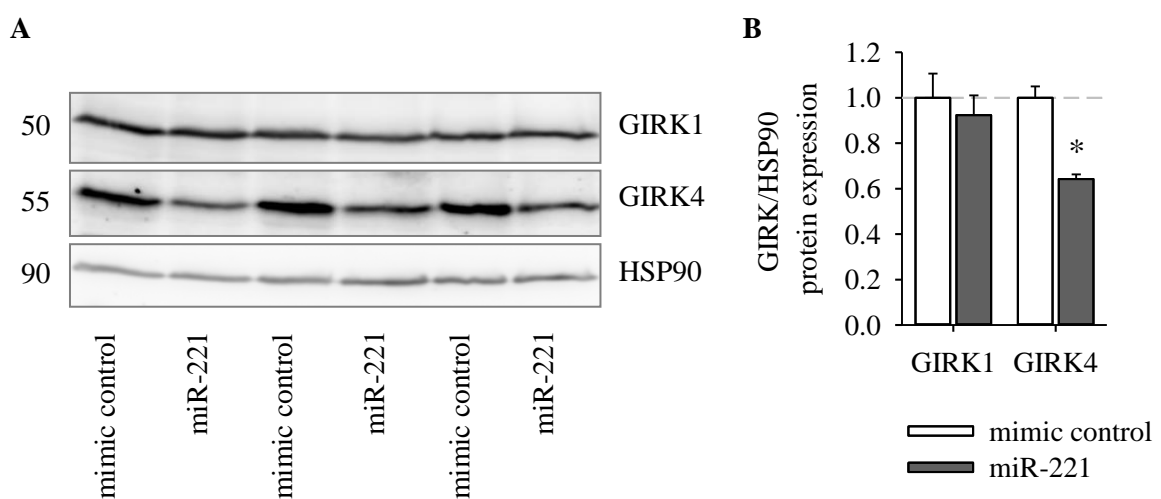
Figure 22. MiR-221 leads to reduced protein expression of GIRK4 but not GIRK1 in HL-1 cells. A Western blot image of 3 different passages of HL-1 cells. The respective size of the proteins is given in kDa on the left side of the images. **B** GIRK protein expression was normalized to HSP90 expression. Data are shown as mean $\pm$ sem, * indicates $p < 0.05$, n=3.

4.2.2 Thallium ion flux through GIRK1/4 is reduced by miR-221/222

GIRK1/4 is a G-protein-activated ion channel that can be activated by stimulation of the muscarinic acetylcholine receptor type 2 (M2R) (Dascal & Kahanovitch, 2015). For this purpose, acetylcholine or its stable analog carbachol can be used.

After confirming the direct interaction of miR-221/222 with Girk4 mRNA, which leads to reduced GIRK4 protein expression, the next step was to analyze whether there is also a functional impact

of aberrant miR expression. The classical way to investigate ion channel function is patch clamp analysis. Unfortunately, $I_{K,ACh}$ could be detected only in about 10% of HL-1 cells in patch clamp measurements (observation; see Fig. 23 for representative current tracings). Thus, another option to analyze GIRK1/4 channel function was exploited, a Thallium ion (Tl^+) flux assay originally developed by Weaver et al. (Weaver et al., 2004). To test and optimize this assay, HEK-293 cells were used initially. As HEK-293 cells are not expected to express GIRK1/4 or M2R, all necessary components of this system were transiently transfected into the cells, in accordance with previous studies (Nobles et al., 2010).
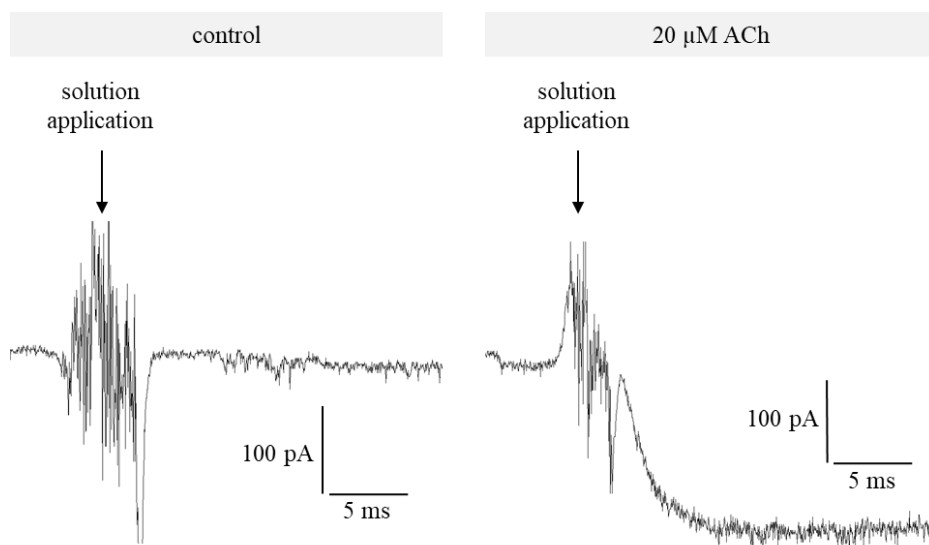
Figure 23. Acetylcholine (ACh) elicits an inward current in HL-1 cells. $I_{K,ACh}$ was induced after application of the test solution (20 µM ACh) at a holding potential of -90 mV. For control measurements water was applied. Representative current tracings show artefacts from adding control or test solution and the ACh-mediated inward current ($I_{K,ACh}$).

4.2.3 Fluxor signal intensity depends on [Tl^+] and GIRK1/4 expression in HEK cells

To determine the optimal Tl^+ concentration, a concentration series was performed. As expected, a higher Tl^+ concentration leads to a higher fluorescence signal (Fig. 24 A). As Tl^+ flows through potassium channels in general, the fluorescence signal is not GIRK1/4-specific. Because of this, cells that are transfected with only the transfection control RFP also show a concentration-dependent increase in fluorescence signal intensity, although this effect is smaller compared to GIRK1/4-transfected cells. This background fluorescence in HEK-293 cells is mediated by endogenous K^+ channels (Raphemot et al., 2013).

Interestingly, even in the unstimulated state (i.e. without carbachol) GIRK1/4-M2R-transfected cells show higher signal intensities compared to cells transfected only with RFP with 1 mM Tl^+ (Fig. 24 B-C #). This can be explained by a higher flux density due to overexpression of GIRK1/4 which is associated with a higher probability of channels in the open state.

From the concentrations tested, only 1 mM Tl^+ leads to a significant difference between cells transfected with GIRK1/4 and RFP (area under the curve: GIRK1/4: 2948.4 ± 242.9 vs. RFP: 2158.9 ± 161.6 (F/F$_0$ x s)). Therefore, to improve the signal-to-noise ratio, all following experiments were performed with 1 mM Tl^+.
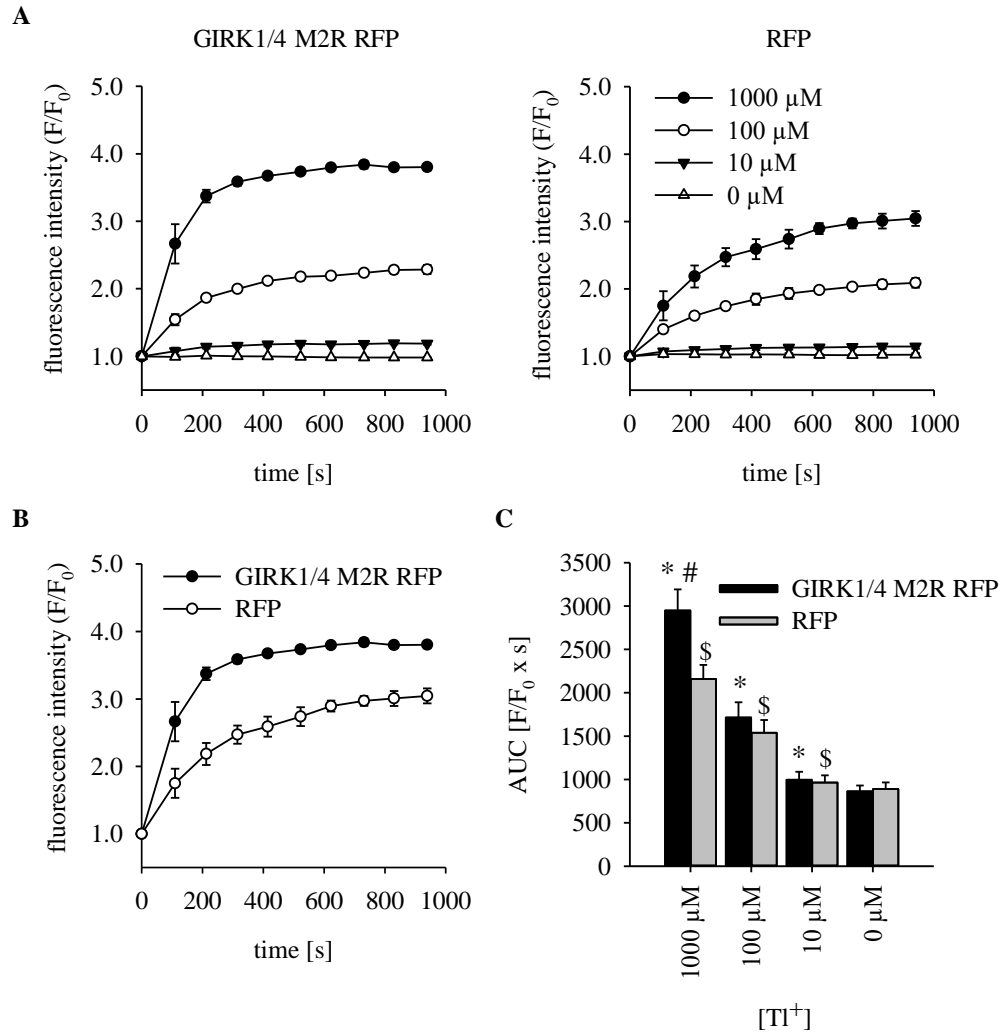

Figure 24. Fluxor fluorescence signal intensity depends on Thallium ion concentration and GIRK1/4 expression in HEK-293 cells. A A Thallium ion concentration series in cells transfected with GIRK1/4, M2R, RFP (left side) and only with RFP (right side) shows a dose-dependent effect of $[Tl^+]$ on fluorescence intensity in the unstimulated state. **B** Direct comparison of fluorescence intensity in both groups at 1000 µM Tl^+ reveals a higher fluorescence level in GIRK1/4-transfected cells even without stimulation of GIRK1/4. **C** Statistical analysis of the area under the whole curves (AUC). Symbols indicate $p < 0.05$ using paired t test: # GIRK1/4 M2R RFP vs. RFP at same $[Tl^+]$, * and $ correspond to respective control of 0 µM Tl^+ in each transfection group. N=3, n=9 (mean of RFP+ cells from each well).

48

4.2.4 Tl$^+$ flux in GIRK1/4/M2R-transfected HEK cells is stimulated by carbachol

To determine GIRK1/4 function, the channel was indirectly stimulated by carbachol-mediated activation of M2R. Incubation with 10 µM carbachol leads to a significantly higher Tl$^+$ influx compared to background activity (Fig. 25), but only in GIRK1/4-M2R-transfected cells (Fig. 25 A, E; area under the curve: CCH: 3123.6 ± 36.6 vs. control: 2915.1 ± 50.3 (F/F$_0$ x s)). As there is no significant carbachol effect in only M2R-transfected cells, it can be concluded that HEK-293 cells do not express GIRK1/4 channels, at least not in the sufficient amount.

Statistical analysis of the areas under the whole curves (AUC) revealed another significant difference in RFP-transfected cells (Fig. 25 E). However, looking at the initial course of the curves (Fig. 25 C), there is no difference between control and carbachol-treated cells in contrast to the curves of GIRK1/4-transfected cells (Fig. 25 A).
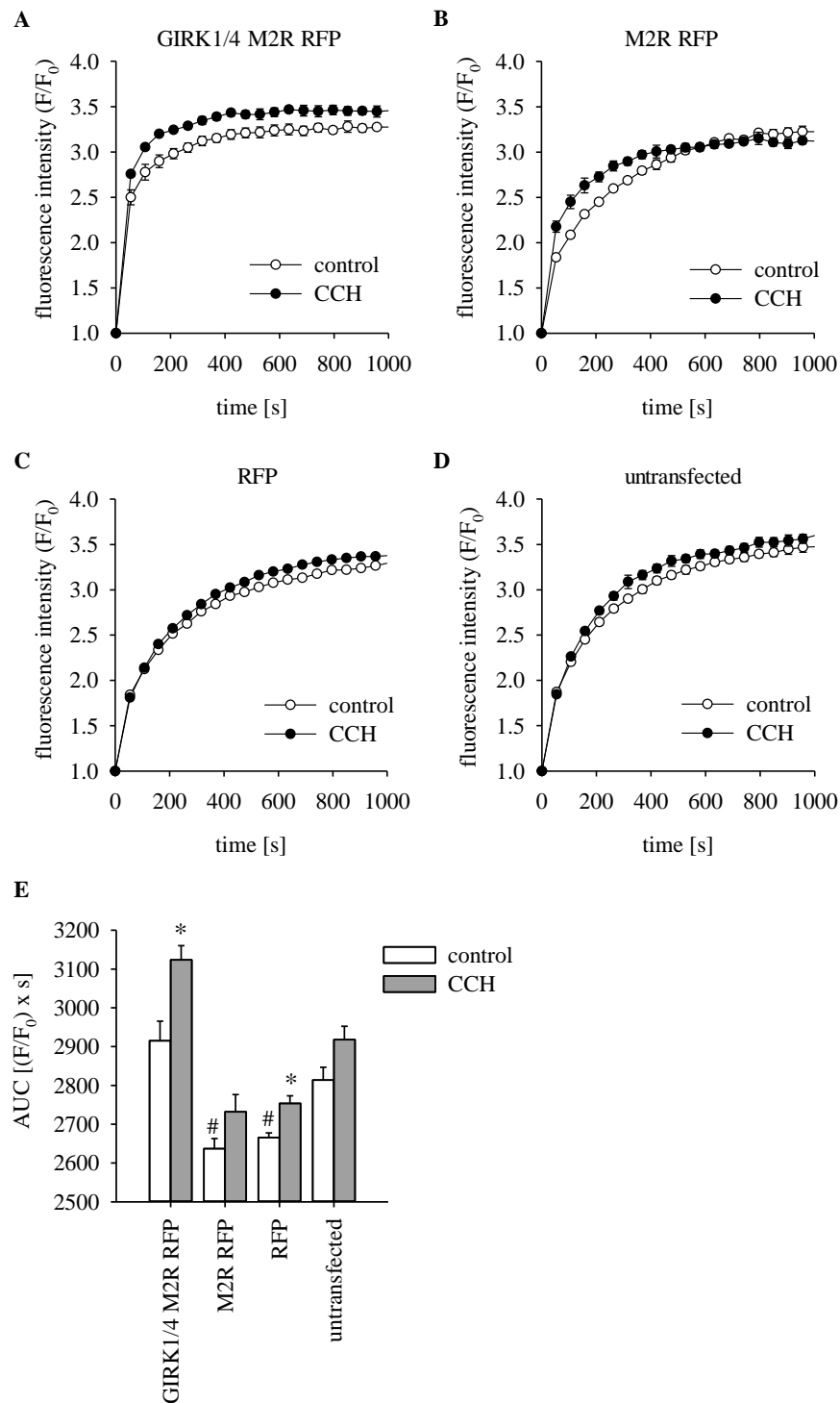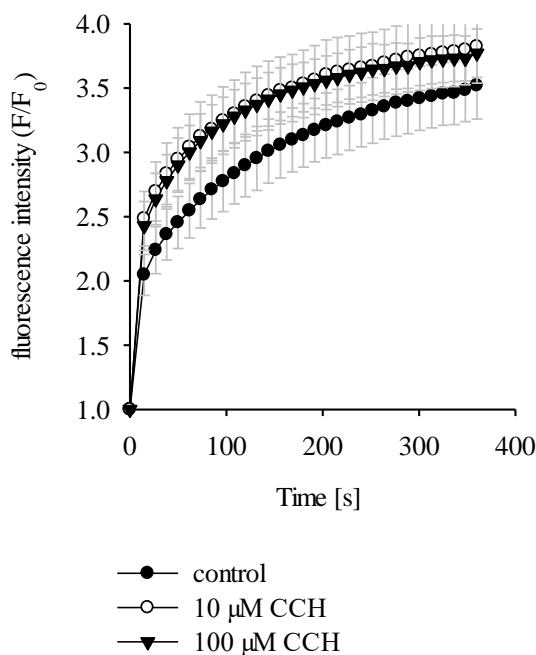
Figure 25. CCH elicits an increase in Tl$^+$ flux in HEK-293 cells only when they are transfected with GIRK1/4. A-D Time course of fluorescence intensity after initial basal measurement (t=0 s) and subsequent addition of CCH or control in different transfection groups. To compare transfected an untransfected cells, all cells were analysed, not only RFP-positive cells, as untransfected cells did not contain RFP. **E** Statistical analysis of the area under the whole curves (AUC). Symbols indicate $p < 0.05$ using unpaired t tests: * CCH vs. control in each transfection group, # vs. untransfected cells of the same treatment (control or CCH). N = 3 with each about 500-600 single cells. CCH: carbachol.

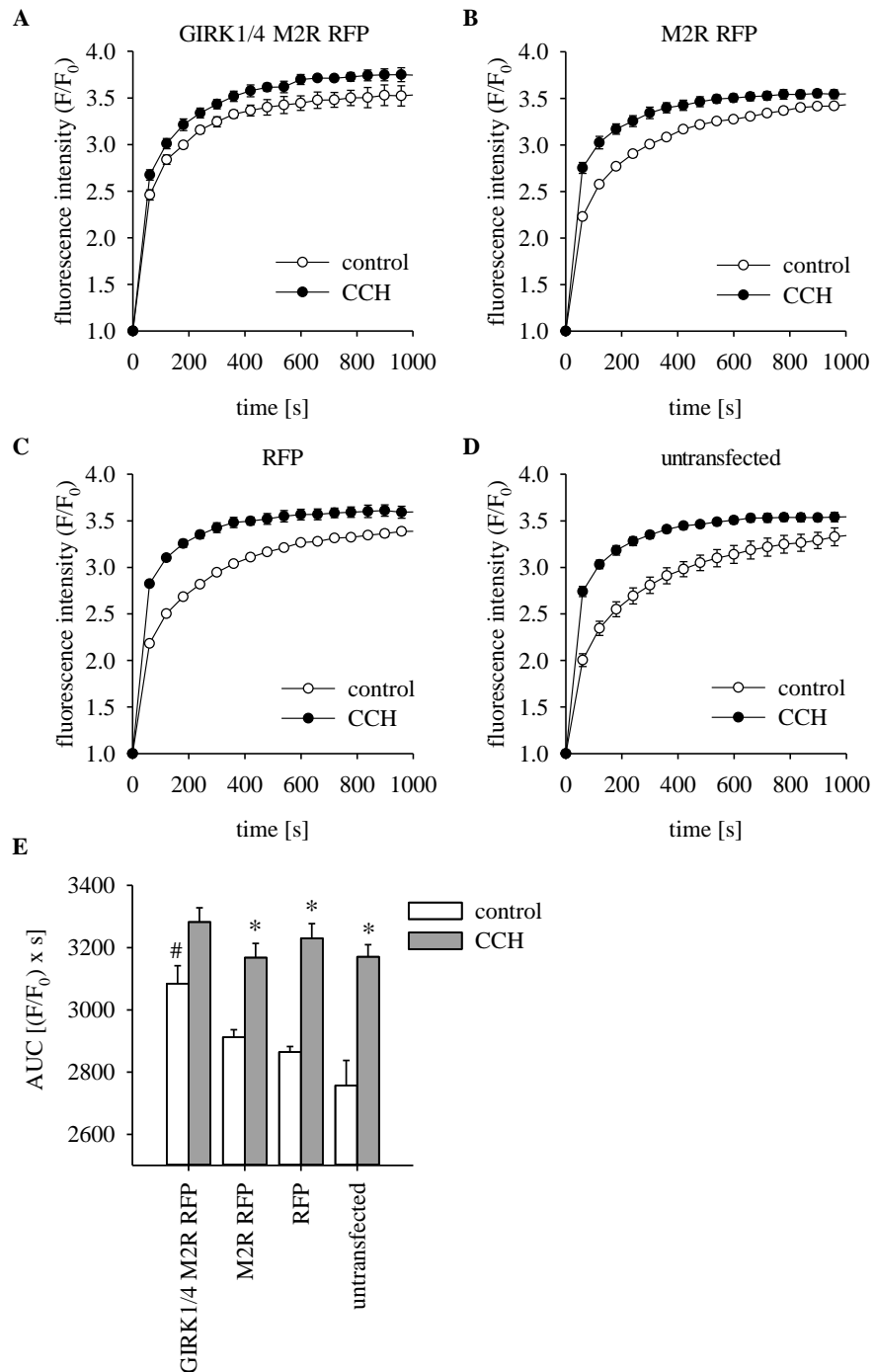**4.2.5 Tl⁺ flux in untransfected HL-1 cells is increased by carbachol**

The assay was then repeated in the cardiomyocyte cell line HL-1. At first, HL-1 cells were also transiently transfected to express RFP, M2R, GIRK1 and GIRK4.

A higher concentration of CCH (100 µM) was also tested but did not increase the carbachol effect further in HL-1 cells (Fig. 26). Further experiments were performed in untransfected HL-1 cells with 10 µM carbachol.

In contrast to HEK-293 cells, GIRK1/4-transfected HL-1 cells do not show a clear carbachol effect (Fig. 27 A, E; AUC: control 3084.5 ± 57.6 vs. CCH 3282.4 ± 45.4 (F/F_0 x s)). Interestingly, stimulation of untransfected HL-1 cells with carbachol leads to significantly increased fluorescence signals (Fig. 27 D; AUC: control 2757.3 ± 80.4 vs. CCH 3170.7 ± 39.1 (F/F_0 x s)), implying that HL-1 cells may express GIRK1/4 and M2R endogenously. This carbachol effect is also observed in M2R-RFP- and RFP-transfected cells (Fig. 27 B, C). The reason of the discrepancy between the group of GIRK1/4-transfected cells and the remaining three groups probably lies in the GIRK1/4 activity under control conditions: GIRK1/4-transfected cells show a significantly higher baseline fluorescence in the control group compared to untransfected control cells (Fig. 27 A, E; AUC control GIRK1/4 3084.5 ± 57.6 vs. untransfected control 2757 ± 80.4 (F/F_0 x s)). The overexpression of GIRK1/4 in these cells seems to enhance the overall open probability of GIRK1/4 channels leading to increased fluorescence even in the absence of carbachol. Additionally, overexpression of M2R might also contribute to activation of GIRK1/4, even in the absence of ligands (Posokhova et al., 2013).

Figure 26. There is no difference between 10 µM CCH and 100 µM CCH in untransfected HL-1 cells. Sampling interval circa 12 s. Data are presented as mean ± sem, N=3, n=12 wells per treatment group. CCH: carbachol.

Figure 27. While CCH elicits an increase in Tl$^+$ flux in untransfected HL-1 cells, this effect is lost in GIRK1/4-transfected cells. A-D Time course of fluorescence intensity after initial basal measurement (t=0s) and subsequent addition of CCH or control in different transfection groups. To compare transfected an untransfected cells, all cells were analysed, not only RFP-positive cells, as untransfected cells did not contain RFP. **E** Statistical analysis of the area under the whole curves (AUC). Symbols indicate $p < 0.05$ using unpaired t tests: * CCH vs. control in each transfection group, # vs. untransfected cells of the same treatment (control). N = 3 with each about 400-600 single cells. CCH: carbachol.
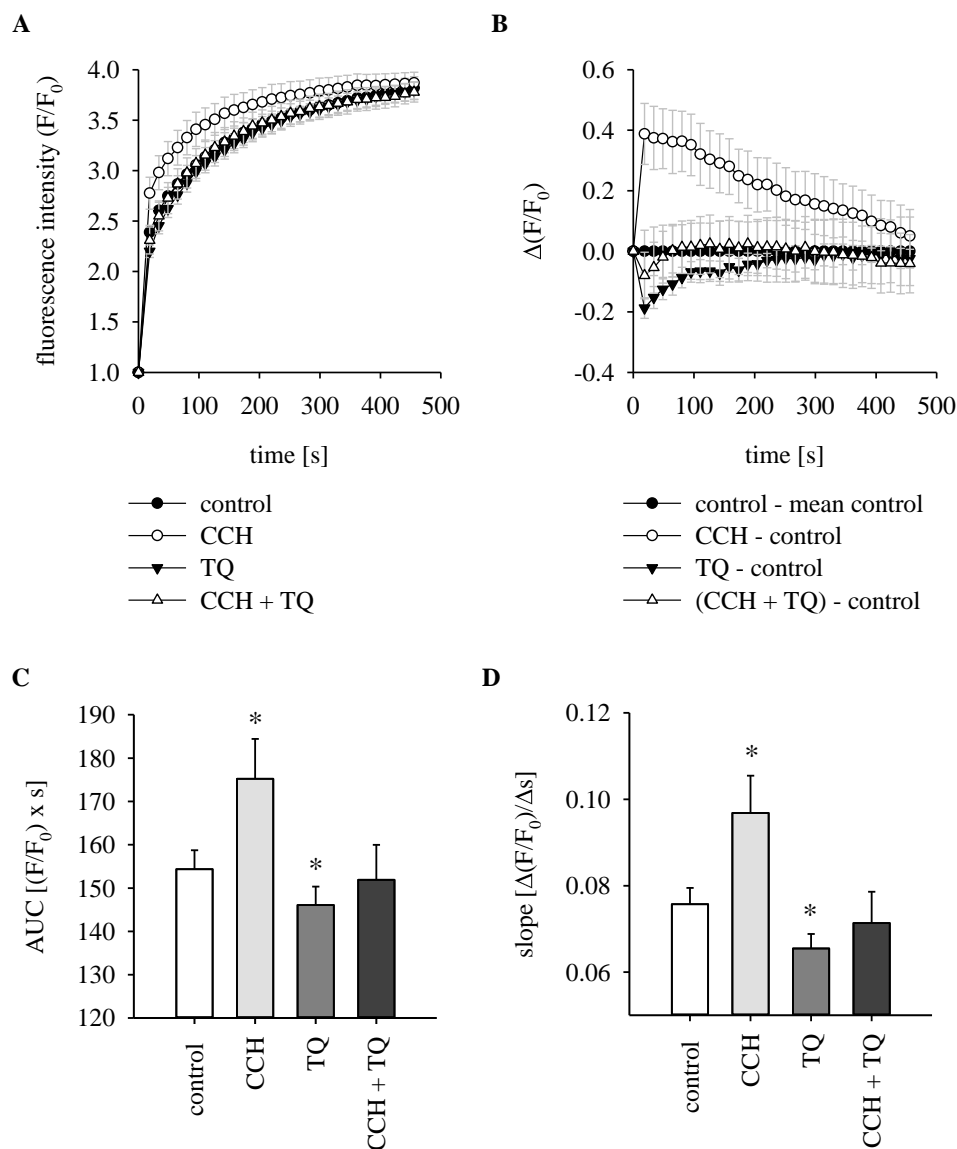
4.2.6 GIRK1/4 inhibitor tertiapin q completely abolishes the CCH effect

To evaluate whether the CCH-induced flux is indeed GIRK1/4-dependent, experiments with tertiapin q (TQ), an inhibitor of GIRK1/4, were performed in HL-1 cells.

While CCH elicits an increase in Tl^+ flux measured by elevated fluorescence intensities (Fig. 28 A, B; CCH: 2.65 ± 0.13 vs. control: 2.34 ± 0.07 at timepoint 2), double incubation of the cells with CCH and TQ prevented the CCH effect completely (CCH+TQ: 2.21 ± 0.12 vs. control: 2.34 ± 0.07 at timepoint 2). Furthermore, application of TQ alone initially leads to fluorescence intensities even lower than control levels (TQ: 2.16 ± 0.06 vs. control: 2.34 ± 0.07 at timepoint 2). This could mean that some GIRK1/4 channels are open even under unstimulated conditions (control) which can be inhibited by TQ and therefore lead to fluorescence intensities below control levels.

To statistically evaluate the effect of CCH and TQ on the time course of Tl^+ flux, the area under the curve (AUC) as well as the slope of the initial increase in fluorescence were calculated. The AUC of the first five time points (65 s) clearly shows that CCH alone evokes a statistically significant increase in Tl^+ flux (Fig. 28 D; CCH: 175.23 ± 9.21 vs. control: 154.37 ± 4.38 ((F/F_0) x s)), while co-incubation with TQ abolishes the CCH-induced increase in Tl^+ flux (CCH+TQ: 151.91 ± 8.08 vs. control: 154.37 ± 4.38 ((F/F_0) x s)). Considering the slope of the first 18 s, i.e. between baseline fluorescence and the first time point after substance and Tl^+ application, confirms these observations: the increase in fluorescence is steeper with CCH and flattened with TQ compared to control (Fig. 28 D; CCH: 0.10 ± 0.009 and TQ: 0.07 ± 0.003 vs. control: 0.08 ± 0.004 ((F/F_0)/s)).

All in all, application of GIRK1/4 inhibitor TQ could abolish the CCH effect completely, meaning that the CCH-induced flux is mediated by GIRK1/4 alone and not by other channels.

A

B

C

D

Figure 28. GIRK1/4 inhibitor TQ completely abolishes the CCH effect in HL-1 cells. A Time course of fluorescence intensity after application of either CCH or TQ or the combination of both. **B** Corresponding calculated CCH effect over time. **C** Area under the curve (AUC) of the first 65 s after substance application. **D** Slope of the initial increase in fluorescence signal after substance application (18 s). Data are displayed as mean ± sem, * indicates $p < 0.05$ (paired t test), N=4, n=12 (wells). CCH: carbachol, TQ: tertiapin q.

4.2.7 Tl$^+$ flux through GIRK1/4 is reduced by miR-221/222

After it was established that the CCH-induced flux is mediated by GIRK1/4 alone, the influence of miR-221/222 on flux through this channel was investigated. HL-1 cells transfected with either miR-221 or -222 show significantly reduced CCH-activated Tl$^+$ flux through GIRK1/4 (Fig. 29; CCH effect on AUC [(F/F$_0$) x s]: control: 145.36 ± 26.11; miR-221: 59.61 ± 12.75; miR-222: 82.13 ± 25.55). Thus, miR-221/222 have a direct impact on GIRK1/4 channel expression and thereby influence the function of this channel in cardiomyocytes.
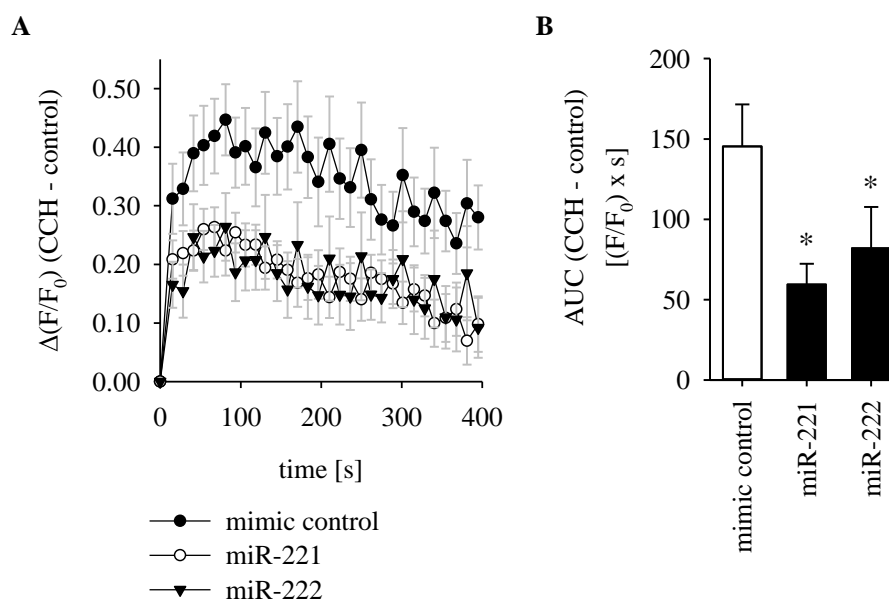
Figure 29. Tl$^+$ flux through GIRK1/4 is reduced by miR-221/222. A CCH effect. **B** Area under the whole curve of the CCH effect. Data are displayed as mean ± sem, * indicates p < 0.05 (paired t test), N=5, n=14. CCH: carbachol.

4.3 L-type Ca^{2+} channel function is impaired by miR-221/222

Previously our group could show that Cacna1c, Cacnb2 and Cacna2d1 mRNA expression was decreased in mouse models with increased miR-221/222 levels (EGFR KO, AngII) (Binas et al., 2020). Additionally, in order to determine a possible impact of miR-221/222-dependent regulation on ion channel function, LTCC current density was analysed by whole cell patch clamp recording. HL-1 cells transfected with miR-221 or -222 mimics showed a reduction in LTCC current density while the voltage-dependence of activation was not altered (Binas et al., 2020).

4.3.1 LTCC-mediated Ca^{2+} influx is slower in miR-transfected HL-1 cells

Dual luciferase assays confirmed LTCC subunit Cacna1c as a target of miR-221/222. To investigate if this regulation has an impact on Ca^{2+} homeostasis, ratiometric fluorescence microscopy was performed using HL-1 cells. Two different mechanisms to increase cytosolic Ca^{2+} concentrations were tested: 1) a depolarization-independent increase mediated by AngII and 2) a depolarization-dependent increase due to elevated extracellular K$^+$ concentration (Fig. 30 A). To discriminate between dead cells and cells not responding to the respective stimuli, ionomycin was added to the superfusion at the end of each experiment. AngII was used to investigate depolarization-independent effects of miR-221/222 on intracellular calcium release. Application of AngII evokes a transient increase in intracellular calcium concentration via an IP3/SR-dependent mechanism (Egger & Domenighetti, 2010) and should therefore lead to a primarily LTCC-independent rise in intracellular calcium. Application of 25 mM KCl leads to cell membrane depolarization and subsequent LTCC activation causing a constantly increasing intracellular Ca^{2+} concentration up to a plateau level (baseline shift).

Transfection of HL-1 cells with miR-221 or -222 has no impact on the AngII-induced calcium transient (Fig. 30 B, C): Neither on peak height (mimic control (mc): 0.20 ± 0.03; miR-221: 0.16 ± 0.01; miR-222: 0.16 ± 0.01 $\Delta(F_{340}/F_{380})$), nor on the area under the curve (mc: 144.86 ± 1.47; miR-221: 142.88 ± 0.46; miR-222: 143.68 ± 0.86 (F_{340}/F_{380})s) which implicates kinetic parameters such as the rise and decay of the curve. Furthermore, the percentage of cells not responding to AngII is also not affected by miR-221/222 (Fig. 30 D; mc: $9.06 \pm 2.71\%$; miR-221: $15.43 \pm 3.96\%$; miR-222: $14.25 \pm 4.10\%$). Thus, miR-221/222 do not interfere with AngII-mediated depolarization-independent calcium signaling.

In contrast to this, LTCC-dependent calcium signaling is altered by miR-221/222. The KCl-induced plateau height (Fig. 30 E; mc: 0.23 ± 0.03; miR-221: 0.17 ± 0.02; miR-222: 0.19 ± 0.02 $\Delta(F_{340}/F_{380})$) is decreased by trend by miR-221 and -222. The area under the curve (Fig. 30 G; mc: 163.92 ± 2.34; miR-221: 156.99 ± 2.23; miR-222: 159.47 ± 2.44 (F_{340}/F_{380})s) is significantly reduced in miR-221-transfected cells and the time needed to reach maximum plateau Ca^{2+} levels is significantly prolonged by both miRs compared to control (Fig. 30 F; mc: 166.80 ± 12.65 s; miR-221: 204.59 ± 9.37 s; miR-222: 204.22 ± 7.27 s). Additionally, miR-221 significantly

increased the proportion of non-responding cells (Fig. 30 H; mc: $0.44 \pm 0.19\%$; miR-221: $1.66 \pm 0.44\%$; miR-222: $1.25 \pm 0.62\%$). These results show that miR-221/222 reduce depolarization-dependent Ca^{2+} influx in HL-1 cells.
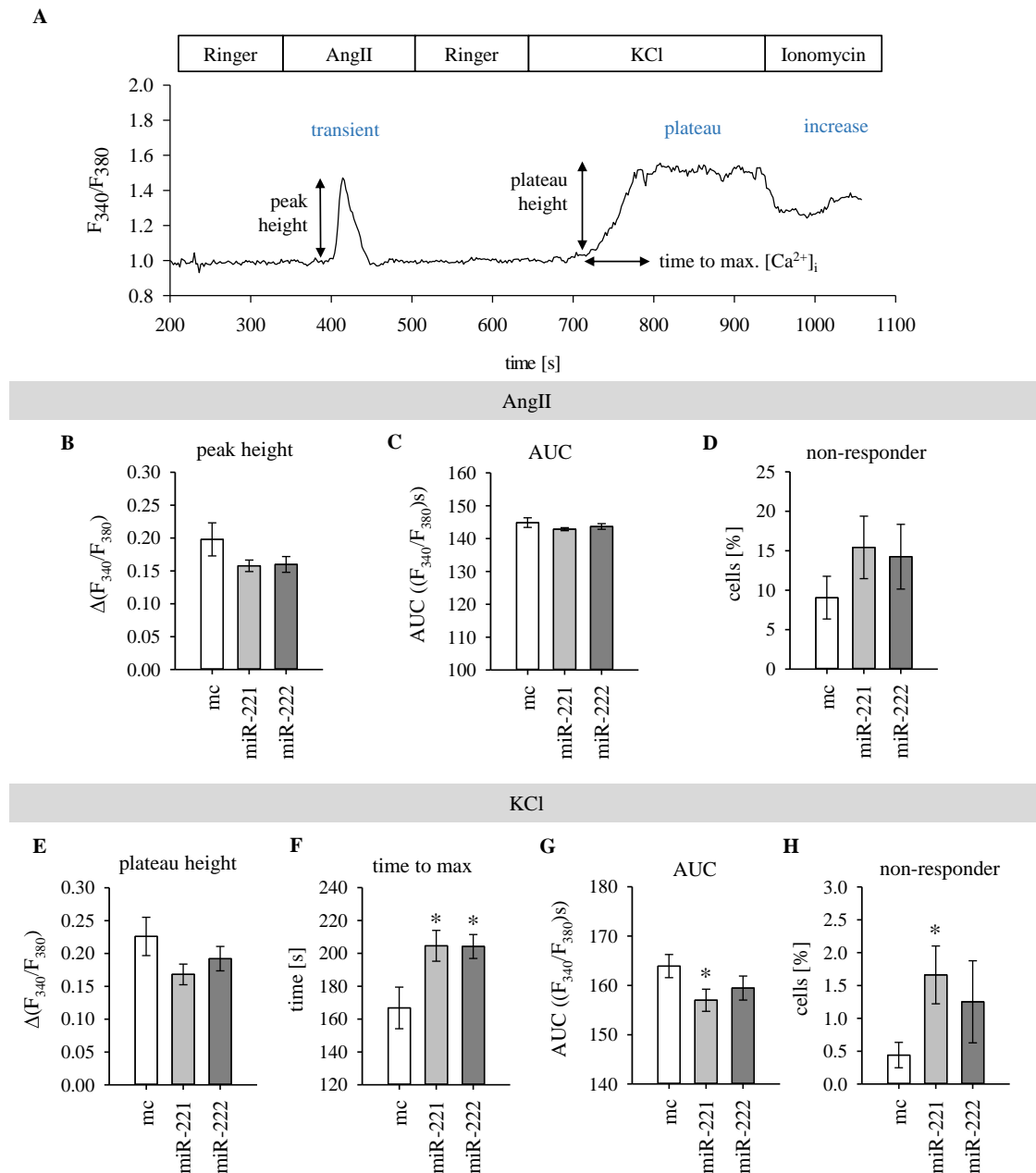

Figure 30. LTCC-mediated increase in cytosolic [Ca^{2+}] is slower in miR-221/222-transfected HL-1 cells. A Scheme of the applied superfusion protocol and typical response of a cell to 100 nM AngII, 25 mM KCl and 1 µM ionomycin. **B-D** AngII elicits a transient increase in [Ca^{2+}]$_i$. Peak height, percentage of non-responding cells and area under the curve (AUC) are not significantly altered compared to mimic control. **E-H** KCl leads to a baseline shift of [Ca^{2+}]$_i$ up to a plateau level. The baseline shift is reduced by trend by miR-221/222. The AUC is significantly reduced in miR-221-transfected cells and miR-221/222 both lead to a significantly slower increase in [Ca^{2+}]$_i$ up to the plateau level. The proportion of non-responding cells is significantly increased in miR-221-transfected cells. Data are displayed as mean $\pm$ sem, * indicates $p < 0.05$, N=13-14 experiments per group, n=27-115 cells per experiment.

To verify that AngII- and KCl-induced calcium signals are indeed mediated by AT1R and LTCC, respectively, experiments with appropriate inhibitors were performed in untransfected HL-1 cells (Fig. 31). AT1R inhibitor losartan significantly reduces the AngII-induced calcium transient in comparison to control-treated cells. Due to an increased population of cells that are no longer responding to AngII upon losartan application (Fig. 31 C; losartan: $55.45 \pm 13.78\%$ vs. control: $19.16 \pm 9.63\%$), the overall peak height of all cells (Fig. 31 A; losartan: 0.06 ± 0.02 vs. control: 0.19 ± 0.03 $\Delta(F_{340}/F_{380})$) is even more reduced than that of the population of responding cells (Fig. 31 B; losartan: 0.08 ± 0.004 vs. control: 0.21 ± 0.001 $\Delta(F_{340}/F_{380})$).

LTCC blocker verapamil prevents the KCl-induced intracellular calcium increase by enlarging the population of non-responding cells (Fig. 31 E; verapamil: $86.67 \pm 5.25\%$ vs. control: $3.53 \pm 1.97\%$). In line with this, when considering the overall response of all cells, the plateau height is dramatically reduced in verapamil-treated cells (Fig. 31 D; verapamil: 0.03 ± 0.002 vs. control: 0.18 ± 0.007 $\Delta(F_{340}/F_{380})$).

Both losartan and verapamil diminish the response elicited under control conditions. Thus, the observed cellular calcium response to AngII and KCl is indeed mediated by AT1R and LTCC, respectively.

In conclusion, the results of calcium measurements in HL-1 cells indicate that miR-221/222 do not influence the IP3/SR-mediated cytosolic calcium increase but have an effect on the depolarization-dependent (e.g. action potential-dependent) intracellular calcium increase in cardiomyocytes. Thus, downregulation of LTCCs by miR-221/222 may have an effect on depolarization kinetics in cardiomyocytes.
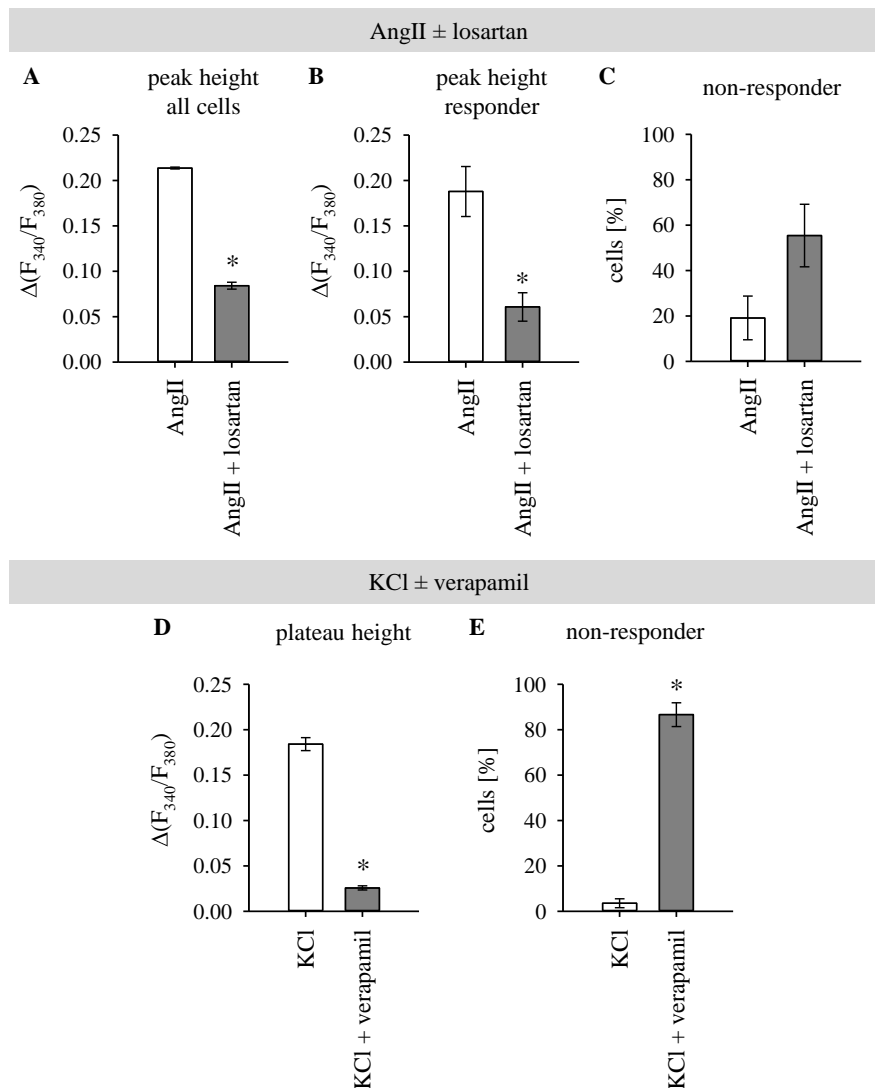
Figure 31. AngII- and KCl-induced changes in $[Ca^{2+}]_i$ are mediated by AT1R or LTCC, respectively.
A-C AT1R inhibitor losartan significantly reduces the AngII-induced calcium transient in HL-1 cells. Cells were superfused either with 100 nM AngII (control) or with AngII plus 10 µM losartan. **A** Calcium transient peak of all cells (responding and non-responding cells combined) is reduced in losartan-treated cells. **B** Losartan also leads to diminished calcium transients in responding cells. **C** The proportion of non-responding cells is increased by losartan. Control: N=2, n=42-66 cells, losartan: N=2, n=24-39 cells. **D-E** LTCC blocker verapamil significantly reduces intracellular calcium increase in response to 25 mM KCl in HL-1 cells. Cells were superfused either with KCl (control) or with KCl plus verapamil. The baseline shift upon KCl superfusion is significantly reduced in verapamil-treated cells (non-responder and responder) (**D**). **F** The dramatically reduced response when analysing all cells in this setting is in part due to an increase of non-responding cells. Concentration of verapamil: 20 µM, data are displayed as mean ± sem, * indicates $p < 0.05$, N=4, n=54-78 cells each.

4.3.2 NeoCMs form functional cell clusters or monolayers in culture

To further investigate the impact of miR-221/222 on calcium homeostasis, the next experiments were performed using neonatal mouse cardiomyocytes (neoCMs). Freshly isolated neoCMs have several properties that make them a very valuable tool to study calcium signaling in a more physiological setting. In contrast to HL-1 cells, neoCMs are a more homogeneous cell population (channel expression etc.) and show much higher spontaneous beating activity after a few days in culture.

Figure 32 shows that isolated neoCMs form cell clusters after a few days in culture. Although a pre-plating step was added to the protocol to eliminate most of the non-cardiomyocytes (especially fibroblasts) from the cell suspension, it is not possible to exclude all of them. Therefore, these cell clusters are formed by cardiomyocytes and fibroblasts together and they start to contract spontaneously after a few days in culture.
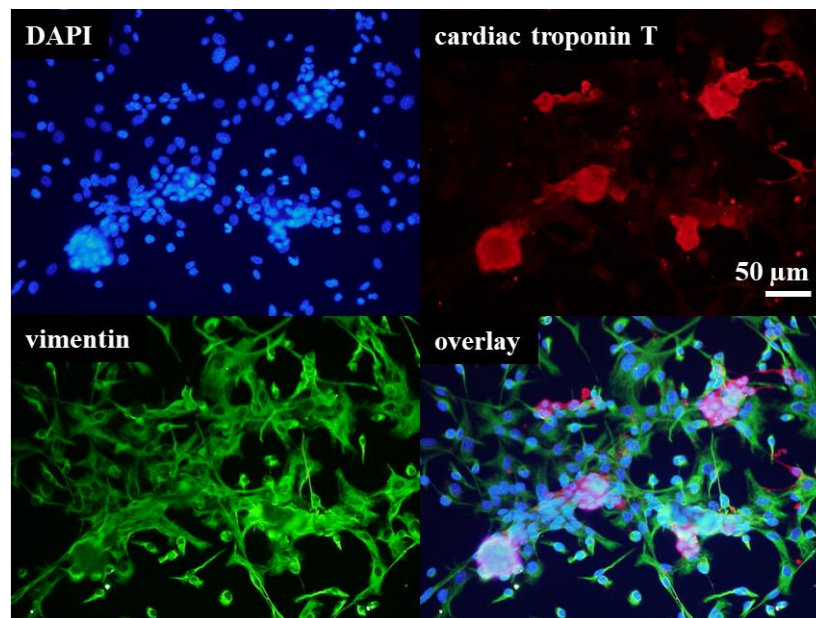
Figure 32. NeoCMs form cell clusters with cardiac fibroblasts in culture. Immunofluorescence staining of ventricular neoCMs after 6 days in culture. DAPI: nuclei, cardiac troponin T: cardiomyocytes, vimentin: fibroblasts. Scale bar indicates 50 µm.

However, neoCM clusters proved difficult to manipulate because transfection reagents or fura-2 did not reach the inner cells of the clusters (observation) and even verapamil could not inhibit spontaneous contractions in bigger clusters compared to small clusters or single cells (observation; recording and quantification for one petri dish: Fig. 33, ROI overview and movies on supplementary DVD, see appendix for file list). On the other hand, calcium measurement in single cells was also not an option because the fluorescence signal intensities were too low. Therefore, calcium measurements were performed with confluent neoCM monolayer cultures. Monolayers are achieved by plating a higher cell density. Cardiomyocytes within these

monolayers show synchronized spontaneous activity, especially at 37°C. Thus, synchronized calcium signals were obtained from all cells within the field of view. This enabled an optimized signal-to-noise ratio. Calcium measurements in neoCMs were performed at room temperature and this resulted in lower spontaneous activity. Therefore, calcium transients were electrically evoked in case of no spontaneous activity.
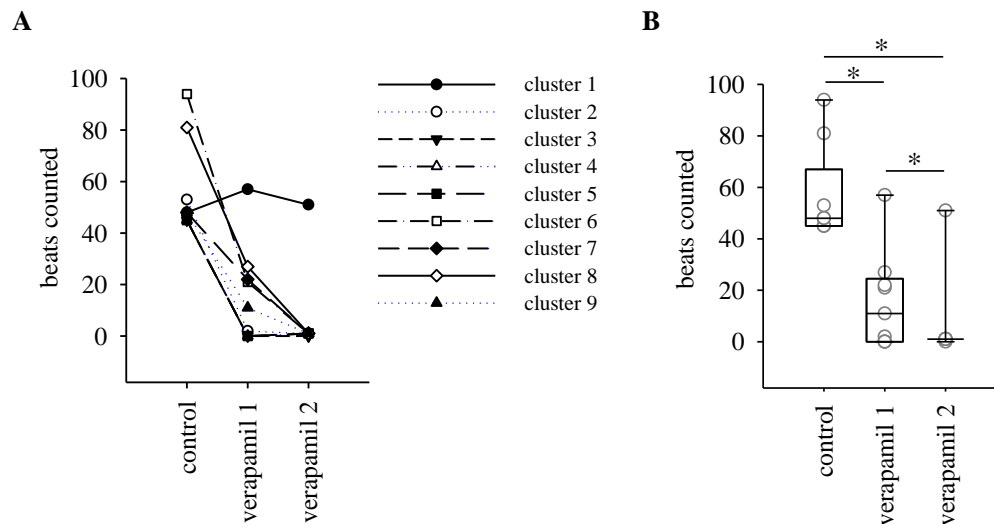
Figure 33. Contraction-inhibiting effect of verapamil depends on neoCM cluster size. Spontaneous beating activity at room temperature was measured under control conditions (for ca. 54 s) and at two successive time periods after solution change to 10 µM verapamil (verapamil 1: ca. 54 s movie, verapamil 2: ca. 58 s movie). Beats were analysed using Myocyter Image J plugin with manual ROI selection. **A** Cluster-specific beating activity. **B** Statistical analysis. N=1, n=9 cluster, paired t-test, * indicates $p < 0.05$. The corresponding movies and ROI overviews can be found on the supplementary DVD (list of files in appendix).

Prior to the next experiments transient transfection with mimics for miR-221 or miR-222 was tested once in neoCMs. Figure 34 shows that miR-transfection greatly increases expression of the respective miR.
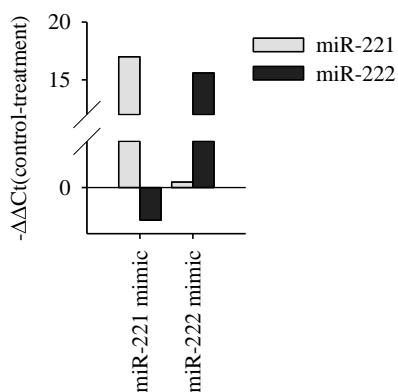

Figure 34. MiR-221/222 expression in neoCMs transiently transfected with 30 nM miR mimics. Proof of principle for miR transfection. MiR-221/222 expression was measured by qRT-PCR 48 h after transfection and normalized to mimic control. n=1, qPCR was performed with technical triplicates.

4.3.3 Basal calcium transient characteristics are not affected by miR-221/222

To investigate whether miR-221/222 influence basal calcium handling in neoCMs, calcium transients were measured under control conditions for 2 min. Both spontaneous calcium transients and electrically evoked transients were recorded. Monotonic transient analysis was performed to evaluate transient parameters for the baseline (Fig. 35 A), departure (Fig. 35 B, C), peak (Fig. 35 D-G) and return phases of the calcium transients (Fig. 35 H, I). There was no statistically significant difference in calcium transient parameters between miR-221/222 and mimic control. The high variability observed especially in departure velocity, peak height and return velocity in mc-transfected cells can be explained by the fact that these data contain more spontaneous transients. In contrast to electrically paced transients where the whole monolayer is always synchronized at sufficient pulse voltage, spontaneous transients can arise from the whole monolayer but also from different loci within the monolayer. Additionally, the duration and therefore also the kinetic parameters of spontaneous calcium transients are not as uniformly as in paced transients since the impulse is not applied externally with fixed time intervals, but rather depends on internal cellular processes of the cardiomyocytes.
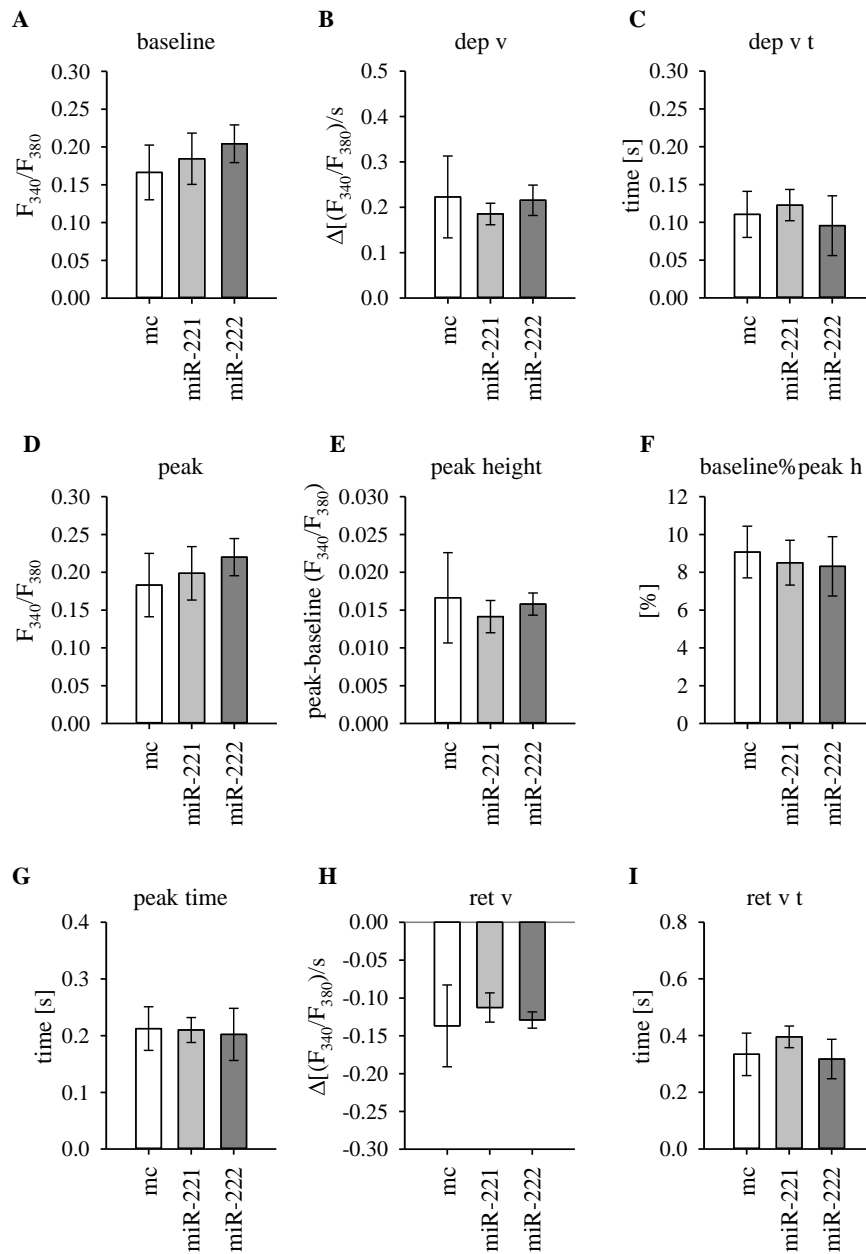
Figure 35. Basal calcium transient characteristics are not affected by miR-221/222 in spontaneously active or paced neoCMs. Spontaneous or electrically evoked calcium transients were measured in monolayers under control conditions for 2 min. Monotonic transient analysis was performed to evaluate transient parameters for the baseline (**A**), departure (**B-C**), peak (**D-G**) and return phases (**H-I**) of the calcium transients. There is no significant difference between miR-221/222 and mimic control (mc). Data are displayed as mean ± sem. mc: N=4-5, miR-221: N=6-7, miR-222: N=4.

4.3.4 The effect of ISO on calcium transients is lost in miR-222-transfected neoCMs

To compare cellular responses in miR-221-, miR-222- or mimic control-transfected neoCM monolayers, cells were stimulated with ISO to elicit an activating effect on LTCC and calcium-induced calcium release (CICR). Figure 36 shows the ISO effect in mimic control-, miR-221- and miR-222-transfected monolayers. Due to variability of calcium transients between different neoCM preparations, transient characteristics under ISO were directly compared to the respective control. For this, the ISO effect was calculated as follows: mean transient parameter(ISO)/mean transient parameter(control). Therefore, data are represented as x-fold change of control.

The results show that mimic control-transfected neoCM monolayers react to ISO (Fig. 36 A). Exposure to 10 µM ISO for in total 5-9 min significantly increased baseline fluorescence (Fig. 36 D). As expected, departure velocity of the calcium transients was elevated as well (Fig. 36 E). The time of maximal departure velocity (dep v t, Fig. 36 F) was slightly, but not significantly reduced. Peak and peak height of the calcium transients were elevated as well (Fig. 36 G, H). The parameter baseline%peak height describes the peak amplitude as percent change of basal calcium levels in the cells. In contrast to peak height, this parameter provides higher comparability of the ISO effect between samples. Accordingly, the ISO effect on baseline%peak height is highly significant (Fig. 36 I; 1.29 ± 0.11; p=0.0292). While ISO slightly reduced time to peak, return velocity and time to reach maximal return velocity (Fig. 36 J-L), these results did not reach statistical significance. Again, this might be explained by the higher variability due to included spontaneous transients. All in all, there is a measurable ISO effect on departure velocity and peak amplitude in spontaneous or pacing-evoked calcium transients of mimic control-transfected neoCM monolayers. ISO application led to differential results in miR-transfected cells. While ISO evoked a response similar to mc in miR-221-transfected cells (Fig. 36 B), virtually no effect of ISO could be detected in miR-222-transfected cells (Fig. 36 C). Apart from return velocity, which is minimally increased, no parameter is significantly changed upon ISO addition in miR-222-transfected neoCMs.
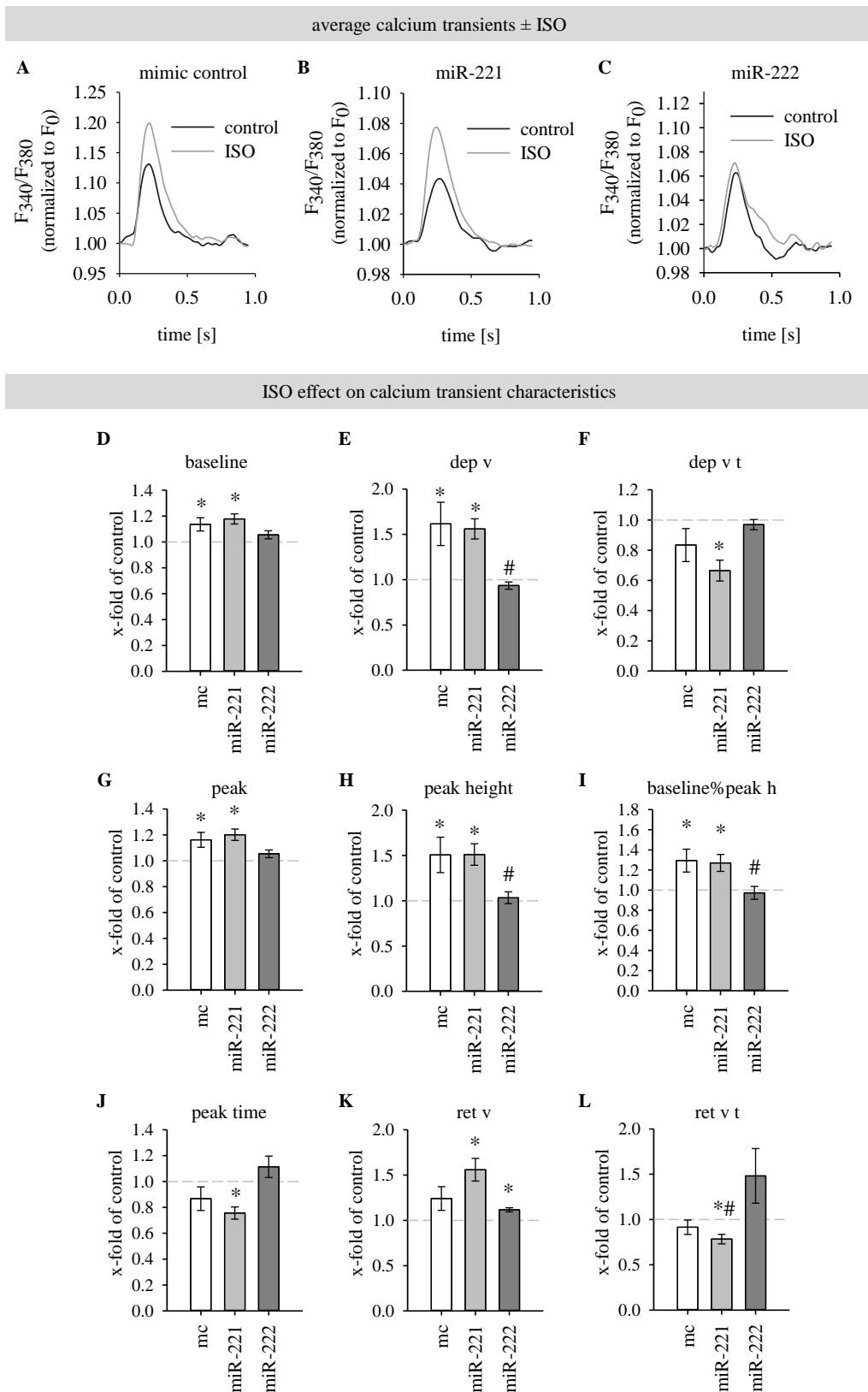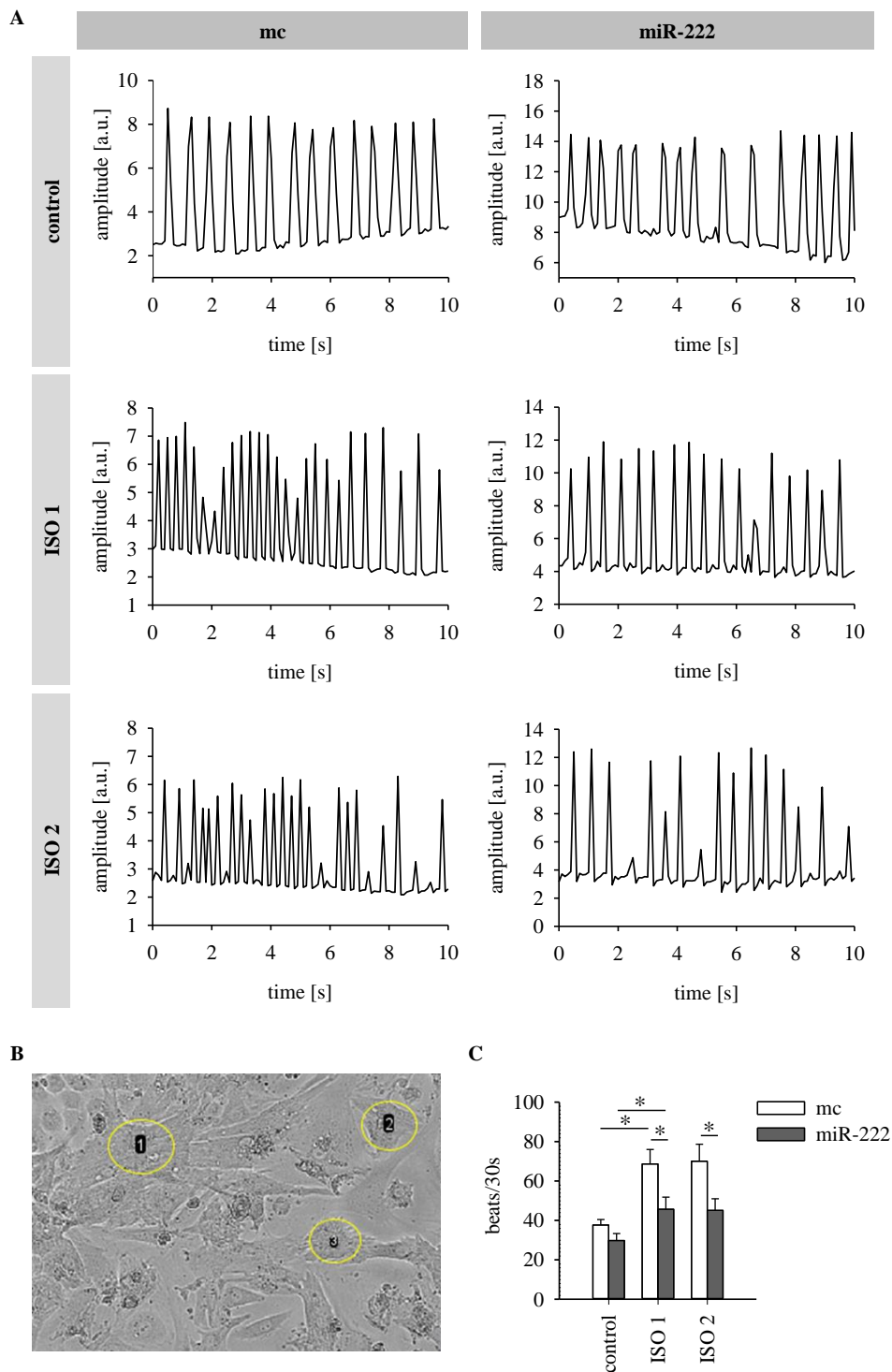
Figure 36. The positive inotropic effect of ISO on [Ca²⁺]ᵢ is lost in miR-222-transfected, but not in miR-221-transfected neoCM monolayers. A-C Average calcium transients show differential response to ISO in miR-222-transfected monolayers. Exemplary average transients are obtained from paced transients only (at least 5 transients) from one measurement each. Transients are representative for ISO effect on transient amplitude characteristics, not for baseline and kinetic parameters since data were normalized to fluorescence ratio at timepoint 0 (,,F₀") and kinetic parameters vary slightly between measurements within one group. **D-L** Spontaneous or electrically evoked calcium transients were measured in monolayers under

control conditions for 2 min, and after ISO addition after further 2 and 6 min for 3 min each. Following monotonic transient analysis, the ISO effect was calculated as ratio of mean transient parameter under ISO exposure divided by mean transient parameter under control conditions for each monolayer. ISO effect is shown for parameters describing baseline (**D**), departure (**E, F**), peak (**G-J**) and return phase (**K, L**) of calcium transients. While ISO accelerates and enhances increase in cytosolic $[Ca^{2+}]$ in neoCMs transfected with mimic control and miR-221, this effect is lost in miR-222-transfected monolayers. Data are displayed as mean ± sem. Paired t test was used to directly compare the calcium transient parameters under control condition and after ISO application for each monolayer. Therefore, data are shown as x-fold of control. For units of the shown parameters and absolute values under control conditions see Fig. 3. *$p<0.05$ ISO effect: ISO compared to respective control (no ISO = 1), # $p<0.05$ ISO effect in miR-transfected cells compared to ISO effect in mc-transfected cells. Mc: N=8, miR-221: N=12-13, miR-222: N=6-7.

4.3.5 The ISO-induced increase in spontaneous contraction frequency is abolished by miR-222

After the impact of miR-221/222 on calcium entry and calcium transients due to depolarization or β-adrenergic stimulation was established, the next question was if miR-221/222 also affect cardiomyocyte contractility. Since miR-221 had no effect on calcium transients in neoCMs, spontaneous contractions were only measured in miR-222-transfected neoCMs and compared to mimic control. Occurrence of spontaneous beating was recorded for 30 s each under control conditions and after ISO addition. As expected, ISO induces an increase in spontaneous contraction frequency (positive chronotropic effect) in mimic control-transfected cells (Fig. 37, movies S3-S8 on supplemental DVD). At 37°C the basal spontaneous beating frequency is 37.4±3.3 beats per 30 s and it is increased to 71.7±8.5 beats after addition of ISO (ISO1; Fig. 37 C). There was no significant difference in spontaneous contraction frequency between mimic control and miR-222 treated neoCMs under baseline conditions. However, the increase in spontaneous contraction frequency by ISO is strongly diminished in miR-222-transfected cells. Here, cells contracted 28.4±4.0 times in 30 s and ISO addition led to an increase to only 40.8±7.1 beats (ISO1). Since calcium measurements in HL-1 cells revealed that intracellular calcium increase was slowed in miR-transfected cells, the possibility of a delayed onset of ISO response was tested by including a second recording after ISO1 (ISO2). However, there was no change in beating frequency between both time points (ISO2: mc: 72.4±10 beats/30 s vs. miR-222: 40.5±7.1 beats/30 s).

Figure 37. The positive chronotropic effect of ISO is significantly reduced in miR-222-transfected neoCMs. Spontaneous contraction activity was recorded at 37°C for 30 s each. ISO1 was measured 2 min after buffer change to ISO and ISO2 was measured 1.5 min after ISO1 (for exact timeline, see Methods section). **A** Representative contraction tracings are shown for mimic control (mc) and miR-222 for 10 s each. **B** Exemplary section of an ROI overview image of a neoCM monolayer (mc). Shown are three manually placed ROIs (yellow circles). **C** While the number of spontaneous contractions was almost doubled in mc-transfected cells, this effect is significantly reduced in miR-222-transfected cells. There is no difference between both ISO time points within each group. Data include 3 independent experiments, N=11 petri dishes for each group with n=5-37 cells or cell clusters, depending on size of clusters or confluence of monolayer. Data are displayed as mean ± sem, * p < 0.05 respective to mc or corresponding control conditions as indicated.

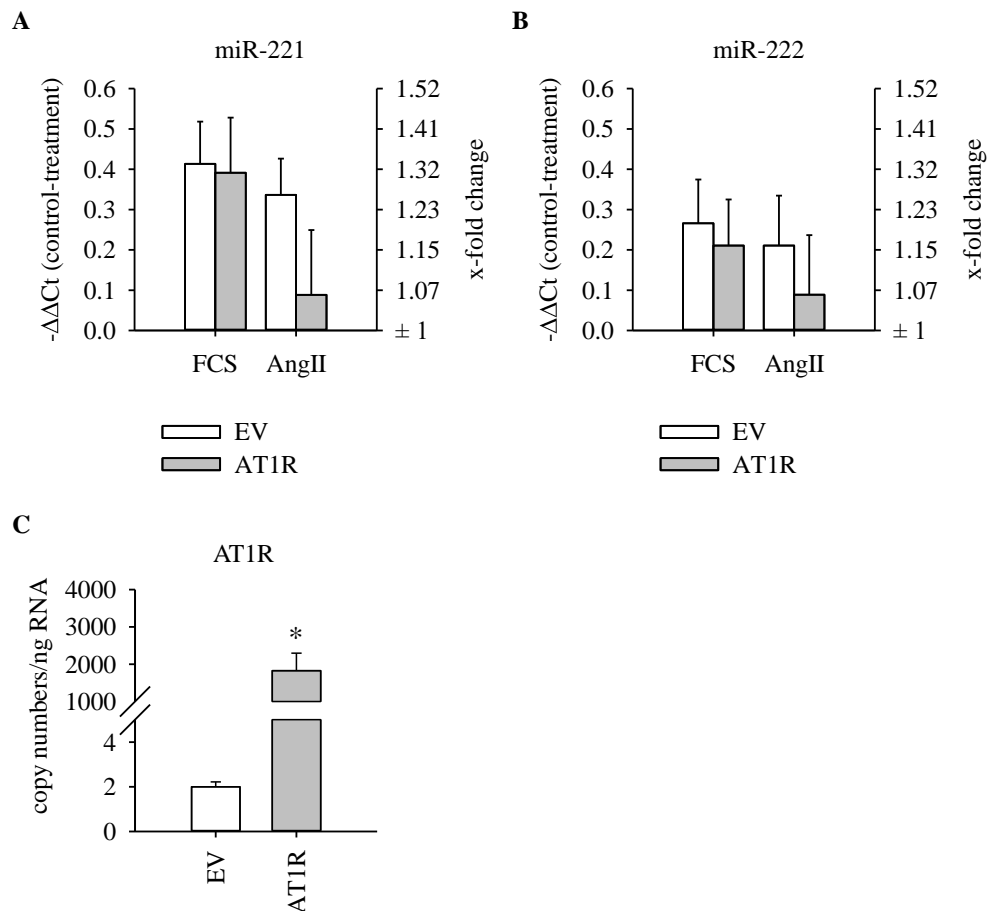## 4.4 Regulation of miR-221/222 expression

After determining the impact of aberrant miR-221 and miR-222 on ion channel expression and function, the question of how the expression of miR-221/222 is regulated remained. Beside upregulation of miR-221/222 in hearts of EGFR KO mice, miR-221 and miR-222 levels were also increased in the hearts of AngII-treated mice (Binas et al., 2020). Furthermore, miR-222 was higher expressed in hearts of ISO-treated mice, while there was no difference in miR-221 expression (Binas et al., 2020). Thus, AngII and ISO seemed to be particularly interesting candidates to test for differential miR-221/222 expression in cell culture.

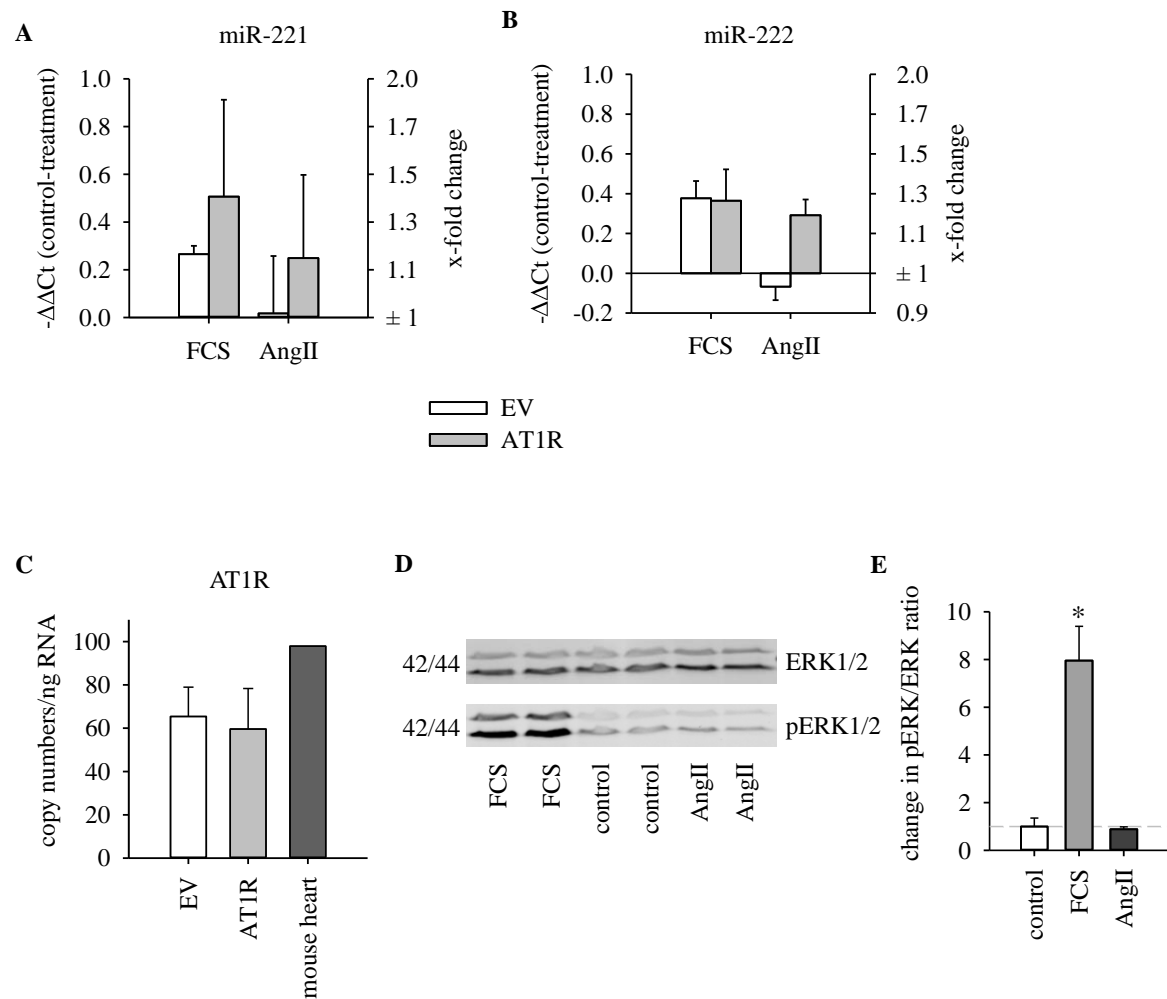### 4.4.1 AngII has no effect on miR-221/222 expression in vitro

AT1R was transiently transfected into the cells and AT1R mRNA copy number was measured by ddPCR. In HEK-293 cells AT1R transfection worked well with 1829.38 ± 469.24 copy numbers per ng RNA of AT1R transcript in the transfected samples compared to 2.00 ± 0.22 copy numbers in the empty vector control samples (Fig. 38 C). In contrast to this, in HL-1 cells there is no significant difference in AT1R copy numbers between AT1R-transfected and control cells (Fig. 39 C; EV: 65.41 ± 13.53 vs. AT1R: 59.58 ± 18.77 copy numbers/ng RNA). However, AT1R transcript copy numbers were approximately in the same range as in mouse heart (97.9 copy numbers/ng RNA; Fig. 39 C).

To further validate AT1R signaling in Hl-1 cells, activation status of ERK1/2, a well-known downstream component of the AT1R signaling cascade (Forrester et al., 2018), was evaluated. For this, HL-1 cells were stimulated with AngII for 10 min, samples were immediately lysed for protein isolation and phosphorylation status of ERK1/2 was measured. 10% FCS were used as a positive control. In contrast to FCS, AngII alone does not lead to ERK1/2 phosphorylation in HL-1 cells (Fig. 39 D, E).

Although the aforementioned mouse models showed differential miR-221/222 expression, this could not be reproduced in vitro. AngII incubation for 48 h has no effect on miR expression, neither in AT1R-transfected HEK-293 nor in AT1R-transfected HL-1 cells (Fig. 38 and 39).

Figure 38. AngII has no effect on miR-221/222 expression in AT1R-transfected HEK-293 cells. MiR expression was analyzed by Taqman qPCR after incubation with 100 nM AngII or 10% FCS for 48 h. **A** Expression of miR-221 is not significantly affected by FCS, AngII or AT1R transfection per se (N=7-8, n=21-24). **B** Expression of miR-222 is also not altered by FCS, AngII or AT1R transfection (N=5-6, n=15-18). **C** To check for AT1R expression, ddPCR was performed using control samples without further stimulation, N=7, n=7, Mann-Whitney rank sum test, * p<0.001.

Figure 39. AngII has no effect on expression of miR-221 (A) or miR-222 (B) in AT1R-transfected HL-1 cells. A-B MiR expression was analyzed by Taqman qPCR. Data are displayed as mean ± sem, * indicates $p < 0.05$, paired t test, N=3, n=4-6. **C** To check for AT1R expression, ddPCR was performed using control samples without further stimulation, N=3, n=3; mouse heart: n=1. **D-E** AngII alone does not elicit ERK1/2 activation. Representative western blot image (**D**) and evaluation of all performed western blots (**E**) shows that 10 min incubation with AngII is not stimulating ERK1/2 phosphorylation (pERK1/2) in untransfected HL-1 cells. The respective size of the proteins is given in kDa on the left side of the western blot images. N=3 passages, n=4-6, data are displayed as mean ± sem, * indicates $p < 0.05$, Wilcoxon signed rank test: FCS vs. control: p=0.031, paired t test: AngII vs. control: p=0.304.

Since it is possible that cardiac fibroblasts are the main source of miR-221/222 in the heart (Verjans et al., 2018), isolated adult cardiac fibroblasts from WT or EGFR KO mice were also incubated with AngII and ISO to test for miR-221/222 expression. Additionally, TGFβ was used because according to Verjans et al., TGFβ leads to reduced miR-221/222 expression neonatal rat cardiac fibroblasts (Verjans et al., 2018). However, neither miR-221 (Fig. 40 A) nor miR-222 (Fig. 40 B) expression is altered by AngII, ISO or TGFβ in adult cardiac fibroblasts.
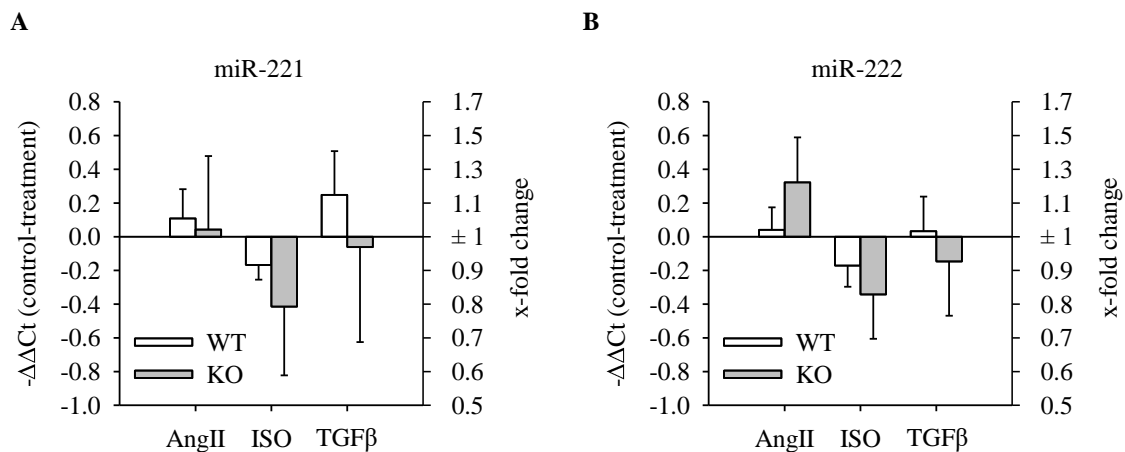
**Figure 40. Incubation of adult cardiac fibroblasts with AngII, ISO or TGFβ does not affect miR-221/222 expression.** Neither miR-221 (**A**) nor miR-222 (**B**) expression is altered by AngII, ISO or TGFβ, independent of EGFR. Freshly isolated fibroblasts from WT (N=8 animals) or EGFR KO (N=10 animals) were plated onto uncoated 5 mm petri dishes at first and were then subcultured on coated 6 well plates. For the experiments passages 1-3 were used. Data are displayed as mean ± sem.

4.4.2 Co-culture of cardiomyocytes and fibroblasts does not affect miR-221/222 levels

In the recent experiments cardiomyocytes and fibroblasts were observed in isolation. However, in vivo they occur in a complex network of cell types, extracellular matrix and communication pathways (e.g. soluble messengers, exosomes). The next set of experiments was therefore performed in co-culture, using mouse fibroblasts (NIH-3T3) and cardiomyocytes (HL-1). NIH-3T3 cells were cultured at the bottom of the well of a 6 well plate and HL-1 cells on the porous membrane of the insert, allowing exchange of soluble substances. However, there is no significant effect of AngII, ISO or TGFβ on miR-221/222 expression in neither cell line (Fig. 41). Additionally, co-culture per se has no significant impact on miR expression in these cells (Fig. 42).
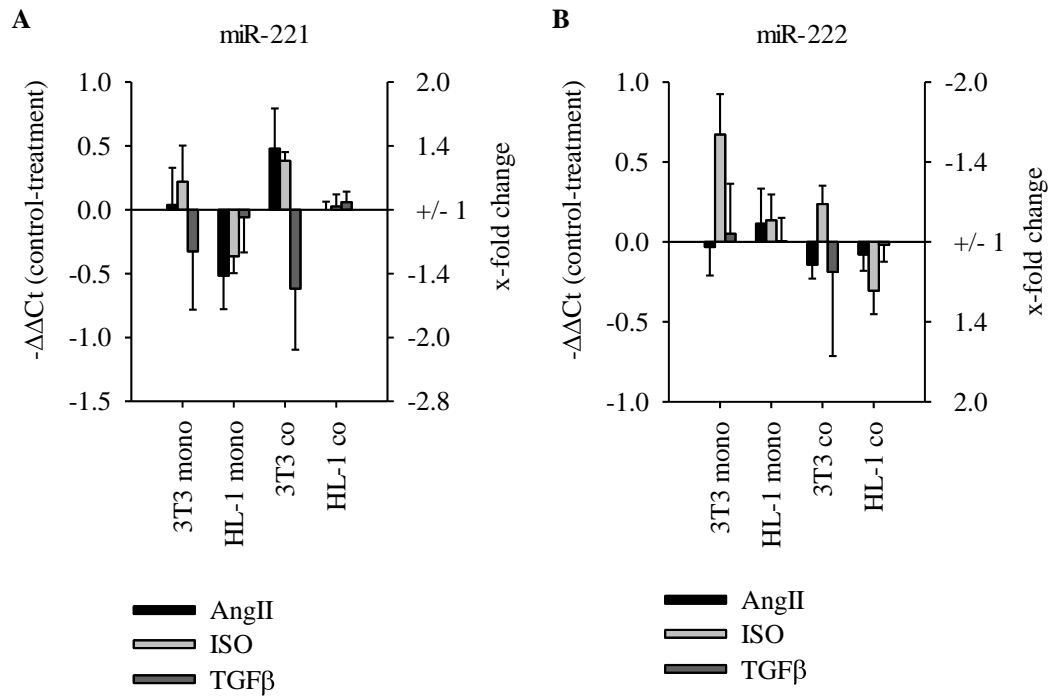
Figure 41. There is no effect of AngII, ISO or TGFβ on miR-221/222 expression in NIH-3T3 and HL-1 cells independently of culture conditions. NIH-3T3 and HL-1 cells were incubated either in mono culture or co-culture for 48 h. MiR-221 (**A**) and miR-222 (**B**) expression was analysed by Taqman qPCR. Data are displayed as mean ± sem, * indicates $p < 0.05$, N=4, n=4 except for TGFβ: N=3, n=3.
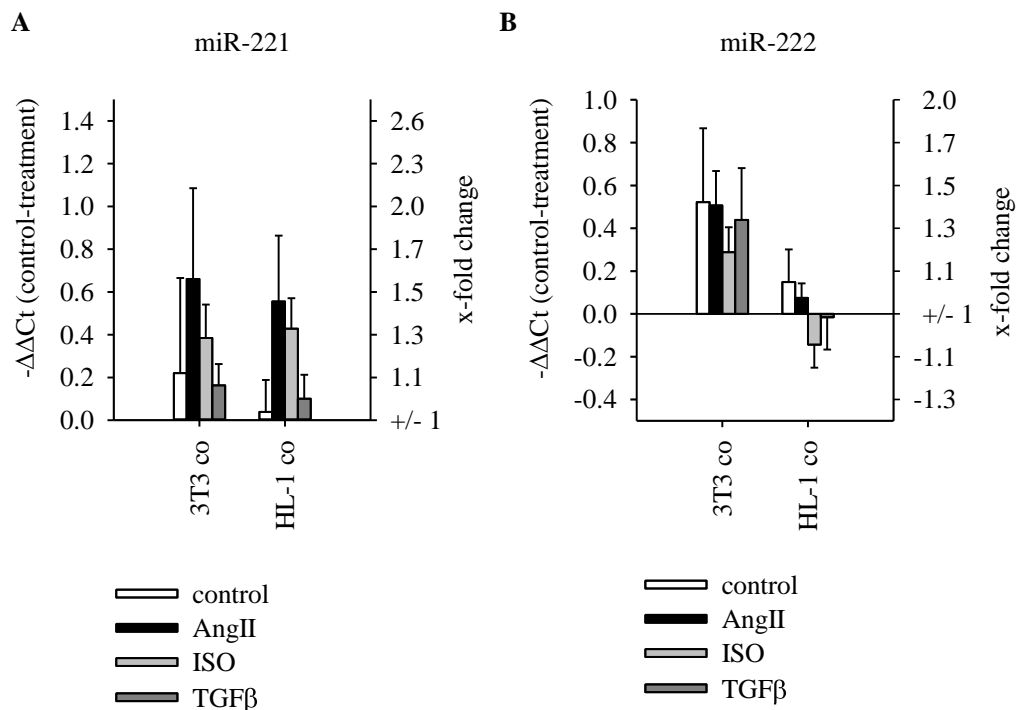
Figure 42. There is no co-culture effect on miR-221/222 expression in NIH-3T3 and HL-1 cells. NIH-3T3 and HL-1 cells were incubated either in mono culture or co-culture for 48 h. MiR-221 (**A**) and -222 (**B**) expression was analysed by qPCR. Data are displayed as mean ± sem, * indicates $p < 0.05$, N=4, n=4 except for TGFβ: N=3, n=3.

To check AT1R signaling in NIH-3T3 cells as well, stimulation experiments were performed as with HL-1 cells before. However, AngII has no activating effect on downstream components of AT1R signaling (Fig. 43). Only the positive control (10% FCS) leads to enhanced phosphorylation of AKT (Fig. 43 A; control: 0.20 ± 0.07 vs. FCS: 1.03 ± 0.44 pAKT/AKT) and ERK (Fig. 43 B; control: 0.08 ± 0.01 vs. FCS: 0.75 ± 0.03 pERK/ERK).
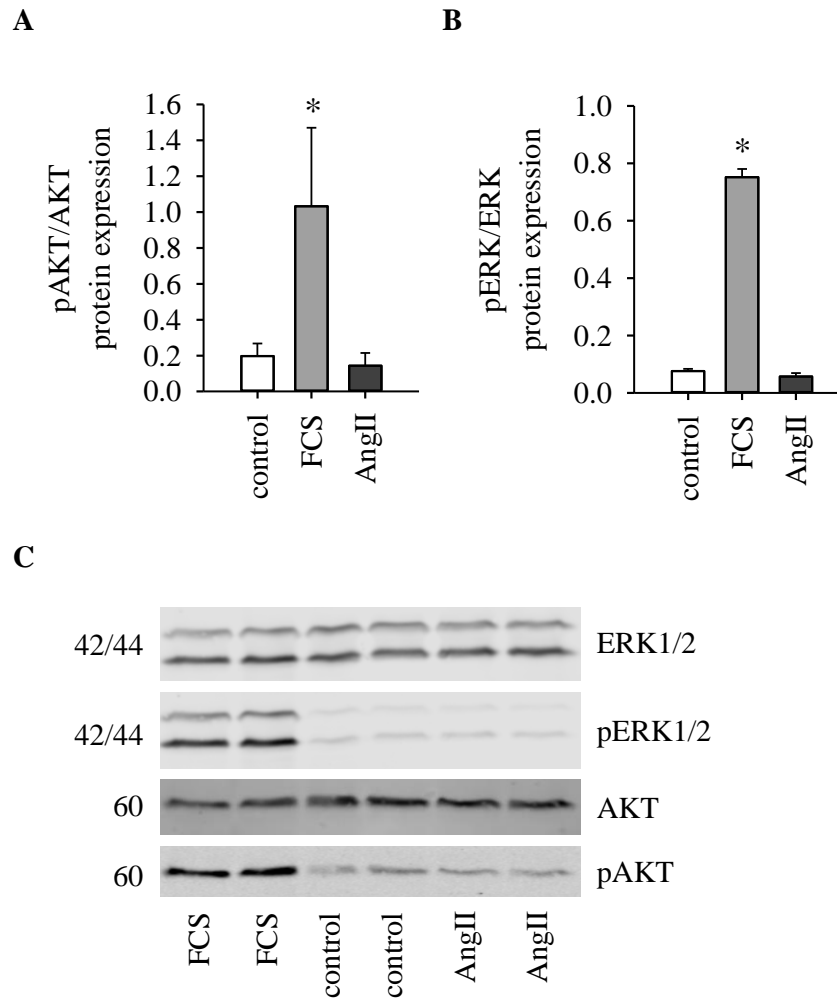
Figure 43. AngII does not lead to downstream ERK activation in NIH-3T3 cells. Neither p(phosphorylated)AKT/AKT (**A**) nor pERK1/2/ERK1/2 ratios (**B**) were affected by AngII. Only FCS leads to more phosphorylation and thereby activation of AKT and ERK1/2. Data are displayed as mean $\pm$ sem, N=3, n=5-6, * indicates $p < 0.05$ after paired t test. **C** Representative Western blot images from one passage of cells. The respective size of the proteins is given in kDa on the left side of the western blot images.

4.4.3 Indirect stimulation of AT1R signaling affects miR-221/222 promoter activity

To directly test possible stimulants of miR-221/222 expression, further experiments were performed in HEK-293 cells using a reporter construct containing a human miR-221/222 promoter fragment (pGL3-hmiR-221). PGL3 basic served as empty vector control for this plasmid. Additionally, cells were co-transfected with AT1R or the respective empty vector control. In the presence of AT1R basal promoter activity is about two-fold higher, even under control conditions (Fig. 44 A, C control). Adding AngII as a stimulant does not enhance promoter activity further (control: 1.95 ± 0.11 vs. AngII: 1.83 ± 0.18 relative luciferase activity; Fig. 44 A). However, 10% FCS could induce promoter activity up to three-fold (3.15 ± 0.36 relative luciferase activity, Fig. 44 A). Thus, some component of FCS is stimulating miR-221/222 promoter activity in the presence of AT1R. In the following experiments, the aim was to find a signaling pathway that is activated by FCS to induce promoter activity. Therefore, inhibitors of possible pathways were employed: AG1478 as an EGFR inhibitor and IKK inhibitor IV to block NFkB signaling. Adding AG1478 to FCS does not influence the FCS-mediated induction of promoter activity (Fig. 44 B). This means that the activating effect is presumably not due to AT1R-mediated transactivation of EGFR. When FCS is combined with IKK inhibitor IV, this leads to a significant decrease in promoter activity compared to FCS alone (FCS: 2.43 ± 0.13 vs. FCS+IKK inhib. IV: 1.91 ±0.08 relative luciferase activity; Fig. 44 C).
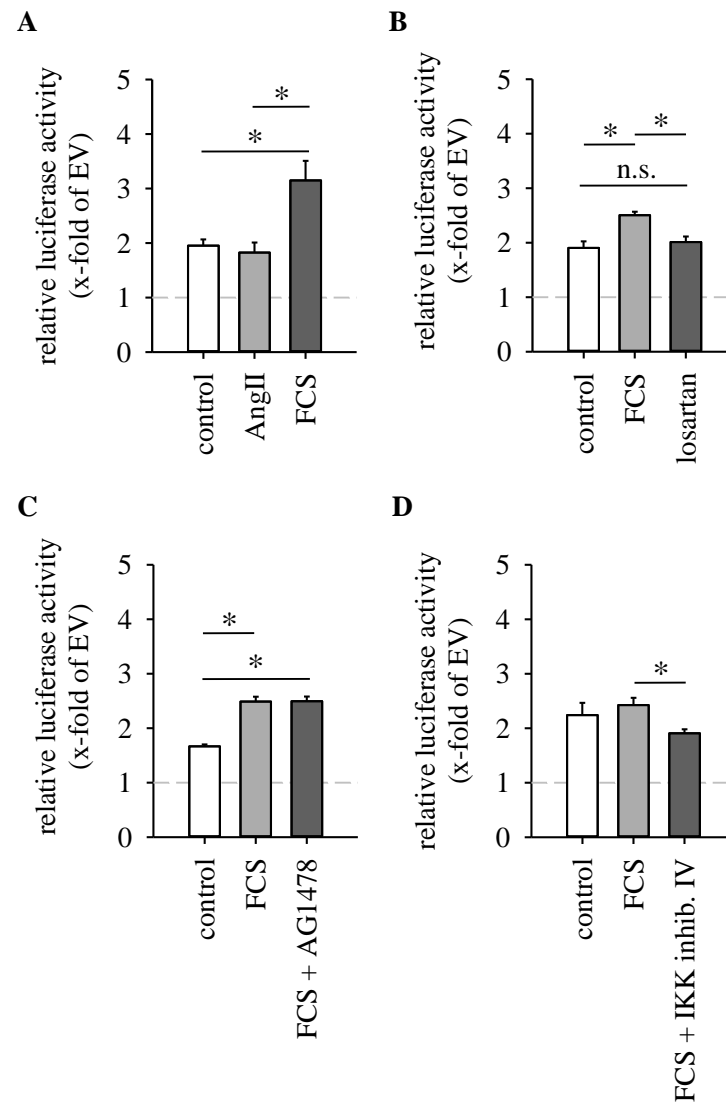
Figure 44. Indirect stimulation of AT1R signaling affects miR-221/222 promoter activity. HEK-293 cells were transiently transfected with pGL3-hmiR-221 (miR-221/222 promoter fragment) and either pAT1R or empty vector control (EV; SEAPbasic). **A** Incubation with 100 nM AngII alone does not alter promoter activity, but 10% FCS leads to significantly increased promoter activity. **B** Incubation with 1 µM losartan does not alter promoter activity compared to control. **C** Incubation with 1 µM EGFR inhibitor AG1478 does not change the FCS-induced promoter activation. **D** Incubation with 5 µM IKK inhibitor IV attenuates the FCS-induced stimulation of promoter activity. Firefly data were normalized to β-galactosidase activity. Data are displayed as mean ± sem, * indicates $p < 0.05$, AngII: N=3, n=6-9; AG1478: N=3, n=9; IKK inhibitor IV: N=2, n=6.

5. Discussion

5.1 Cacna1c and Girk4 3'-UTRs are targets of miR-221/222

Dual luciferase assays revealed that although both miR-221 and miR-222 share the same seed sequence they display differential targeting in transfected HEK-293 cells. They already show differences in downregulating their respective positive control. While 30 nM of miR-222 led to a 64% reduction of pMiR-222 luciferase activity, the same amount of miR-221 only led to a 35% reduction. On the other hand, when using each miR in combination with the non-corresponding positive control vector, the effect on luciferase activity was reduced for both miRs. Since both pMiR-221 and pMiR-222 differ only in their mature miR inserts, it is likely that not only the seed sequences but also the surrounding sequences of the miRs are important for differential targeting. This has been described before for other targets of miR-221 and miR-222 using miR-specific knockout cell lines (Jeong et al., 2017).

Differential targeting is also seen in regulation of the analyzed ion channel 3'-UTRs. While Cacna1c and Girk4 3'-UTRs are regulated by both miR-221 and -222, only miR-222 regulates Cacnb2, Cacna2d1 and Kcnd2. However, in contrast to the strong effect of miR-222 on its positive control, the effect on Cacnb2, Kcnd2 and Cacna2d1 3'-UTR was very low. Therefore, further experiments were focused on L-type calcium channel (especially Cacna1c) and Girk4.

Subsequent mutagenesis of putative binding sites within Cacna1c and Girk4 3'-UTRs provided proof for the direct interaction of miR-221 with Cacna1c and Girk4 3'-UTRs. Since mutated Cacna1c_b was still downregulated although not at the same extent as the wild type form, there might be another binding site for miR-221 present. However, this could not be seen with miR-222. Until now we do not know why there is such a discrepancy between these results and the results of the first luciferase experiments where miR-222 lead to a significant downregulation of luciferase activity by binding to Girk4 3'-UTR. Luciferase assays with the mutated form were performed in independent experiments with other cell passages. Nevertheless, subsequent functional experiments provided evidence for the role of not only miR-221 but also miR-222 in ion channel remodeling.

5.2 Limitations of transient miR transfection in luciferase and functional assays

There are some limitations with the luciferase and following functional experiments regarding transient miR transfection.

First, in luciferase assays only 3'-UTRs were analysed. However, miR binding could also take place within the 5'-UTR or coding sequence/open reading frame of target mRNAs (Moretti et al., 2010). This was not further analysed in this study.

Second, since miR-221/222 are clustered miRs they are expected to be regulated/expressed together and here both miRs were used separately in luciferase and functional assays. Possible combinatorial effects were tested exemplarily with Cacna1c_b 3'-UTR. Combination of miR-221 and miR-222 had the same effect on Cacna1c_b luciferase activity as miR-221 alone. At least for Cacna1c_b 3'-UTR, there was no combinatorial effect of both miR-221 and -222. In the following experiments, both miRs were again used separately to identify miR-specific effects.

Third, transient transfection with miR mimics likely led to miR levels that exceeded physiological concentrations that could be found in cardiomyocytes. qPCR revealed $\Delta\Delta Ct$ values of 17 and 15.6 for miR-221 and miR-222, respectively. However, results of quantitative measurements of transfected miRs from whole cell lysates should be interpreted with caution since a large proportion of transfected miRs tends to stay inside intracellular vesicles and is therefore not available for functional regulation of transcripts (Thomson et al., 2013). However, other groups also used a mimic concentration of 30 nM in luciferase experiments (Cañón et al., 2016). On the other hand, the luciferase assay system is highly artificial and plasmids are also transfected into the cells. Therefore, it is more important to optimize the ratio of miR and plasmid for analyzing possible direct interactions rather than achieving physiologically relevant concentrations. Enhancing the miR/plasmid ratio did not lead to further downregulation of luciferase activity. Furthermore, higher concentration of miR-221 did not lead to less Cacna1c_b luciferase activity. With miR-222, using 60 instead of 30 nM even abolishes any miR-effect on Cacna1c_b luciferase activity, indicating possibly an interfering effect of too high miR expression. From this one can conclude that the used miR concentration was appropriate in combination with these plasmids. Additionally, using 40 ng instead of 10 ng Girk4 3'-UTR did not reduce the miR effect on luciferase activity, suggesting the miRs are still in excess compared to the plasmids. In functional assays using cardiomyocytes with endogenous target gene expression cells were also transfected with 30 nM mimics or mimic control.

Fourth, the exact stoichiometry of miR-221 to miR-222 was disregarded in luciferase experiments and following functional assays. Clustered miRs like miR-221/222 are expected to be expressed together from one pri-miR transcript (Kabekkodu et al., 2018). Theoretically, expression levels should be equal. However, it has been shown that this may not always be the case. In hearts of

EGFR KO mice, miR-221/222 expression was upregulated about 2-fold but basal miR-222 levels were lower compared to miR-221 (Binas et al., 2020).

5.3 GIRK1/4 expression and function are reduced by miR-221/222

Overexpression of miR-221 in HL-1 cells led to reduced GIRK4, but not GIRK1, protein expression. Since GIRK1 cannot form functional channels alone (Kennedy et al., 1999), overall GIRK1/4 channel expression should be reduced in these cells. Furthermore, a study with GIRK4 knockout mice suggested that GIRK1 is unstable in the absence of GIRK4 (Wickman et al., 1998). Co-regulation of Girk4 and Girk1 on mRNA level was also suggested (Mintert-Jancke, 2010). However, in the present study GIRK1 was not affected by miR-221 48 h after transfection. Since the postulated effect on GIRK1 may be indirect compared to direct miR-dependent regulation of GIRK4 mRNA, future experiments should include later time points to analyze this possibility. However, the thallium flux assay results suggest that GIRK1/4 function is decreased, likely due to reduced protein expression.

In HL-1 cells, the overexpression of GIRK1/4 seems to enhance the overall open probability of GIRK1/4 channels leading to increased Tl^+ flux even in the absence of CCH. It has been shown that overexpression of GIRK4 leads to higher basal GIRK4-mediated currents (Mintert et al., 2007). Additionally, overexpression of M2R might also contribute to activation of GIRK1/4, even in the absence of ligands since spontaneous, ligand-independent M2R activity was suggested (Posokhova et al., 2013). This over-activity of GIRK1/4 and/or M2R under control conditions could prevent or mask additional effects by CCH. In line with this notion, no significant CCH effect was observed in GIRK1/4-M2R-transfected HL-1 cells. Thus, further experiments were performed with untransfected HL-1 cells and therefore endogenous M2R and GIRK1/4 expression only.

Endogenous M2R expression and activity was reported for HL-1 cells (Nenasheva et al., 2013). Additionally, Nobles et al. showed comparable CCH-induced currents in atrial cardiomyocytes, HL-1 cells and HEK-293 cells with stable expression of GIRK1/4 and M2R (Nobles et al., 2010). In contrast to their data obtained by patch clamp measurements, we could not measure Tl^+ flux in a comparable temporal resolution. The shortest interval between two measurements of the same well was 15 s, so it is likely that the actual initial increase in CCH-induced fluorescence is underestimated in these experiments. On the one hand, this method allowed for higher throughput since all cells of one measurement field in one well were captured and many wells could be measured in one batch. This was important because of our previous experience with the low fraction of HL-1 cells that showed $I_{K,ACh}$. But on the other hand, current characteristics like exact kinetics of activation and desensitization cannot be measured with this technique.

Tl^+ flux assays can deliver an estimate of the time needed to reach steady-state fluorescence. After an initial fast increase in fluorescence a steady-state level is reached. The level of steady-state fluorescence is a parameter for overall Tl^+ conductance of the cells. Since the concentration gradient for Tl^+ was the same in control and CCH settings, the overall fluorescence intensity (normalized to t_0) is associated with Tl^+ conductance. This can be quantified by the area under the curve. Eventually, CCH and control curves approach each other probably due to increasing concentration balance of Tl^+ intra- and extracellularly (reduced driving force) through background channels or saturation of Tl^+-specific dye. While in untransfected HL-1 cells there is an initial difference between control and CCH treatment, in the end the steady state levels approach similar fluorescence intensities. In this case, both cell populations are expected to have roughly the same expression of GIRK1/4 and M2R. In line with this, overexpression of GIRK1/4 and M2R in HEK and HL-1 cells keeps the steady state level of the CCH group above the control group.

In untransfected HL-1 cells steady-state is reached earlier with CCH treatment and on a higher level of fluorescence. This can be explained by a higher number of open GIRK1/4 channels due to CCH stimulation, so the concentration balance of Tl^+ is reached faster. Another parameter that can be used is the initial slope of fluorescence increase, i.e. the change in fluorescence between 0 and 1 mM Tl^+. There is good agreement between data from the area under the whole curve and the initial slope.

To determine whether the CCH-induced Tl^+ flux is indeed carried by GIRK1/4 only, the GIRK1/4 inhibitor tertiapin Q (TQ) was used. TQ is an oxidation-resistant mutant from tertiapin, a peptide toxin from honey bee venom (Jin et al., 1999). It is highly specific for GIRK1/4 (IC_{50}=8 nM) (Kitamura et al., 2000). It has been shown to inhibit also other GIRK channels like ROMK1 (KCNJ1, Kir1.1; IC50) and GIRK2 (KCNJ6, Kir3.2), but they are predominantly expressed in kidney and brain, not in cardiomyocytes (Hibino et al., 2010). Additionally, TQ inhibits BK-type K^+ channel in a concentration- and voltage-dependent manner (Kanjhan et al., 2005), however, it was reported that there was no native BK current detectable in HL-1 cells (Stimers et al., 2015). Furthermore, Nobles et al. demonstrated that TQ abolishes CCH-induced current in HL-1 cells as well as in HEK-293 cells stably expressing GIRK1/4 and M2R (Nobles et al., 2010). In line with this, co-incubation of HL-1 cells with CCH and TQ completely blocked the CCH-induced increase in Tl^+ flux and fluorescence intensity (CCH effect). Thus, the CCH effect is mediated by GIRK1/4. Interestingly, applying TQ alone led to fluorescence levels even below control levels. This supports the notion that there might be a certain basal activity of GIRK1/4 channels even without stimulation by CCH.

Transfection of HL-1 cells with miR-221 or miR-222 led to a significantly reduced CCH effect on Tl^+ flux through GIRK1/4. Therefore, miR-221/222 directly impair GIRK1/4 function.

All in all, in line with the initial luciferase results and western blot data, miR-221/222 lead to reduced GIRK1/4 function due to posttranscriptional regulation of GIRK4 protein expression.

5.4 L-type Ca^{2+} channel function and calcium handling are impaired by miR-221/222

5.4.1 miR-221/222 impair LTCC-induced Ca^{2+} increase but not intracellular Ca^{2+} release

Measurements of cytosolic calcium in HL-1 cells clearly showed that miR-221/222 reduce LTCC-mediated calcium increase due to significantly prolonged time to reach plateau calcium levels (miR-221/222) as well as significantly increased proportion of non-responding cells (miR-221). That the plateau height of responding cells was not significantly altered can be explained by the fact that the driving force for calcium was not changed. Thus, with fewer LTCCs due to downregulation by miR-221/222, it takes longer to reach plateau calcium levels.

AngII-induced calcium transients were unaffected by miR-221/222. Since AngII elicits the observed transient increase in cytosolic calcium through release from intracellular stores (Egger & Domenighetti, 2010), it can be used to estimate influence of miR-221/222 on SR calcium load. While miR-221/222 impair LTCC-dependent calcium entry, handling of intracellular stores does not seem to be affected. This supports the notion that the miR-effect is mainly due to LTCC regulation. To study SR calcium load in more detail, RyR and SERCA2a function could be analysed in future experiments, using caffeine to activate RyR2 and thapsigargin to block SERCA2a.

That the respective effects were mediated by AT1R or LTCC was proven by incubation with losartan or verapamil. Although co-application of losartan with AngII or verapamil with KCl did not completely block the responses to AngII or KCl, the percentage of non-responding cells increased and the response of responding cells decreased significantly.

In conclusion, miR-221/222 affect the depolarization-dependent LTCC-initiated intracellular calcium increase in HL-1 cells. This could influence action potential generation, propagation and excitation-contraction coupling in cardiomyocytes in the heart.

5.4.2 miR-222 abolishes the ISO-induced inotropic effect on intracellular Ca^{2+} transients in neoCMs

As expected, ISO had a positive inotropic effect on intracellular calcium transients in neoCMs. With miR-222, this ISO effect was completely gone. This is in good agreement with our previous results from luciferase assay (Binas et al., 2020), calcium measurements in HL-1 cells and also patch clamp measurements (Binas et al., 2020) showing that LTCC subunits are targets of miR-222.

But, in contrast to miR-222, there was no alteration of the ISO effect in miR-221-transfected neoCMs. However, calcium measurements and also patch clamp in HL-1 cells showed an influence of miR-221 on LTCC-dependent calcium handling. This discrepancy can be explained by the different methods and thereby the different read-outs. Intracellular calcium in HL-1 cells was measured after application of KCl until a clear plateau phase was observed - for 300 s in total. In this case, there was maximum activation of LTCC channels. Similar to this, $I_{Ca,L}$ current was also measured at maximum activation of LTCC channels, so the impact of miR-221/222 on peak calcium current was analyzed. In contrast to these measurements, in neoCMs no maximum activation but rather the more dynamic calcium handling important for excitation-contraction coupling was analyzed. NeoCMs were paced at 1 Hz if there was no spontaneous activity, so calcium cycling had to be much faster and there probably was no maximum activation of all LTCCs at each transient. This suggests that the miR-221 effect might only be seen at maximum activation. However, since the results from neoCM dynamic calcium handling are functionally more relevant to the in vivo situation, miR-222 seems to be more important than miR-221 in regulating LTCC.

There are some limitations with calcium measurements in neoCMs. Although a pre-plating step was added during isolation to reduce the number of non-cardiomyocytes, neoCM monolayers are not only cardiomyocytes (Ehler et al., 2013) (see also Fig. 32). Since neoCMs need a few days after preparation to fully regain their properties and then have to be transiently transfected, measurements could only be performed after about seven days in culture. At this point, there was a considerable number of non-cardiomyocytes in the neoCM culture. So, it cannot be excluded that measured effects are also due to interaction of miR-transfected fibroblasts or endothelial cells with cardiomyocytes. Additionally, there is likely an underestimation of the miR effect because probably not all cells in the monolayer are transfected and cells are still proliferating after transfection, thereby further diluting the proportion of transfected cells and the observable miR effect.

Furthermore, there are some technical implications of analyzing neoCM clusters vs. monolayers [see also (Belostotskaya & Golovanova, 2014)]. As shown exemplarily with the verapamil incubation, bigger clusters are not easy to manipulate because transfection reagents and also substances like stimulants or fura-2 are probably not reaching the inner cell layers thereby preventing conclusive results.

Zhu et al. showed variability of spontaneous activity among and even within clusters of cardiomyocytes derived from human embryonic stem cells (Zhu et al., 2016). Although in this study neoCMs, and not embryonic stem cell-derived cardiomyocytes, were used, they originated from whole heart preparations. So, there is also a possibility of variability in electrophysiological behaviour due to different origins of the cells and clusters. However, compared to adult CMs, neoCMs do not show the same high level of specificity depending on their location within the

heart. For instance, in contrast to adult CMs, ventricular CMs in the postnatal stage have been shown to be spontaneously active which is attributed to I_f current and Ca^{2+} clock mechanisms (Louch et al., 2015) or mitochondrial calcium signaling (Zhang et al., 2015). But there is still some level of specialization which could lead to variable spontaneous behaviour. Inter-preparation differences can also account for variability. That is why the ISO effect was always analysed in direct comparison to the respective control measurement. Additionally, because of the mentioned differences between different developmental stages of CMs the transferability of the results from murine neoCMs to adult CMs or even human CMs should be treated with caution. In summary, for neoCMs, there is likely an underestimation of the miR effect because probably not all cells in the monolayer are transfected and cells are still proliferating after transfection thereby further diluting the proportion of transfected cells and thus the observable miR effect.

5.4.3 The ISO-induced increase in spontaneous contraction frequency is reduced by miR-222

NeoCMs react to ISO not only with faster and higher calcium transients, they also increase their spontaneous beating activity, thus implementing a positive chronotropic response.

MiR-222 did not only influence the effect of ISO on calcium transients but also on spontaneous contractility in neoCMs. While basal spontaneous contraction activity was similar in control and miR-222-transfected neoCMs, the response to ISO was significantly reduced. This suggests reduced β-adrenergic responsiveness in miR-222-transfected cells which is an important feature of CMs in heart failure (El-Armouche & Eschenhangen, 2009). Since miR-221 had no effect on the ISO response regarding the calcium transients, it was not further analysed. The effect of miR-222 is probably due to regulating LTCC expression, as it is known that verapamil blocks spontaneous calcium transients (Li et al., 2017) and contractions (Fig. 33, movies S1-S2, supplemental DVD).

In contrast to calcium measurements, contractions were recorded in unstained neoCM monolayers with brightfield illumination, so there was no problem with dye loading or photobleaching. Keeping the neoCMs at 34-37°C during the measurements increased their spontaneous activity immensely. Previous calcium measurements were performed at room temperature and often there was no spontaneous activity so that calcium transients had to be evoked electrically.

Analysis with the Image J plugin Myocyter had several advantages. In contrast to common software for analysis of CM characteristics, it is not dependent on single, rod-shaped CMs with clear and high-contrast edges. Myocyter is suitable for neoCM monolayers because it compares frame-to frame pixel intensity between corresponding pixels and can therefore analyse cell morphology over time (Grune et al., 2019; Kijlstra et al., 2015). However, with the current system the highest possible temporal resolution was 10 Hz. Because of this low temporal resolution only the parameter "beats counted" was analysed. Although the heart rate of mice is around 600 beats

per minute and thus 10 Hz (Wickman et al., 1998), isolated neoCMs showed lower beating frequencies (observation during IonOptix calcium measurements at room temperature and even at 37°C). This is in line with a report that murine SAN cells had a spontaneous beating frequency of 2-3 Hz (Posokhova et al., 2013). Therefore, 10 Hz sampling rate was appropriate to measure the beating frequency. However, further analysis of kinetic properties of the contractions like contraction and relaxation velocities would require a sampling rate of around 100-200 Hz. This could be achieved e.g. with a smartphone camera (at least 120-240 frames per second) with an appropriate adapter to the microscope (Häseli et al., 2020).

5.5 Regulation of miR-221/222 expression

In contrast to the previous experiments on the functional impact of aberrant miR-221/222 expression, experiments regarding the regulation of miR-221/222 did not yield conclusive results. Our group has recently shown that AngII infusion led to significantly increased miR-221/222 levels, while ISO treatment only increased miR-222 (Binas et al., 2020). Furthermore, a publication by Verjans et al. suggests TGFβ may also play an important role in regulating miR-221/222 expression (Verjans et al., 2018). To analyze the potential influence of AngII, ISO and TGFβ incubation experiments were performed in HEK-293, HL-1 cells and adult cardiac fibroblasts, and co-culture was done with HL-1 and NIH-3T3 cells.

To be sure that AT1R is present in most cells, HEK-293 and HL-1 cells were transiently transfected with pAT1R. Surprisingly, when AT1R transcript copy numbers were measured by ddPCR later on, there was no significant difference between empty vector control and pAT1R in HL-1 cells, in contrast to HEK cells where the transfection led to a highly significant increase in AT1R mRNA copy numbers. Possible explanations include lower transfection efficiency in HL-1 cells compared to HEK cells, at least for vectors, or AT1R degradation. Despite no difference between transfected and untransfected HL-1 cells, AT1R transcript copy numbers still were in the same range as in freshly isolated whole mouse heart, so theoretically there should be enough AT1R present. In addition, during calcium measurements there was a direct response to AngII observable which could also be inhibited by AT1R blocker losartan. This suggests that AngII-AT1R signaling is generally working in HL-1 cells but has no influence on miR-221/222 expression. On the other hand, western blot analysis did not show activation of ERK upon 10 min AngII incubation in untransfected HL-1 cells. ERK is a downstream target of AT1R signaling in neonatal and adult CM (Schlüter & Wenzel, 2008). Since AngII elicited a fast response in calcium imaging in HL-1 cells, the incubation time of 10 min for ERK activation should not be too short. A possible explanation for the discrepancies between the effect seen after AngII application in calcium imaging on single cell level and no effect of AngII incubation on ERK activation is that HL-1 cells may not express the EGFR ligand HB-EGF. HB-EGF is necessary for AT1R-dependent EGFR transactivation which mediates e.g. ERK activation (Forrester et al., 2018). In

FCS, however, HB-EGF should be present and this could, at least in part, explain the effect on ERK activation seen after FCS incubation.

Furthermore, miR expression was not altered by AngII, ISO or TGFβ in adult cardiac fibroblasts. This contradicts data from Verjans et al. who showed that TGFβ incubation (also 10 ng/ml for 24 h) leads to reduced miR-221/222 expression in neonatal rat cardiac fibroblasts (Verjans et al., 2018).

It has been shown that paracrine signaling is of importance for cardiomyocyte-fibroblast crosstalk, e.g. in hypertrophy (Bang et al., 2014; Cartledge et al., 2015; Pellman et al., 2016). TGFβ was identified as a key signaling molecule for this crosstalk (Cartledge et al., 2015). Furthermore, AngII was shown to be a stimulator for cardiac fibroblasts to release exosomes leading to increased AngII and AT1R production in cardiomyocytes (Lyu et al., 2015). This is suggested to promote pathological hypertrophy of the heart through AngII (Lyu et al., 2015). Verjans et al. demonstrated a non-significant increase of miR-221/222 by AngII in whole heart extracts and they suggested this may be due to an altered composition of cell types in the heart and not due to transcriptional regulation (Verjans et al., 2018).

They also suggested that fibroblasts are the main source of miR-221/222 in the heart (Verjans et al., 2018), so culturing CM together with fibroblasts could lead to higher miR-221/222 levels in CM, e.g. due to exosomal miR transfer. However, this assumption could not be verified in co-culture experiments. Incubation with AngII, ISO or TGFβ also had no effect on miR-221/222 expression when co-culturing HL-1 cells with the fibroblast cell line NIH-3T3. For co-culture a transwell system was used where both cell types remain physically separated but can exchange soluble mediators through the medium in a paracrine manner. Admittedly, NIH-3T3 originate from embryonic mouse fibroblasts and may therefore miss some features cardiac-specific fibroblasts may possess. Cartledge et al. demonstrated differences in cardiomyocyte-fibroblast crosstalk depending on the fibroblasts used. They analysed fibroblast cell lines, freshly isolated fibroblasts and cultured fibroblasts. Although there were differences, all fibroblast types did influence cardiomyocytes in regard to viability and calcium transient amplitude (Cartledge et al., 2015). Good alternatives to NIH-3T3 would be adult and neonatal cardiac fibroblasts. However, performing co-culture experiments with adult CM is not feasible as they cannot be kept in culture for several days (Peter et al., 2016) and as mentioned above discriminating between CMs and nonCMs from neoCM preparations is very difficult because they already grow in direct co-culture. Further complicating matters, there might be differences in AngII response and signaling depending on the developmental stage of the CM (Schlüter & Wenzel, 2008).

Furthermore, there is also evidence that the important cell type in influencing CM is not fibroblasts but rather endothelial cells. Lee et al. showed that maturation of murine embryonic stem cell-derived CMs was promoted in co-culture with rat endothelial cells, but not with mouse fibroblasts (D. S. Lee et al., 2015). They also demonstrated that a combination of four miRs (miR-

125-5p, miR-199a-5p, miR-221-3p, miR-222-3p) may at least in part be responsible for the observed effects on CM maturity.

Further underlining the potential importance of endothelial cells are newer studies on the cellular composition of the heart that suggest, in contrast to older studies (Banerjee et al., 2007), that not fibroblasts but endothelial cells are the major cell type of the heart or the major nonCM cell type (Pinto et al., 2016; Zhou & Pu, 2016). In line with this, while our group observed an increase in both mature miR-221/222 and pri-miR-221/222 expression in whole heart extracts and isolated CM of EGFR KO mice compared to WT, there was no difference in miR-221/222 expression in isolated fibroblasts from these animals (Binas et al., 2020). So, it would be very interesting to analyse co-culture of CM with endothelial cells with respect to miR-221/222 effects.

Promoter studies showed that AT1R transfection leads to a two-fold induction of miR-221/222 promoter activity, even in the absence of AngII. This suggests a ligand-independent activation which is possibly due to overexpression of the AT1R. In line with this, adding AngII did not further increase the effect on miR promoter activity. However, losartan also had no effect on promoter activity in the presence of AT1R. This suggests that the transfected AT1R is somehow unresponsive to external stimuli but still endogenously active compared to EV control. But FCS together with AT1R increased promoter activity even more, up to three-fold. This effect is not due to AT1R-mediated transactivation of the EGFR since adding EGFR inhibitor AG1478 to the FCS incubation did not lead to an altered effect on promoter activity. There has to be some other stimulant within FCS that additionally to or together with AT1R signaling further activates the promoter. When IKK inhibitor IV, an inhibitor of NFkB signaling, was added to FCS in the presence of AT1R, the promoter activity was significantly reduced. This is in line with the observation that AngII (AT1R signaling) leads to activation of several transcription factors including AP-1 and NFkB in cardiomyocytes (Schlüter & Wenzel, 2008). These results suggest that NFkB may stimulate miR-221/222 expression and that the AT1R may be involved. NFkB involvement in miR-221/222 transcriptional regulation has been observed in prostate carcinoma and glioblastoma cells (Galardi et al., 2011).

A limitation of the promoter experiments is that the used promoter fragment is not the whole regulatory unit for miR-221/222 transcriptional regulation. Sun et al. located a potential promoter region 23.3 kb upstream of the miR-221/222 gene (T. Sun et al., 2018). Furthermore, Bouvy-Liivrand et al. reported enhancer elements involved in the regulation of miR-221/222 transcription that are not only more distant from the promoter and the transcription start site, but are dependent on chromatin architecture (Bouvy-Liivrand et al., 2017). These studies were performed with human cell lines and whether miR-221/222 regulation is comparable in mouse cells is not known until now.

5.6 Impact of miR-221/222 in cardiac disease

MiR-221/222 have been frequently reported as upregulated in cardiac remodeling and disease. However, it remains unclear whether their activity is cardioprotective or part of pathological remodeling. This study provides evidence that miR-221/222 regulate two ion channels in cardiomyocytes: GIRK1/4 and LTCC. Altered ion channel expression contributes to cardiac electrical remodeling as discussed below.

5.6.1 Possible impact of reduced GIRK4 expression on cardiac function

Traditionally, GIRK1/4 expression was assigned to SAN, conduction system and atria, but the possible role of GIRK1/4 in ventricles is just emerging and has to be further characterized, also in regard to possible pathophysiological relevance. Reduced GIRK4 expression would have numerous implications within the complex interplay of specialized cell types in the heart.

In sinoatrial node cells, reduced GIRK4 expression and therefore reduced $I_{K,ACh}$ would impact pacemaker activity. Mice with GIRK4 KO showed reduced heart rate variability but no alteration in resting heart rate (Wickman et al., 1998). Another study with GIRK4 KO mice found mildly reduced resting heart rate and significantly delayed recovery of resting heart rate after sympathetic activation (Mesirca et al., 2013). Further studies showed that the delayed recovery of resting heart rate may be attributed to I_f (Mesirca et al., 2014). In a mouse model with silenced I_f the resulting cardiac arrhythmias could be prevented by genetic GIRK4 inactivation, thus adding $I_{K,ACh}$ to the group of ion channels contributing to cardiac automaticity (Mesirca et al., 2014). Resting heart rate as well as the relative degree of heart rate regulation may not be highly influenced by reduced $I_{K,ACh}$ since there are numerous redundant pathways ensuring maintained pacemaker activity (Mesirca et al., 2013). However, low heart rate variability has been associated with high morbidity and mortality in heart diseases (Posokhova et al., 2013).

Atrial fibrillation is associated with reduced agonist-evoked $I_{K,ACh}$, but increased constitutively active $I_{K,ACh}$ and I_{K1} (Dobrev et al., 2001, 2002, 2005). Together both currents promote hyperpolarization of the cell membrane and could release Nav channels from inactivation which could further contribute to atrial fibrillation (Liang et al., 2014). In this case reduced GIRK1/4 channel expression would be beneficial as it would reduce shortening of AP duration (APD) and hyperpolarization. GIRK1/4 channels have been suggested as new atria-specific targets for therapy of atrial fibrillation (Ehrlich et al., 2008; Ravens, 2017). But apart from promising effects of GIRK1/4 inhibition in animal models, e.g. with tertiapin Q in a dog model of atrial fibrillation (Cha et al., 2006), it remains unclear whether GIRK1/4 inhibition is effective in human patients (Ravens, 2017; Walfridsson et al., 2015). In addition, it is not clear until now whether GIRK4 homotetramers play a relevant role in atrial cardiomyocytes. They were initially purified from

bovine atria and have been shown to be functional in GIRK4 overexpression studies in adult rat atrial CM (Bender et al., 2001; Corey & Clapham, 1998). However, reduced GIRK4 but unaltered GIRK1 expression would favour heterotetramer formation. This is in line with observations that high GIRK1-to-GIRK4 ratios seem to ensure proper heterotetramer formation under physiological conditions (Mintert et al., 2007).

The role of parasympathetic input and GIRK1/4 current in the ventricles is controversially discussed. In contrast to earlier assumptions, there is a growing body of literature suggesting widespread parasympathetic innervation in the ventricles (Coote, 2013; Liang et al., 2014) and relevance of GIRK1/4 or $I_{K,ACh}$ in ventricular myocardium (Takahashi et al., 2003; Y. Yang et al., 2010). Thus, miR-induced downregulation of GIRK4 expression might have an impact on ventricular electrophysiology. It was demonstrated that CCH can induce a small current in ventricular CM, similar to $I_{K,ACh}$ but with slower kinetics, and that this current was not present in CM of either GIRK1 or GIRK4 KO mice (Anderson et al., 2018). Application of either adenosine receptor agonist CPA or M2R agonist CCH led to APD shortening in rat papillary muscle preparations from ventricles (Liang et al., 2014). Furthermore, application of TQ prolonged APD and depolarized the membrane even in absence of exogenous stimuli (Liang et al., 2014). Although the action of endogenous adenosine could not be excluded in this setting, the authors conclude that GIRK1/4 may contribute to ventricular repolarization. Another study investigated the impact of GIRK1/4 on the ventricle specifically, but found no effect on heart rate, heart rate variability or ECG under control conditions or with CCH application (Anderson et al., 2018). Ventricular knockout was achieved by using the promoter of the ventricle-specific isoform of myosin light chain (MLCv2) for Cre recombinase expression (J. Chen et al., 1998). However, they used ablation of only GIRK1, so it could be argued that the remaining GIRK4 would still form functional channels and thus there was no full ablation of $I_{K,ACh}$. In line with this notion, GIRK4 was still found at the outer plasma membrane as well as in t-tubules in ventricular tissue from GIRK1 KO mice, while there was no GIRK4 staining in cardiac tissue of GIRK4 KO mice (Liang et al., 2014).

Furthermore, cyclic vagus nerve stimulation improves cardiac function, even in healthy rats (S. W. Lee et al., 2016). Vagal stimulation led to APD shortening and increased myocardial conduction velocity while not affecting ventricular ejection fraction and spatial dispersion of APD. It also reduced susceptibility to ventricular arrhythmias ex vivo (S. W. Lee et al., 2016). This beneficial effect should, at least in part, be due to $I_{K,ACh}$. However, this effect may apply only to the ventricle since slowing of conduction velocity is one mode of action for anti-arrhythmic drugs in atrial fibrillation (Geng et al., 2020) and increased $I_{K,ACh}$/GIRK current leading to AP shortening may cause arrhythmias in the atria (see above). Another study linked a GIRK4 mutation to Long QT Syndrome (Y. Yang et al., 2010). The mutation led to loss of $I_{K,ACh}$ due to

decreased stability and trafficking of the channel to the membrane. Thus, in contrast to atrial fibrillation, ventricular arrhythmias might be caused, among others, by decreased $I_{K,ACh}$.

Disentangling the roles of parasympathicus and M2R/GIRK1/4 in the ventricles is going to be very complicated since the dogma of neuronal-derived ACh and M2R/GIRK1/4 is questioned in several studies. One study suggested that the vagal effect might be independent from M2R/$I_{K,ACh}$ (Kulkarni et al., 2018) and other studies suggested an intrinsic non-neuronal ACh system in the myocardium that exerts its effects independently from vagal input (Oikawa et al., 2021; Saw et al., 2018; Takahashi et al., 2003).

Although the precise mechanisms are not fully understood, contribution of GIRK1/4 to ventricular repolarization is likely. This implies that miR-221/222-induced downregulation of GIRK4 would undermine electrical stability in the myocardium and promote susceptibility to ventricular dysrhythmias.

In this study GIRK1/4 function was measured in the atrial cell line HL-1. Furthermore, Girk4 mRNA expression was decreased in whole heart NGS analysis from EGFR KO mice (Binas et al., 2020). Therefore, an effect of reduced GIRK1/4 expression on the whole heart cannot be excluded. However, atrial versus ventricular GIRK1/4 function was not analysed.

5.6.2 Possible influence of reduced LTCC expression on calcium homeostasis in the heart

Since the LTCC is essential for action potential conduction and excitation-contraction coupling throughout the heart, a reduction in functional channel density could greatly impair cardiac function. MiR-221/222 transfection led to several alterations in calcium handling in HL-1 cells and neoCMs that would impact the whole heart. **First**, under unstimulated conditions, KCl-induced Ca^{2+} entry was slowed and reduced in miR-transfected HL-1 cells compared to mimic control. This implies that basal LTCC activity is reduced in these cells, most likely due to posttranscriptional downregulation by miR-221/222. In the present study the previously reported direct interaction of miR-221/222 with Cacna1c mRNA, which encodes the Cav1.2 pore forming subunit, was associated with a reduction in channel function. Furthermore, the effect of miR-221/222 on L-type Ca^{2+} current ($I_{Ca,L}$) density was analyzed by whole cell patch clamp recording (Binas et al., 2020). It has been reported that HL-1 cells express several voltage-gated Ca^{2+} channels. Apart from LTCCs, of which Cav1.2 is higher expressed and mostly localized on the cell surface while Cav1.3 is lowly expressed and mostly located intracellularly, they also express T-type Ca^{2+} channels (TTCC) (Xia et al., 2004). To ensure that the observed Ca^{2+} current was mediated by LTCC and not TTCC, $I_{Ca,L}$ was elicited at -40 mV which is too low for TTCC activation (Xia et al., 2004). TTCCs activate at around -70 mV (Xia et al., 2004). Transfection

with mimics for both miRs decreased $I_{Ca,L}$ density in HL-1 cells significantly, however, the voltage-dependence of activation was not altered (Binas et al., 2020). Thus, the downregulation of peak $I_{Ca,L}$ seems to be mainly due to transcriptional regulation of LTCC subunit mRNAs by miR-221/222.

The **second observation** was that β-adrenergic stimulation with ISO resulted in a reduced calcium transient amplitude in neoCM monolayers transfected with miR-222 compared to mimic control. This suggests a reduced positive inotropic effect of ISO due to miR-222. Since contractility per se was not measured, the effect of miR-221/222 on inotropy can only be discussed insofar as the calcium transient amplitude is thought to correlate with force development (Saleem et al., 2020). However, an inadequate response to β-adrenergic stimulation impairs the ability of the heart to adapt the cardiac output to differing needs and thus impairs cardiac function. This is in line with the observation that the β-adrenergic reserve is reduced in heart failure (X. Chen et al., 2002).

This also fits well to the **third observation**, that β-adrenergic stimulation resulted in a reduced positive chronotropic response in miR-222-transfected neoCMs compared to mimic control. Ventricular neoCMs exhibit spontaneous beating activity because they still express HCN channels (I_f), TTCC and Cav1.3 as well as other components of the Ca^{2+} clock (Louch et al., 2015). They express less TTCC than LTCC and the t-tubules are still in development but CICR, RyR, SERCA and SR calcium buffering are present (Louch et al., 2015). In the heart the positive chronotropic effect of ISO is mediated by sinoatrial node (SAN), atrioventricular node (AVN) and conduction within the myocardium.

Transferring these results to the whole heart could mean that either pacemaking frequency is still increased due to ISO but conduction to or within the myocardium is slowed or that pacemaking frequency itself cannot adapt to ISO. Since SAN and AVN cells express mainly Cav1.3 and not Cav1.2 and until now we do not know whether miR-221/222 target also Cav1.3, heart rate may not be altered under control conditions. However, the most problematic result would be that the Ca^{2+} entry and therefore the contractility of the working myocardium in atria and ventricles is reduced under β-adrenergic stimulation because they express mainly Cav1.2 (atria also Cav1.3). The reduced cardiac function would lead to an elevated β-adrenergic tone but together with the reduced responsiveness to catecholamines this initiates and reinforces a vicious circle that in the end leads to failing of the heart (El-Armouche & Eschenhangen, 2009). Further experiments are necessary to determine the role of miR-221/222 on contractility of neoCMs.

That basal calcium transients as well as spontaneous beating frequency were not affected by the miRs could be explained by a certain buffering in LTCC biosynthesis as described by Rosati et

al. (Rosati et al., 2011). If this was the case, LTCC expression may be reduced by miR-222, but would still be sufficient to ensure spontaneous activity. However, then the β-adrenergic reserve would be too low to allow for adequate increase in intracellular Ca^{2+} transient amplitude with ISO. In contrast to patch clamp and KCl where peak current and maximum Ca^{2+} entry were measured, spontaneous contractions under unstimulated conditions should not require maximal activation of all LTCCs present and thus even reduced LTCC expression should be sufficient. An alternative explanation would be that LTCC expression is reduced to a greater extent by miR-221/222 and that the fewer channels are in a more active state even under control conditions. In this case, ISO-induced PKA-dependent phosphorylation of LTCC could not increase LTCC activity and thus beating frequency any further.

MiR-221/222 are frequently upregulated in cardiac disease (Coskunpinar et al., 2016; Huang et al., 2020; Kakimoto et al., 2018; Lok et al., 2015; Sayed et al., 2007; Tatsuguchi et al., 2007; C. Wang et al., 2012) and seem to be associated with cardiac remodeling. Two studies with cardiac-specific overexpression of miR-221 or miR-222 in mice demonstrated cardiac hypertrophy and heat failure following miR overexpression (Su et al., 2015, 2016). This confirmed findings from other studies linking miR-221 and especially miR-222 to cardiac hypertrophy (X. Liu et al., 2015; C. Wang et al., 2012). Although cardiac hypertrophy is thought to arise due to increased Ca^{2+} entry or $[Ca^{2+}]_i$ (X. Chen et al., 2011), there is also evidence for the opposite situation. Mice with cardiac-specific heterozygous Cav1.2 deletion developed even more pronounced cardiac hypertrophy under β-adrenergic activation and reduced ventricular function than control mice (Goonasekera et al., 2012). In contrast to the two studies of Su et al., miR-221 and especially miR-222 have been shown to be more cardioprotective than detrimental, so the question arises whether a reduction of LTCC expression is beneficial. In fact, studies with LTCC inhibitors point in this direction. Benidipine inhibited cardiac hypertrophy and prevented heart failure in a mouse model with pressure overload (Y. Liao et al., 2005) and diltiazem prevented disruption of SR Ca^{2+} homeostasis in mice with hypertrophic cardiomyopathy (Semsarian et al., 2002). Whether miR-221/222 promote remodeling or protection may depend on the precise context of the respective cardiac disease.

5.6.3 Differential effects of miR-221 and miR-222

It seems that miR-222 elicits a stronger effect on LTCC in neoCMs than miR-221, which is therefore also detectable even when LTCC is not maximally activated. While miR-221 also reduced peak $I_{Ca,L}$ and slowed KCl-induced increase in $[Ca^{2+}]_i$ it had no effect on the response to β-adrenergic stimulation, in contrast to miR-222. The β-subunit (Cacnb2) that enhances LTCC trafficking to the cell membrane is a confirmed target of miR-222 (Carrillo et al., 2011). Loss of this subunit could, at least in part, explain the stronger effect of miR-222 on calcium handling in

cardiomyocytes. It is also conceivable that miR-221 may also target regulators of $I_{Ca,L}$, e.g. phosphatases, contributing to preserved LTCC function. Differential targeting of miR-221/222 despite sharing the same seed sequence has been described before (Jeong et al., 2017). There is evidence that also the central and 3'-region of a miR may be important for target binding (Jeong et al., 2017) and this could explain the differential effects of miR-221/222.

Additionally, miR-222 was lower expressed than miR-221 in hearts from WT and EGFR KO mice (Binas et al., 2020). This suggests independent transcription (Ramalingam et al., 2014) or posttranscriptional regulation of miR transcripts (Ryazansky et al., 2011) which could further strengthen differential effects of miR-221 and -222.

5.6.4 Outlook

An additional indirect effect of miR-221/222 on neoCM calcium handling and beating cannot be excluded. For example, RyR was also among the predicted targets of miR-221/222 that were also downregulated in EGFR KO mice (Binas et al., 2020). Until now this putative target was not confirmed but it likely would contribute to electrical remodeling, further reducing SR calcium load and thereby contractility. Another interesting target for future experiments is connexin 43 which is an important part of cardiomyocyte gap junctions and a direct target of miR-221/222 in astrocytes (Shen et al., 2018). There is also evidence that miR-221/222 indirectly impact NO production (Evangelista et al., 2013) and therefore nitrosylation of LTCC, RyR and SERCA (Gonzalez et al., 2007; J. Sun et al., 2006, 2007)

5.7 Conclusion

All in all, this study adds a new role of miR-221/222 in cardiac electrical remodeling by showing the impact on GIRK1/4-mediated ion flux, β-adrenergic regulation of LTCC function, cardiomyocyte calcium handling and contractility.

Future studies in neoCMs over a prolonged time or in mouse models are necessary to uncover potential miR-221/222-induced compensatory mechanisms caused by reduced LTCC expression and their effect on long-term cardiac remodeling and function. Effects on GIRK1/4 and LTCC have been discussed separately, but of course in the heart the regulation would occur simultaneously, adding further complexity. Furthermore, cell type-specific actions of miR-221/222 are a very interesting topic. To further investigate the role of miR-221/222 in cardiac remodeling, mouse models with cell type-specific miR-221/222 overexpression or decreased miR-221/222 expression due to infusion of miR inhibitors would be necessary.

6. Summary

Cardiovascular diseases are the leading cause of death worldwide. Cardiac remodeling comprises all changes in molecular, cellular and interstitial composition of the heart and can lead to cardiac dysfunction, malignant arrhythmias, sudden cardiac arrest or heart failure (Azevedo et al., 2016). Electrical remodeling including altered ion channel expression and imbalance of calcium homeostasis can have detrimental effects on cardiac function (Aiba & Tomaselli, 2010). MicroRNAs have been implicated in cardiac remodeling and disease. This study is about the role of miR-221/222 in electrical remodeling in cardiomyocytes.

While it is established that miR-221/222 are associated with cardiac remodeling and disease the precise role remains unclear. Our group previously showed that upregulated miR-221/222 expression in hearts from EGFR KO mice was correlated to downregulated cardiac ion channel genes which are predicted targets of both miRs. Thus, miR-221/222 could be involved in electrical remodeling in the heart by targeting ion channel mRNAs. Among the regulated ion channel genes were subunits of the L-type Ca^{2+} channel (Cacna1c as pore-forming subunit, Cacnb2 and Cacna2d1 as auxiliary subunits) and two K^+ channels (Kcnd2 as subunit of the Kv4.2 channel and Girk4 as subunit of the G protein-activated inwardly rectifying K^+ channel GIRK1/4). The aim of this study was to analyse the possible role of miR-221/222 in electrical remodeling in cardiomyocytes.

Dual luciferase reporter assays revealed Cacna1c and Girk4 as direct targets of miR-221/222 which could be verified with mutation of the predicted binding sites, at least for miR-221.

Furthermore, miR-221 led to reduced protein expression of GIRK4, but not GIRK1. Additionally, carbachol-induced Tl^+ flux through GIRK1/4 was significantly reduced in miR-221- or miR-222-transfected cells.

Previously our group could show that Cacna1c, Cacnb2 and Cacna2d1 mRNA expression was decreased in mouse models with increased miR-221/222 levels (EGFR KO, AngII). Additionally, in order to determine a possible impact of miR-221/222-dependent regulation on ion channel function, LTCC current density was analysed by whole cell patch clamp recording. HL-1 cells transfected with miR-221 or -222 mimics showed a reduction in LTCC current density while the voltage-dependence of activation was not altered. To investigate if this regulation has an impact on Ca^{2+} homeostasis, ratiometric fluorescence microscopy was performed in HL-1 cells and calcium and contractility measurements were performed in neoCMs. Transient transfection of HL-1 cells with miR-221/222 mimics led to slower depolarization-dependent Ca^{2+} entry and increased proportion of non-responding cells. Angiotensin II-induced Ca^{2+} release from the SR was not affected by miR-221/222. Furthermore, in miR-222-transfected neoCMs the ISO-induced positive inotropic effect on the intracellular Ca^{2+} transient was lost and the positive chronotropic effect on spontaneous beating activity was strongly reduced. This could have severe consequences

for cardiomyocytes and could lead to a reduced contractility and systolic dysfunction of the whole heart.

To investigate possible mechanisms that regulate miR-221/222 expression HL-1 cells were incubated with AngII, ISO or TGFβ. However, this did not alter miR-221/222 expression levels. Co-culture with NIH-3T3 fibroblasts also had no effect. Only miR-221/222 promoter studies using luciferase assays revealed an activating indirect impact of AT1R that seems to involve NFkB signaling.

All in all, this study adds a new role of miR-221/222 in cardiac electrical remodeling by showing the impact on GIRK1/4-mediated ion flux, β-adrenergic regulation of L-type Ca^{2+} channel function, cardiomyocyte calcium handling and contractility.

7. References

Agarwal, V., Bell, G. W., Nam, J. W., & Bartel, D. P. (2015). Predicting effective microRNA target sites in mammalian mRNAs. *ELife*, *4*(AUGUST2015), 1–38. https://doi.org/10.7554/eLife.05005

Aiba, T., & Tomaselli, G. F. (2010). Electrical remodeling in the failing heart. *Current Opinion in Cardiology*, *25*(1), 29–36. https://doi.org/10.1097/HCO.0b013e328333d3d6

Amini, S., Abak, A., Sakhinia, E., & Abhari, A. (2019). MicroRNA-221 and microRNA-222 in common human cancers: Expression, function, and triggering oftumor progression as a key modulator. *Lab Medicine*, *50*(4), 333–347. https://doi.org/10.1093/labmed/lmz002

Anderson, A., Kulkarni, K., Marron Fernandez De Velasco, E., Carlblom, N., Xia, Z., Nakano, A., Martemyanov, K. A., Tolkacheva, E. G., & Wickman, K. (2018). Expression and relevance of the G protein-gated K+ channel in the mouse ventricle. *Scientific Reports*, *8*(1), 1–14. https://doi.org/10.1038/s41598-018-19719-x

Azevedo, P. S., Polegato, B. F., Minicucci, M. F., Paiva, S. A. R., & Zornoff, L. A. M. (2016). Cardiac Remodeling: Concepts, Clinical Impact, Pathophysiological Mechanisms and Pharmacologic Treatment. *Arquivos Brasileiros de Cardiologia*, *106*(1), 62–69. https://doi.org/10.5935/abc.20160005

Baggish, A. L., Hale, A., Weiner, R. B., Lewis, G. D., Systrom, D., Wang, F., Wang, T. J., & Chan, S. Y. (2011). Dynamic regulation of circulating microRNA during acute exhaustive exercise and sustained aerobic exercise training. *Journal of Physiology*, *589*(16), 3983–3994. https://doi.org/10.1113/jphysiol.2011.213363

Banerjee, I., Fuseler, J. W., Price, R. L., Borg, T. K., & Baudino, T. A. (2007). Determination of cell types and numbers during cardiac development in the neonatal and adult rat and mouse. *American Journal of Physiology - Heart and Circulatory Physiology*, *293*(3), 1883–1891. https://doi.org/10.1152/ajpheart.00514.2007

Bang, C., Batkai, S., Dangwal, S., Gupta, S. K., Foinquinos, A., Holzmann, A., Just, A., Remke, J., Zimmer, K., Zeug, A., Ponimaskin, E., Schmiedl, A., Yin, X., Mayr, M., Halder, R., Fischer, A., Engelhardt, S., Wei, Y., Schober, A., … Thum, T. (2014). Cardiac fibroblast-derived microRNA passenger strand-enriched exosomes mediate cardiomyocyte hypertrophy. *Journal of Clinical Investigation*, *124*(5), 2136–2146. https://doi.org/10.1172/JCI70577

Bartos, D. C., Grandi, E., & Ripplinger, C. M. (2015). Ion channels in the heart. *Comprehensive Physiology*, *5*(3), 1423–1464. https://doi.org/10.1002/cphy.c140069

Bauersachs, J., & Thum, T. (2011). Biogenesis and regulation of cardiovascular MicroRNAs. *Circulation Research*, *109*(3), 334–347. https://doi.org/10.1161/CIRCRESAHA.110.228676

Belostotskaya, G. B., & Golovanova, T. A. (2014). Characterization of contracting cardiomyocyte colonies in the primary culture of neonatal rat myocardial cells: A model of in vitro cardiomyogenesis. *Cell Cycle*, *13*(6), 910–918. https://doi.org/10.4161/cc.27768

Bender, K., Wellner-Kienitz, M. C., Inanobe, A., Meyer, T., Kurachi, Y., & Pott, L. (2001). Overexpression of monomeric and multimeric GIRK4 subunits in rat atrial myocytes removes fast desensitization and reduces inward rectification of muscarinic K+ current (IK(ACh)). Evidence for functional homomeric GIRK4 channels. *Journal of Biological Chemistry*, *276*(31), 28873–28880. https://doi.org/10.1074/jbc.M102328200

Bers, D. M. (2002). Cardiac excitation-contraction coupling. *Nature*, *415*, 198–205.

Bers, D. M. (2008). Calcium cycling and signaling in cardiac myocytes. *Annual Review of Physiology*, *70*, 23–49. https://doi.org/10.1146/annurev.physiol.70.113006.100455

Binas, S., Knyrim, M., Hupfeld, J., Kloeckner, U., Rabe, S., Mildenberger, S., Quarch, K., Strätz, N., Misiak, D., Gekle, M., Grossmann, C., & Schreier, B. (2020). miR-221 and -222 target CACNA1C and KCNJ5 leading to altered cardiac ion channel expression and current density. *Cellular and Molecular Life Sciences*, *77*(5), 903–918. https://doi.org/10.1007/s00018-019-03217-y

Bootman, M. D., Fearnley, C., Smyrnias, I., MacDonald, F., & Roderick, H. L. (2009). An update on nuclear calcium signalling. *Journal of Cell Science*, *122*(14), 2337–2350. https://doi.org/10.1242/jcs.028100

Bootman, M. D., Higazi, D. R., Coombes, S., & Roderick, H. L. (2006). Calcium signalling during excitation-contraction coupling in mammalian atrial myocytes. *Journal of Cell Science*, *119*(19), 3915–3925. https://doi.org/10.1242/jcs.03223

Bouvy-Liivrand, M., De Sande, A. H., Pölönen, P., Mehtonen, J., Vuorenmaa, T., Niskanen, H., Sinkkonen, L., Kaikkonen, M. U., & Heinäniemi, M. (2017). Analysis of primary microRNA loci from nascent transcriptomes reveals regulatory domains governed by chromatin architecture. *Nucleic Acids Research*, *45*(17), 9837–9849. https://doi.org/10.1093/nar/gkx680

Cañón, S., Caballero, R., Herraiz-Martínez, A., Pérez-Hernández, M., López, B., Atienza, F., Jalife, J., Hove-Madsen, L., Delpón, E., & Bernad, A. (2016). miR-208b upregulation interferes with calcium handling in HL-1 atrial myocytes: Implications in human chronic atrial fibrillation. *Journal of Molecular and Cellular Cardiology*, *99*, 162–173. https://doi.org/10.1016/j.yjmcc.2016.08.012

Carmeliet, E. (2019). Pacemaking in cardiac tissue. From IK2 to a coupled-clock system. *Physiological Reports*, *7*(1), 1–11. https://doi.org/10.14814/phy2.13862

Carrillo, E. D., Escobar, Y., González, G., Hernández, A., Galindo, J. M., García, M. C., & Sánchez, J. A. (2011). Posttranscriptional regulation of the β 2-subunit of cardiac L-type Ca 2+ channels by microRNAs during long-term exposure to isoproterenol in Rats. *Journal of Cardiovascular Pharmacology*, *58*(5), 470–478. https://doi.org/10.1097/FJC.0b013e31822a789b

Cartledge, J. E., Kane, C., Dias, P., Tesfom, M., Clarke, L., Mckee, B., Al Ayoubi, S., Chester, A., Yacoub, M. H., Camelliti, P., & Terracciano, C. M. (2015). Functional crosstalk between cardiac fibroblasts and adult cardiomyocytes by solublemediators. *Cardiovascular Research*, *105*(3), 260–270. https://doi.org/10.1093/cvr/cvu264

Cha, T. J., Ehrlich, J. R., Chartier, D., Qi, X. Y., Xiao, L., & Nattel, S. (2006). Kir3-based inward rectifier potassium current: Potential role in atrial tachycardia remodeling effects on atrial repolarization and arrhythmias. *Circulation*, *113*(14), 1730–1737. https://doi.org/10.1161/CIRCULATIONAHA.105.561738

Chen, C., Ridzon, D. A., Broomer, A. J., Zhou, Z., Lee, D. H., Nguyen, J. T., Barbisin, M., Xu, N. L., Mahuvakar, V. R., Andersen, M. R., Lao, K. Q., Livak, K. J., & Guegler, K. J. (2005). Real-time quantification of microRNAs by stem-loop RT-PCR. *Nucleic Acids Research*, *33*(20), 1–9. https://doi.org/10.1093/nar/gni178

Chen, J., Kubalak, S. W., Minamisawa, S., Price, R. L., Becker, K. D., Hickey, R., Ross, J., & Chien, K. R. (1998). Selective requirement of myosin light chain 2v in embryonic heart function. *Journal of Biological Chemistry*, *273*(2), 1252–1256. https://doi.org/10.1074/jbc.273.2.1252

Chen, Q., Zhou, Y., Richards, A. M., & Wang, P. (2016). Up-regulation of miRNA-221 inhibits hypoxia/reoxygenation-induced autophagy through the DDIT4/mTORC1 and Tp53inp1/p62 pathways. *Biochemical and Biophysical Research Communications*, *474*(1), 168–174. https://doi.org/10.1016/j.bbrc.2016.04.090

Chen, X., Nakayama, H., Zhang, X., Ai, X., Harris, D. M., Tang, M., Zhang, H., Szeto, C., Stockbower, K., Berretta, R. M., Eckhart, A. D., Koch, W. J., Molkentin, J. D., & Houser, S. R. (2011). Calcium influx through Cav1.2 is a proximal signal for pathological cardiomyocyte hypertrophy. *Journal of Molecular and Cellular Cardiology*, *50*(3), 460–470. https://doi.org/10.1016/j.yjmcc.2010.11.012

Chen, X., Piacentino, V., Furukawa, S., Goldman, B., Margulies, K. B., & Houser, S. R. (2002). L-type Ca2+ channel density and regulation are altered in failing human ventricular myocytes and recover after support with mechanical assist devices. *Circulation Research*, *91*(6), 517–524. https://doi.org/10.1161/01.RES.0000033988.13062.7C

Cheng, Y., Du, L., Shi, Q., Jiao, H., Zhang, X., Hao, Y., Rong, H., Zhang, J., Jia, X., Guo, S., Kuang, W., Zhang, H., Chen, C., & Wang, F. (2013). Identification of miR-221 and -222 as important regulators in genotype IV swine hepatitis E virus ORF3-expressing HEK 293 cells. *Virus Genes*, *47*(1), 49–55. https://doi.org/10.1007/s11262-013-0912-4

Claycomb, W. C., Lanson, N. A., Stallworth, B. S., Egeland, D. B., Delcarpio, J. B., Bahinski, A., & Izzo, N. J. (1998). HL-1 cells: A cardiac muscle cell line that contracts and retains phenotypic characteristics of the adult cardiomyocyte. *Proceedings of the National Academy of Sciences of the United States of America*, *95*(6), 2979–2984. https://doi.org/10.1073/pnas.95.6.2979

Coote, J. H. (2013). Myths and realities of the cardiac vagus. *Journal of Physiology*, *591*(17), 4073–4085. https://doi.org/10.1113/jphysiol.2013.257758

Corey, S., & Clapham, D. E. (1998). Identification of native atrial G-protein-regulated inwardly rectifying K+ (GIRK4) channel homomultimers. *Journal of Biological Chemistry*, *273*(42), 27499–27504. https://doi.org/10.1074/jbc.273.42.27499

Corsten, M., Heggermont, W., Papageorgiou, A. P., Deckx, S., Tijsma, A., Verhesen, W., Van Leeuwen, R., Carai, P., Thibaut, H. J., Custers, K., Summer, G., Hazebroek, M., Verheyen, F., Neyts, J., Schroen, B., & Heymans, S. (2015). The microRNA-221/-222 cluster balances the antiviral and inflammatory response in viral myocarditis. *European Heart Journal*, *36*(42), 2909–2919. https://doi.org/10.1093/eurheartj/ehv321

Coskunpinar, E., Cakmak, H. A., Kalkan, A. K., Tiryakioglu, N. O., Erturk, M., & Ongen, Z. (2016). Circulating miR-221-3p as a novel marker for early prediction of acute myocardial infarction. *Gene*, *591*(1), 90–96. https://doi.org/10.1016/j.gene.2016.06.059

Da Costa Martins, P. A., Bourajjaj, M., Gladka, M., Kortland, M., Van Oort, R. J., Pinto, Y. M., Molkentin, J. D., & De Windt, L. J. (2008). Conditional Dicer gene deletion in the postnatal myocardium provokes spontaneous cardiac remodeling. *Circulation*, *118*(15), 1567–1576.

https://doi.org/10.1161/CIRCULATIONAHA.108.769984

Dascal, N., & Kahanovitch, U. (2015). Structure to Function of G Protein-Gated Inwardly Rectifying (GIRK) Channels. Chapter Two - The Roles of Gβγ and Gα in Gating and Regulation of GIRK Channels. In *International Review of Neurobiology (editors: Paul A. Slesinger and Kevin Wickman)* (Vol. 123, pp. 27–85).

Davies, A., Hendrich, J., Van Minh, A. T., Wratten, J., Douglas, L., & Dolphin, A. C. (2007). Functional biology of the α2δ subunits of voltage-gated calcium channels. *Trends in Pharmacological Sciences*, *28*(5), 220–228. https://doi.org/10.1016/j.tips.2007.03.005

Davlouros, P. A., Gkizas, V., Vogiatzi, C., Giannopoulos, G., Alexopoulos, D., & Deftereos, S. (2016). Calcium Homeostasis and Kinetics in Heart Failure. *Medicinal Chemistry*, *12*(2), 151–161. https://doi.org/10.2174/1573406412021602090994548

Dobrev, D., Friedrich, A., Voigt, N., Jost, N., Wettwer, E., Christ, T., Knaut, M., & Ravens, U. (2005). The G protein-gated potassium current IK,ACh is constitutively active in patients with chronic atrial fibrillation. *Circulation*, *112*(24), 3697–3706. https://doi.org/10.1161/CIRCULATIONAHA.105.575332

Dobrev, D., Graf, E., Wettwer, E., Himmel, H. M., Hála, O., Doerfel, C., Christ, T., Schüler, S., & Ravens, U. (2001). Molecular Basis of Downregulation of G-Protein – Coupled Inward Rectifying K♭ Current (IK,ACh) in Chronic Human Atrial Fibrillation. *Circulation*, *104*, 2551–2558.

Dobrev, D., Wettwer, E., Kortner, A., Knaut, M., Schüler, S., & Ravens, U. (2002). Human inward rectifier potassium channels in chronic and postoperative atrial fibrillation. *Cardiovascular Research*, *54*(2), 397–404. https://doi.org/10.1016/S0008-6363(01)00555-7

Dobrzynski, H., Marples, D. D. R., Musa, H., Yamanushi, T. T., Henderson, Z., Takagishi, Y., Honjo, H., Kodama, I., & Boyett, M. R. (2001). Distribution of the muscarinic K+ channel proteins Kir3.1 and Kir3.4 in the Ventricle, atrium, and sinoatrial node of heart. *Journal of Histochemistry and Cytochemistry*, *49*(10), 1221–1234. https://doi.org/10.1177/002215540104901004

Dolphin, A. C. (2006). A short history of voltage-gated calcium channels. *British Journal of Pharmacology*, *147*(SUPPL. 1), 56–62. https://doi.org/10.1038/sj.bjp.0706442

Egger, M., & Domenighetti, A. A. (2010). Adaptive and Maladaptive Remodeling of Cardiomyocyte Excitation-Contraction Coupling by Angiotensin II. *Trends in Cardiovascular Medicine*, *20*(3), 78–85. https://doi.org/10.1016/j.tcm.2010.06.001

Ehler, E., Moore-Morris, T., & Lange, S. (2013). Isolation and culture of neonatal mouse cardiomyocytes. *Journal of Visualized Experiments*, *79*, 1–10. https://doi.org/10.3791/50154

Ehrlich, J. R., Biliczki, P., Hohnloser, S. H., & Nattel, S. (2008). Atrial-Selective Approaches for the Treatment of Atrial Fibrillation. *Journal of the American College of Cardiology*, *51*(8), 787–792. https://doi.org/10.1016/j.jacc.2007.08.067

Eisner, D. A., Caldwell, J. L., Kistamás, K., & Trafford, A. W. (2017). Calcium and Excitation-Contraction Coupling in the Heart. *Circulation Research*, *121*(2), 181–195. https://doi.org/10.1161/CIRCRESAHA.117.310230

El-Armouche, A., & Eschenhangen, T. (2009). β-Adrenergic stimulation and myocardial function in the failing heart. *Heart Fail Rev*, *14*, 225–241. https://doi.org/10.1007/s10741-008-9132-8

Evangelista, A. M., Deschamps, A. M., Liu, D., Raghavachari, N., & Murphy, E. (2013). miR-222 contributes to sex-dimorphic cardiac eNOS expression via ets-1. *Physiological Genomics*, *45*(12), 493–498. https://doi.org/10.1152/physiolgenomics.00008.2013

Forrester, S. J., Booz, G. W., Sigmund, C. D., Coffman, T. M., Kawai, T., Rizzo, V., Scalia, R., & Eguchi, S. (2018). Angiotensin II signal transduction: An update on mechanisms of physiology and pathophysiology. *Physiological Reviews*, *98*(3), 1627–1738. https://doi.org/10.1152/physrev.00038.2017

Galardi, S., Mercatelli, N., Farace, M. G., & Ciafrè, S. A. (2011). NF-kB and c-Jun induce the expression of the oncogenic miR-221 and miR-222 in prostate carcinoma and glioblastoma cells. *Nucleic Acids Research*, *39*(9), 3892–3902. https://doi.org/10.1093/nar/gkr006

Gandini, M. A., Sandoval, A., & Felix, R. (2014). Patch-clamp recording of voltage-sensitive Ca2+ channels. *Cold Spring Harbor Protocols*, *2014*(4), 329–335. https://doi.org/10.1101/pdb.top066092

Geng, M., Lin, A., & Nguyen, T. P. (2020). Revisiting Antiarrhythmic Drug Therapy for Atrial Fibrillation: Reviewing Lessons Learned and Redefining Therapeutic Paradigms. *Frontiers in Pharmacology*, *11*(November), 1–23. https://doi.org/10.3389/fphar.2020.581837

Gonzalez, D. R., Beigi, F., Treuer, A. V., & Hare, J. M. (2007). Deficient ryanodine receptor S-nitrosylation increases sarcoplasmic reticulum calcium leak and arrhythmogenesis in cardiomyocytes. *Proceedings of the National Academy of Sciences of the United States of America*, *104*(51), 20612–20617. https://doi.org/10.1073/pnas.0706796104

Goonasekera, S. A., Hammer, K., Auger-Messier, M., Bodi, I., Chen, X., Zhang, H., Reiken, S., Elrod, J. W., Correll, R. N., York, A. J., Sargent, M. A., Hofmann, F., Moosmang, S., Marks, A. R., Houser,

S. R., Bers, D. M., & Molkentin, J. D. (2012). Decreased cardiac L-type Ca 2+channel activity induces hypertrophy and heart failure in mice. *Journal of Clinical Investigation*, *122*(1), 280–290. https://doi.org/10.1172/JCI58227

Grune, T., Ott, C., Häseli, S., Höhn, A., & Jung, T. (2019). The "MYOCYTER" – Convert cellular and cardiac contractions into numbers with ImageJ. *Scientific Reports*, *9*(1), 1–13. https://doi.org/10.1038/s41598-019-51676-x

Ha, M., & Kim, V. N. (2014). Regulation of microRNA biogenesis. *Nature Reviews Molecular Cell Biology*, *15*(8), 509–524. https://doi.org/10.1038/nrm3838

Harada, M., Luo, X., Murohara, T., Yang, B., Dobrev, D., & Nattel, S. (2014). MicroRNA regulation and cardiac calcium signaling: Role in cardiac disease and therapeutic potential. *Circulation Research*, *114*(4), 689–705. https://doi.org/10.1161/CIRCRESAHA.114.301798

Häseli, S., Deubel, S., Jung, T., Grune, T., & Ott, C. (2020). Cardiomyocyte Contractility and Autophagy in a Premature Senescence Model of Cardiac Aging. *Oxidative Medicine and Cellular Longevity*, *2020*. https://doi.org/10.1155/2020/8141307

Hibino, H., Inanobe, A., Furutani, K., Murakami, S., Findlay, I., & Kurachi, Y. (2010). Inwardly rectifying potassium channels: Their structure, function, and physiological roles. *Physiological Reviews*, *90*(1), 291–366. https://doi.org/10.1152/physrev.00021.2009

Hille, B. (1973). Potassium channels in myelinated nerve selective permeability to small cations. *Journal of General Physiology*, *61*(6), 669–686. https://doi.org/10.1085/jgp.61.6.669

Huang, D., Chen, Z., Wang, J., Chen, Y., Liu, D., & Lin, K. (2020). MicroRNA-221 is a potential biomarker of myocardial hypertrophy and fibrosis in hypertrophic obstructive cardiomyopathy. *Bioscience Reports*, *40*(1), 1–13. https://doi.org/10.1042/BSR20191234

Jeong, G., Lim, Y. H., Kim, N. J., Wee, G., & Kim, Y. K. (2017). Knockout of miR-221 and miR-222 reveals common and specific targets for paralogous miRNAs. *RNA Biology*, *14*(2), 197–205. https://doi.org/10.1080/15476286.2016.1269994

Jin, W., Klem, A. M., Lewis, J. H., & Lu, Z. (1999). Mechanisms of inward-rectifier K+ channel inhibition by tertiapin-Q. *Biochemistry*, *38*(43), 14294–14301. https://doi.org/10.1021/bi991206j

Kabekkodu, S. P., Shukla, V., Varghese, V. K., D'Souza, J., Chakrabarty, S., & Satyamoorthy, K. (2018). Clustered miRNAs and their role in biological functions and diseases. *Biological Reviews*, *93*(4), 1955–1986. https://doi.org/10.1111/brv.12428

Kakimoto, Y., Tanaka, M., Hayashi, H., Yokoyama, K., & Osawa, M. (2018). Overexpression of miR-221 in sudden death with cardiac hypertrophy patients. *Heliyon*, *4*(6), e00639. https://doi.org/10.1016/j.heliyon.2018.e00639

Kanjhan, R., Coulson, E. J., Adams, D. J., & Bellingham, M. C. (2005). Tertiapin-Q blocks recombinant and native large conductance K+ channels in a use-dependent manner. *Journal of Pharmacology and Experimental Therapeutics*, *314*(3), 1353–1361. https://doi.org/10.1124/jpet.105.085928

Kennedy, M. E., Nemec, J., Corey, S., Wickman, K., & Clapham, D. E. (1999). GIRK4 confers appropriate processing and cell surface localization to G- protein-gated potassium channels. *Journal of Biological Chemistry*, *274*(4), 2571–2582. https://doi.org/10.1074/jbc.274.4.2571

Kijlstra, J. D., Hu, D., Mittal, N., Kausel, E., Van Der Meer, P., Garakani, A., & Domian, I. J. (2015). Integrated Analysis of Contractile Kinetics, Force Generation, and Electrical Activity in Single Human Stem Cell-Derived Cardiomyocytes. *Stem Cell Reports*, *5*(6), 1226–1238. https://doi.org/10.1016/j.stemcr.2015.10.017

Kitamura, H., Yokoyama, M., Akita, H., Matsushita, K., Kurachi, Y., & Yamada, M. (2000). Tertiapin potently and selectively blocks muscarinic K+ channels in rabbit cardiac myocytes. *Journal of Pharmacology and Experimental Therapeutics*, *293*(1), 196–205.

Kulkarni, K., Xie, X., De Velasco, E. M. F., Anderson, A., Martemyanov, K. A., Wickman, K., & Tolkacheva, E. G. (2018). The influences of the M2R-GIRK4-RGS6 dependent parasympathetic pathway on electrophysiological properties of the mouse heart. *PLoS ONE*, *13*(4), 1–12. https://doi.org/10.1371/journal.pone.0193798

Lai, T. C., Lee, T. L., Chang, Y. C., Chen, Y. C., Lin, S. R., Lin, S. W., Pu, C. M., Tsai, J. S., & Chen, Y. L. (2020). MicroRNA-221/222 Mediates ADSC-Exosome-Induced Cardioprotection Against Ischemia/Reperfusion by Targeting PUMA and ETS-1. *Frontiers in Cell and Developmental Biology*, *8*(December), 1–17. https://doi.org/10.3389/fcell.2020.569150

Landstrom, A. P., Dobrev, D., & Wehrens, X. H. T. (2017). Calcium Signaling and Cardiac Arrhythmias. *Circulation Research*, *120*(12), 1969–1993. https://doi.org/10.1161/CIRCRESAHA.117.310083

Lee, D. S., Chen, J. H., Lundy, D. J., Liu, C. H., Hwang, S. M., Pabon, L., Shieh, R. C., Chen, C. C., Wu, S. N., Yan, Y. T., Lee, S. T., Chiang, P. M., Chien, S., Murry, C. E., & Hsieh, P. C. H. (2015). Defined MicroRNAs Induce Aspects of Maturation in Mouse and Human Embryonic-Stem-Cell-Derived Cardiomyocytes. *Cell Reports*, *12*(12), 1960–1967. https://doi.org/10.1016/j.celrep.2015.08.042

Lee, S. W., Li, Q., Libbus, I., Xie, X., Kenknight, B. H., Garry, M. G., & Tolkacheva, E. G. (2016). Chronic

cyclic vagus nerve stimulation has beneficial electrophysiological effects on healthy hearts in the absence of autonomic imbalance. *Physiological Reports*, *4*(9), 1–8. https://doi.org/10.14814/phy2.12786

Li, X., Shen, L., Zhao, F., Zou, X., He, Y., Zhang, F., Zhang, C., Yu, B., & Cao, Z. (2017). Modification of distinct ion channels differentially modulates Ca2+ dynamics in primary cultured rat ventricular cardiomyocytes. *Scientific Reports*, *7*(November 2016), 1–14. https://doi.org/10.1038/srep40952

Liang, B., Nissen, J. D., Laursen, M., Wang, X., Skibsbye, L., Hearing, M. C., Andersen, M. N., Rasmussen, H. B., Wickman, K., Grunnet, M., Olesen, S. P., & Jespersen, T. (2014). G-protein-coupled inward rectifier potassium current contributes to ventricular repolarization. *Cardiovascular Research*, *101*(1), 175–184. https://doi.org/10.1093/cvr/cvt240

Liao, R., & Jain, M. (2007). Isolation, culture, and functional analysis of adult mouse cardiomyocytes. *Methods in Molecular Medicine*, *139*, 251–262. https://doi.org/10.1007/978-1-59745-571-8_16

Liao, Y., Asakura, M., Takashima, S., Ogai, A., Asano, Y., Asanuma, H., Minamino, T., Tomoike, H., Hori, M., & Kitakaze, M. (2005). Benidipine, a long-acting calcium channel blocker, inhibits cardiac remodeling in pressure-overloaded mice. *Cardiovascular Research*, *65*(4), 879–888. https://doi.org/10.1016/j.cardiores.2004.11.006

Liu, C. M., & Hermann, T. E. (1978). Characterization of ionomycin as a calcium ionophore. *Journal of Biological Chemistry*, *253*(17), 5892–5894. https://doi.org/10.1016/s0021-9258(17)34550-7

Liu, J., Kim, K., Morales, M. J., Heximer, S. P., Hui, C., & Backx, P. H. (2015). Kv4.3-Encoded Fast Transient Outward Current Is Presented in Kv4.2 Knockout Mouse Cardiomyocytes. *PLoS ONE*, *10*(7), 1–15. https://doi.org/10.1371/journal.pone.0133274

Liu, X., Xiao, J., Zhu, H., Wei, X., Platt, C., Damilano, F., Xiao, C., Bezzerides, V., Boström, P., Che, L., Zhang, C., Spiegelman, B. M., & Rosenzweig, A. (2015). MiR-222 is necessary for exercise-induced cardiac growth and protects against pathological cardiac remodeling. *Cell Metabolism*, *21*(4), 584–595. https://doi.org/10.1016/j.cmet.2015.02.014

Lok, S. I., De Jonge, N., Van Kuik, J., Van Geffen, A. J. P., Huibers, M. M. H., Van Der Weide, P., Siera, E., Winkens, B., Doevendans, P. A., De Weger, R. A., & Da Costa Martins, P. A. (2015). MicroRNA expression in myocardial tissue and plasma of patients with end-stage heart failure during LVAD support: Comparison of continuous and pulsatile devices. *PLoS ONE*, *10*(10), 1–13. https://doi.org/10.1371/journal.pone.0136404

Louch, W. E., Koivumäki, J. T., & Tavi, P. (2015). Calcium signalling in developing cardiomyocytes: Implications for model systems and disease. *Journal of Physiology*, *593*(5), 1047–1063. https://doi.org/10.1113/jphysiol.2014.274712

Lyu, L., Wang, H., Li, B., Qin, Q., Qi, L., Nagarkatti, M., Nagarkatti, P., Janicki, J. S., Wang, X. L., & Cui, T. (2015). A critical role of cardiac fibroblast-derived exosomes in activating renin angiotensin system in cardiomyocytes. *Journal of Molecular and Cellular Cardiology*, *89*, 268–279. https://doi.org/10.1016/j.yjmcc.2015.10.022

Mesirca, P., Alig, J., Torrente, A. G., Müller, J. C., Marger, L., Rollin, A., Marquilly, C., Vincent, A., Dubel, S., Bidaud, I., Fernandez, A., Seniuk, A., Engeland, B., Singh, J., Miquerol, L., Ehmke, H., Eschenhagen, T., Nargeot, J., Wickman, K., … Mangoni, M. E. (2014). Cardiac arrhythmia induced by genetic silencing of "funny" (f) channels is rescued by GIRK4 inactivation. *Nature Communications*, *5*(May). https://doi.org/10.1038/ncomms5664

Mesirca, P., Marger, L., Toyoda, F., Rizzetto, R., Audoubert, M., Dubel, S., Torrente, A. G., DiFrancesco, M. L., Muller, J. C., Leoni, A. L., Couette, B., Nargeot, J., Clapham, D. E., Wickman, K., & Mangoni, M. E. (2013). The G-protein-gated K+ channel, IKACh, is required for regulation of pacemaker activity and recovery of resting heart rate after sympathetic stimulation. *Journal of General Physiology*, *142*(2), 113–126. https://doi.org/10.1085/jgp.201310996

Mintert-Jancke, E. (2010). *regulation of cardiac GIRK channels in atrial myocytes Die Rolle von Kir3 . 1- und Kir3 . 4- Untereinheiten in der Regulation kardialer GIRK-Kanäle in Vorhofmyozyten. October.*

Mintert, E., Bösche, L. I., Rinne, A., Timpert, M., Kienitz, M. C., Pott, L., & Bender, K. (2007). Generation of a constitutive Na+-dependent inward-rectifier current in rat adult atrial myocytes by overexpression of Kir3.4. *Journal of Physiology*, *585*(1), 3–13. https://doi.org/10.1113/jphysiol.2007.140772

Moretti, F., Thermann, R., & Hentze, M. W. (2010). Mechanism of translational regulation by miR-2 from sites in the 5′ untranslated region or the open reading frame. *Rna*, *16*(12), 2493–2502. https://doi.org/10.1261/rna.2384610

Nass, R. D., Aiba, T., Tomaselli, G. F., & Akar, F. G. (2008). Mechanisms of Disease: Ion channel remodeling in the failing ventricle. *Nature Clinical Practice Cardiovascular Medicine*, *5*(4), 196–207. https://doi.org/10.1038/ncpcardio1130

Nenasheva, T. A., Neary, M., Mashanov, G. I., Birdsall, N. J. M., Breckenridge, R. A., & Molloy, J. E. (2013). Abundance, distribution, mobility and oligomeric state of M2 muscarinic acetylcholine

receptors in live cardiac muscle. *Journal of Molecular and Cellular Cardiology*, *57*(1), 129–136. https://doi.org/10.1016/j.yjmcc.2013.01.009

Nerbonne, J. M., & Kass, R. S. (2005). Molecular physiology of cardiac repolarization. *Physiological Reviews*, *85*(4), 1205–1253. https://doi.org/10.1152/physrev.00002.2005

Nobles, M., Sebastian, S., & Tinker, A. (2010). HL-1 cells express an inwardly rectifying K+ current activated via muscarinic receptors comparable to that in mouse atrial myocytes. *Pflugers Archiv European Journal of Physiology*, *460*(1), 99–108. https://doi.org/10.1007/s00424-010-0799-z

Oikawa, S., Kai, Y., Mano, A., Ohata, H., Kurabayashi, A., Tsuda, M., & Kakinuma, Y. (2021). Non-neuronal cardiac acetylcholine system playing indispensable roles in cardiac homeostasis confers resiliency to the heart. *The Journal of Physiological Sciences*, *71*(2), 1–20. https://doi.org/10.1186/s12576-020-00787-6

Pandit, S. V. (2018). Ionic Mechanisms of Atrial Action Potentials. In *Cardiac Electrophysiology: From Cell to Bedside* (Seventh Ed, pp. 293–303). Elsevier. https://doi.org/10.1016/B978-0-323-44733-1.00031-6

Park, Y. B. (1994). Ion selectivity and gating of small conductance Ca(2+)-activated K+ channels in cultured rat adrenal chromaffin cells. *The Journal of Physiology*, *481*(3), 555–570. https://doi.org/10.1113/jphysiol.1994.sp020463

Pellman, J., Zhang, J., & Sheikh, F. (2016). Myocyte-fibroblast communication in cardiac fibrosis and arrhythmias: Mechanisms and model systems. *Journal of Molecular and Cellular Cardiology*, *94*, 22–31. https://doi.org/10.1016/j.yjmcc.2016.03.005

Peter, A. K., Bjerke, M. A., & Leinwand, L. A. (2016). Biology of the cardiac myocyte in heart disease. *Molecular Biology of the Cell*, *27*(14), 2149–2160. https://doi.org/10.1091/mbc.E16-01-0038

Pinto, A. R., Ilinykh, A., Ivey, M. J., Kuwabara, J. T., D'antoni, M. L., Debuque, R., Chandran, A., Wang, L., Arora, K., Rosenthal, N. A., & Tallquist, M. D. (2016). Revisiting cardiac cellular composition. *Circulation Research*, *118*(3), 400–409. https://doi.org/10.1161/CIRCRESAHA.115.307778

Posokhova, E., Ng, D., Opel, A., Masuho, I., Tinker, A., Biesecker, L. G., Wickman, K., & Martemyanov, K. A. (2013). Essential role of the m2R-RGS6-IKACh pathway in controlling intrinsic heart rate variability. *PloS One*, *8*(10), 2–11. https://doi.org/10.1371/journal.pone.0076973

Posokhova, E., Wydeven, N., Allen, K. L., Wickman, K., & Martemyanov, K. A. (2010). RGS6/Gβ5 complex accelerates IKACh gating kinetics in atrial myocytes and modulates parasympathetic regulation of heart rate. *Circulation Research*, *107*(11), 1350–1354. https://doi.org/10.1161/CIRCRESAHA.110.224212

Ramalingam, P., Palanichamy, J. K., Singh, A., Das, P., Bhagat, M., Kassab, M. A., Sinha, S., & Chattopadhyay, P. (2014). Biogenesis of intronic miRNAs located in clusters by independent transcription and alternative splicing. *Rna*, *20*(1), 76–87. https://doi.org/10.1261/rna.041814.113

Ramos, A. E., Lo, C., Estephan, L. E., Tai, Y. Y., Tang, Y., Zhao, J., Sugahara, M., Gorcsan, J., Brown, M. G., Lieberman, D. E., Chan, S. Y., & Baggish, A. L. (2018). Specific circulating microRNAs display dose-dependent responses to variable intensity and duration of endurance exercise. *American Journal of Physiology - Heart and Circulatory Physiology*, *315*(2), H273–H283. https://doi.org/10.1152/ajpheart.00741.2017

Raphemot, R., Kadakia, R. J., Olsen, M. L., Banerjee, S., Days, E., Smith, S. S., Weaver, C. D., & Denton, J. S. (2013). Development and validation of fluorescence-based and automated patch clamp-based functional assays for the inward rectifier potassium channel Kir4.1. *Assay and Drug Development Technologies*, *11*(9–10), 532–543. https://doi.org/10.1089/adt.2013.544

Ravegnini, G., Cargnin, S., Sammarini, G., Zanotti, F., Bermejo, J. L., Hrelia, P., Terrazzino, S., & Angelini, S. (2019). Prognostic role of miR-221 and miR-222 expression in cancer patients: A systematic review and meta-analysis. *Cancers*, *11*(7), 1–25. https://doi.org/10.3390/cancers11070970

Ravens, U. (2010). Antiarrhythmic therapy in atrial fibrillation. *Pharmacology & Therapeutics*, *128*(1), 129–145. https://doi.org/10.1016/j.pharmthera.2010.06.004

Ravens, U. (2017). Atrial-selective K+ channel blockers – potential antiarrhythmic drugs in atrial fibrillation? *Canadian Journal of Physiology and Pharmacology*.

Rosati, B., Yan, Q., Lee, M. S., Liou, S. R., Ingalls, B., Foell, J., Kamp, T. J., & Mckinnon, D. (2011). Robust L-type calcium current expression following heterozygous knockout of the Cav1.2 gene in adult mouse heart. *Journal of Physiology*, *589*(13), 3275–3288. https://doi.org/10.1113/jphysiol.2011.210237

Ryazansky, S. S., Gvozdev, V. A., & Berezikov, E. (2011). Evidence for post-transcriptional regulation of clustered microRNAs in Drosophila. *BMC Genomics*, *12*. https://doi.org/10.1186/1471-2164-12-371

Saleem, U., Mannhardt, I., Braren, I., Denning, C., Eschenhagen, T., & Hansen, A. (2020). Force and Calcium Transients Analysis in Human Engineered Heart Tissues Reveals Positive Force-Frequency Relation at Physiological Frequency. *Stem Cell Reports*, *14*(2), 312–324.

https://doi.org/10.1016/j.stemcr.2019.12.011

Saw, E. L., Kakinuma, Y., Fronius, M., & Katare, R. (2018). The non-neuronal cholinergic system in the heart: A comprehensive review. *Journal of Molecular and Cellular Cardiology*, *125*(July), 129–139. https://doi.org/10.1016/j.yjmcc.2018.10.013

Saxena, A., & Tabin, C. J. (2010). miRNA-processing enzyme Dicer is necessary for cardiac outflow tract alignment and chamber septation. *Proceedings of the National Academy of Sciences of the United States of America*, *107*(1), 87–91. https://doi.org/10.1073/pnas.0912870107

Sayed, D., Hong, C., Chen, I. Y., Lypowy, J., & Abdellatif, M. (2007). MicroRNAs play an essential role in the development of cardiac hypertrophy. *Circulation Research*, *100*(3), 416–424. https://doi.org/10.1161/01.RES.0000257913.42552.23

Schlüter, K. D., & Wenzel, S. (2008). Angiotensin II: A hormone involved in and contributing to pro-hypertrophic cardiac networks and target of anti-hypertrophic cross-talks. *Pharmacology and Therapeutics*, *119*(3), 311–325. https://doi.org/10.1016/j.pharmthera.2008.05.010

Schmitz, B., & Brand, S.-M. S. M. (2018). Commentary: MicroRNA-221/222 Family Counteracts Myocardial Fibrosis in Pressure Overload-Induced Heart Failure. *Frontiers in Cardiovascular Medicine*, *5*, 1–2. https://doi.org/10.3389/fcvm.2018.00095

Schreier, B., Rabe, S., Schneider, B., Bretschneider, M., Rupp, S., Ruhs, S., Neumann, J., Rueckschloss, U., Sibilia, M., Gotthardt, M., Grossmann, C., & Gekle, M. (2013). Loss of epidermal growth factor receptor in vascular smooth muscle cells and cardiomyocytes causes arterial hypotension and cardiac hypertrophy. *Hypertension*, *61*(2), 333–340. https://doi.org/10.1161/HYPERTENSIONAHA.112.196543

Schreier, B., Rabe, S., Winter, S., Ruhs, S., Mildenberger, S., Schneider, B., Sibilia, M., Gotthardt, M., Kempe, S., Mäder, K., Grossmann, C., & Gekle, M. (2014). Moderate inappropriately high aldosterone/NaCl constellation in mice: Cardiovascular effects and the role of cardiovascular epidermal growth factor receptor. *Scientific Reports*, *4*. https://doi.org/10.1038/srep07430

Semsarian, C., Ahmad, I., Giewat, M., Georgakopoulos, D., Schmitt, J. P., McConnell, B. K., Reiken, S., Mende, U., Marks, A. R., Kass, D. A., Seidman, C. E., & Seidman, J. G. (2002). The L-type calcium channel inhibitor diltiazem prevents cardiomyopathy in a mouse model. *Journal of Clinical Investigation*, *109*(8), 1013–1020. https://doi.org/10.1172/JCI200214677

Shen, F., Huang, W., Xing, B., Fang, X., Feng, M., & Jiang, C. (2018). Genistein Improves the Major Depression through Suppressing the Expression of miR-221/222 by Targeting Connexin 43. *Psychiatry Investigation*, *15*(10), 919–925. https://doi.org/10.30773/pi.2018.06.29

Shimizu, I., & Minamino, T. (2016). Physiological and pathological cardiac hypertrophy. *Journal of Molecular and Cellular Cardiology*, *97*, 245–262. https://doi.org/10.1016/j.yjmcc.2016.06.001

Smedler, E., & Uhlén, P. (2014). Frequency decoding of calcium oscillations. *Biochimica et Biophysica Acta - General Subjects*, *1840*(3), 964–969. https://doi.org/10.1016/j.bbagen.2013.11.015

Smith, G. L., & Eisner, D. A. (2019). Calcium Buffering in the Heart in Health and Disease. *Circulation*, *139*(20), 2358–2371. https://doi.org/10.1161/CIRCULATIONAHA.118.039329

Soattin, L., Lubberding, A. F., Bentzen, B. H., Christ, T., & Jespersen, T. (2020). Inhibition of Adenosine Pathway Alters Atrial Electrophysiology and Prevents Atrial Fibrillation. *Frontiers in Physiology*, *11*(June), 1–14. https://doi.org/10.3389/fphys.2020.00493

Song, Q., An, Q., Niu, B., Lu, X., Zhang, N., & Cao, X. (2019). Role of miR-221/222 in Tumor Development and the Underlying Mechanism. *Journal of Oncology*, *2019*. https://doi.org/10.1155/2019/7252013

Stimers, J. R., Song, L., Rusch, N. J., & Rhee, S. W. (2015). Overexpression of the large-conductance, Ca2+-activated K+(BK) channel shortens action potential duration in HL-1 cardiomyocytes. *PLoS ONE*, *10*(6), 1–17. https://doi.org/10.1371/journal.pone.0130588

Striessnig, J., Pinggera, A., Kaur, G., Bock, G., & Tuluc, P. (2014). L-type Ca2+ channels in heart and brain. *Wiley Interdisciplinary Reviews: Membrane Transport and Signaling*, *3*(2), 15–38. https://doi.org/10.1002/wmts.102

Su, M., Chen, Z., Wang, C., Song, L., Zou, Y., Zhang, L., Hui, R., & Wang, J. (2016). Cardiac-Specific Overexpression of miR-222 Induces Heart Failure and Inhibits Autophagy in Mice. *Cellular Physiology and Biochemistry*, *39*(4), 1503–1511. https://doi.org/10.1159/000447853

Su, M., Wang, J., Wang, C., Wang, X., Dong, W., Qiu, W., Wang, Y., Zhao, X., Zou, Y., Song, L., Zhang, L., & Hui, R. (2015). MicroRNA-221 inhibits autophagy and promotes heart failure by modulating the p27/CDK2/mTOR axis. *Cell Death and Differentiation*, *22*(6), 986–999. https://doi.org/10.1038/cdd.2014.187

Sun, J., Morgan, M., Shen, R. F., Steenbergen, C., & Murphy, E. (2007). Preconditioning results in S-nitrosylation of proteins involved in regulation of mitochondrial energetics and calcium transport. *Circulation Research*, *101*(11), 1155–1163. https://doi.org/10.1161/CIRCRESAHA.107.155879

Sun, J., Picht, E., Ginsburg, K. S., Bers, D. M., Steenbergen, C., & Murphy, E. (2006). Hypercontractile

female hearts exhibit increased S-nitrosylation of the L-type Ca2+ channel α1 subunit and reduced ischemia/reperfusion injury. *Circulation Research*, *98*(3), 403–411. https://doi.org/10.1161/01.RES.0000202707.79018.0a

Sun, L., Zhu, W., Zhao, P., Zhang, J., Lu, Y., Zhu, Y., Zhao, W., Liu, Y., Chen, Q., & Zhang, F. (2020). Down-Regulated Exosomal MicroRNA-221 – 3p Derived From Senescent Mesenchymal Stem Cells Impairs Heart Repair. *Frontiers in Cell and Developmental Biology*, *8*(May), 1–14. https://doi.org/10.3389/fcell.2020.00263

Sun, T., Du, S. Y., Armenia, J., Qu, F., Fan, J., Wang, X., Fei, T., Komura, K., Liu, S. X., Lee, G. S. M., & Kantoff, P. W. (2018). Expression of lncRNA MIR222HG cotranscribed from the miR-221/222 gene promoter facilitates the development of castration-resistant prostate cancer. *Oncogenesis*, *7*(3). https://doi.org/10.1038/s41389-018-0039-5

Takahashi, H., Maehara, K., Onuki, N., Saito, T., & Maruyama, Y. (2003). Decreased contractility of the left ventricle is induced by the neurotransmitter acetylcholine, but not by vagal stimulation in rats. *Japanese Heart Journal*, *44*(2), 257–270. https://doi.org/10.1536/jhj.44.257

Tang, R., Long, T., Lui, K. O., Chen, Y., & Huang, Z. P. (2020). A Roadmap for Fixing the Heart: RNA Regulatory Networks in Cardiac Disease. *Molecular Therapy - Nucleic Acids*, *20*(June), 673–686. https://doi.org/10.1016/j.omtn.2020.04.007

Tatsuguchi, M., Seok, H. Y., Callis, T. E., Thomson, J. M., Chen, J. F., Newman, M., Rojas, M., Hammond, S. M., & Wang, D. Z. (2007). Expression of microRNAs is dynamically regulated during cardiomyocyte hypertrophy. *Journal of Molecular and Cellular Cardiology*, *42*(6), 1137–1141. https://doi.org/10.1016/j.yjmcc.2007.04.004

Tham, Y. K., Bernardo, B. C., Ooi, J. Y. Y., Weeks, K. L., & McMullen, J. R. (2015). Pathophysiology of cardiac hypertrophy and heart failure: signaling pathways and novel therapeutic targets. *Archives of Toxicology*, *89*(9), 1401–1438. https://doi.org/10.1007/s00204-015-1477-x

Thomson, D. W., Bracken, C. P., Szubert, J. M., & Goodall, G. J. (2013). On Measuring miRNAs after Transient Transfection of Mimics or Antisense Inhibitors. *PLoS ONE*, *8*(1), 1–7. https://doi.org/10.1371/journal.pone.0055214

Tian, Z., Miyata, K., Kadomatsu, T., Horiguchi, H., Fukushima, H., Tohyama, S., Ujihara, Y., Okumura, T., Yamaguchi, S., Zhao, J., Endo, M., Morinaga, J., Sato, M., Sugizaki, T., Zhu, S., Terada, K., Sakaguchi, H., Komohara, Y., Takeya, M., … Oike, Y. (2016). ANGPTL2 activity in cardiac pathologies accelerates heart failure by perturbing cardiac function and energy metabolism. *Nature Communications*, *7*. https://doi.org/10.1038/ncomms13016

Touhara, K. K., & Mackinnon, R. (2018). Molecular basis of signaling specificity between GIRK channels and GPCRs. *ELife*, *7*, 1–23. https://doi.org/10.7554/eLife.42908

Uchida, S., & Dimmeler, S. (2015). Exercise controls non-coding RNAs. *Cell Metabolism*, *21*(4), 511–512. https://doi.org/10.1016/j.cmet.2015.03.014

Uhlén, P., & Fritz, N. (2010). Biochemistry of calcium oscillations. *Biochemical and Biophysical Research Communications*, *396*(1), 28–32. https://doi.org/10.1016/j.bbrc.2010.02.117

Verjans, R., Peters, T., Beaumont, F. J., Van Leeuwen, R., Van Herwaarden, T., Verhesen, W., Munts, C., Bijnen, M., Henkens, M., Diez, J., De Windt, L. J., Van Nieuwenhoven, F. A., Van Bilsen, M., Goumans, M. J., Heymans, S., González, A., & Schroen, B. (2018). MicroRNA-221/222 family counteracts myocardial fibrosis in pressure overload-induced heart failure. *Hypertension*, *71*(2), 280–288. https://doi.org/10.1161/HYPERTENSIONAHA.117.10094

Voigt, N., Abu-Taha, I., Heijman, J., & Dobrev, D. (2014). Constitutive activity of the acetylcholine-activated potassium current IK,ACh in cardiomyocytes. In *Advances in Pharmacology* (Vol. 70, Issue June, pp. 393–409). https://doi.org/10.1016/B978-0-12-417197-8.00013-4

Vujic, A., Lerchenmüller, C., Wu, T. Di, Guillermier, C., Rabolli, C. P., Gonzalez, E., Senyo, S. E., Liu, X., Guerquin-Kern, J. L., Steinhauser, M. L., Lee, R. T., & Rosenzweig, A. (2018). Exercise induces new cardiomyocyte generation in the adult mammalian heart. *Nature Communications*, *9*(1), 1–9. https://doi.org/10.1038/s41467-018-04083-1

Walfridsson, H., Anfinsen, O. G., Berggren, A., Frison, L., Jensen, S., Linhardt, G., Nordkam, A. C., Sundqvist, M., & Carlsson, L. (2015). Is the acetylcholine-regulated inwardly rectifying potassium current a viable antiarrhythmic target? Translational discrepancies of AZD2927 and A7071 in dogs and humans. *Europace*, *17*(3), 473–482. https://doi.org/10.1093/europace/euu192

Walquist, M. J., & El-Gewely, M. R. (2018). Mutagenesis: Site-Directed. *ELS*, *February*, 1–14. https://doi.org/10.1002/9780470015902.a0001000.pub4

Wang, C., Wang, S., Zhao, P., Wang, X., Wang, J., Wang, Y., Song, L., Zou, Y., & Hui, R. (2012). MiR-221 promotes cardiac hypertrophy in vitro through the modulation of p27 expression. *Journal of Cellular Biochemistry*, *113*(6), 2040–2046. https://doi.org/10.1002/jcb.24075

Wang, X., Liang, B., Skibsbye, L., Olesen, S. P., Grunnet, M., & Jespersen, T. (2013). GIRK channel activation via adenosine or muscarinic receptors has similar effects on rat atrial electrophysiology.

Journal of Cardiovascular Pharmacology, *62*(2), 192–198. https://doi.org/10.1097/FJC.0b013e3182965221

Wardle, S. L., Bailey, M. E. S., Kilikevicius, A., Malkova, D., Wilson, R. H., Venckunas, T., & Moran, C. N. (2015). Plasma microRNA levels differ between endurance and strength athletes. *PLoS ONE*, *10*(4), 1–15. https://doi.org/10.1371/journal.pone.0122107

Weaver, C. D., Harden, D., Dworetzky, S. I., Robertson, B., & Knox, R. J. (2004). A thallium-sensitive, fluorescence-based assay for detecting and characterizing potassium channel modulators in mammalian cells. *Journal of Biomolecular Screening*, *9*(8), 671–677. https://doi.org/10.1177/1087057104268749

Wickman, K., Nemec, J., Gendler, S. J., & Clapham, D. E. (1998). Abnormal heart rate regulation in GIRK4 knockout mice. *Neuron*, *20*(1), 103–114. https://doi.org/10.1016/S0896-6273(00)80438-9

Xia, M., Salata, J. J., Figueroa, D. J., Lawlor, A. M., Liang, H. A., Liu, Y., & Connolly, T. M. (2004). Functional expression of L- and T-type Ca2+ channels in murine HL-1 cells. *Journal of Molecular and Cellular Cardiology*, *36*(1), 111–119. https://doi.org/10.1016/j.yjmcc.2003.10.007

Yang, L., Katchman, A., Morrow, J. P., Doshi, D., & Marx, S. O. (2011). Cardiac L-type calcium channel (Cav1.2) associates with gamma subunits. In *Faseb J.* (Vol. 25, Issue 3, pp. 928–936). http://www.ncbi.nlm.nih.gov/pubmed/21127204%5Cnhttp://www.fasebj.org/content/25/3/928.full.pdf

Yang, Y., Yang, Y., Liang, B., Liu, J., Li, J., Grunnet, M., Olesen, S. P., Rasmussen, H. B., Ellinor, P. T., Gao, L., Lin, X., Li, L., Wang, L., Xiao, J., Liu, Y., Liu, Y., Zhang, S., Liang, D., Peng, L., … Chen, Y. H. (2010). Identification of a Kir3.4 Mutation in Congenital Long QT Syndrome. *American Journal of Human Genetics*, *86*(6), 872–880. https://doi.org/10.1016/j.ajhg.2010.04.017

Yu, B., Gong, M., Wang, Y., Millard, R. W., Pasha, Z., Yang, Y., Ashraf, M., & Xu, M. (2013). Cardiomyocyte Protection by GATA-4 Gene Engineered Mesenchymal Stem Cells Is Partially Mediated by Translocation of miR-221 in Microvesicles. *PLoS ONE*, *8*(8), 1–12. https://doi.org/10.1371/journal.pone.0073304

Zamponi, G. W., Striessnig, J., Koschak, A., & Dolphin, A. C. (2015). The physiology, pathology, and pharmacology of voltage-gated calcium channels and their future therapeutic potential. *Pharmacological Reviews*, *67*(4), 821–870. https://doi.org/10.1124/pr.114.009654

Zhang, X. H., Wei, H., Šarić, T., Hescheler, J., Cleemann, L., & Morad, M. (2015). Regionally diverse mitochondrial calcium signaling regulates spontaneous pacing in developing cardiomyocytes. *Cell Calcium*, *57*(5–6), 321–336. https://doi.org/10.1016/j.ceca.2015.02.003

Zhao, Y., Ransom, J. F., Li, A., Vedantham, V., von Drehle, M., Muth, A. N., Tsuchihashi, T., McManus, M. T., Schwartz, R. J., & Srivastava, D. (2007). Dysregulation of Cardiogenesis, Cardiac Conduction, and Cell Cycle in Mice Lacking miRNA-1-2. *Cell*, *129*(2), 303–317. https://doi.org/10.1016/j.cell.2007.03.030

Zheng, S., & Kruse, A. C. (2019). Solving a specificity mystery Differences. *ELife*, *8*, 1–3. https://doi.org/10.7554/eLife.44298

Zhou, P., & Pu, W. T. (2016). Recounting cardiac cellular composition. *Circulation Research*, *118*(3), 368–370. https://doi.org/10.1161/CIRCRESAHA.116.308139

Zhu, R., Millrod, M. A., Zambidis, E. T., & Tung, L. (2016). Variability of Action Potentials Within and among Cardiac Cell Clusters Derived from Human Embryonic Stem Cells. *Scientific Reports*, *6*(January), 1–12. https://doi.org/10.1038/srep18544

Zylbergold, P., Ramakrishnan, N., & Hébert, T. E. (2010). The role of G proteins in assembly and function of Kir3 inwardly rectifying potassium channels. *Channels*, *4*(5). https://doi.org/10.4161/chan.4.5.13327

8. Appendix

8.1 Abbreviations

$[Ca^{2+}]_i$	intracellular calcium ion concentration
AC	adenylyl cyclase
aCFB	adult cardiac fibroblasts
ACh	acetylcholine
aCM	adult cardiomyocytes
AKT	AKT kinase (protein kinase B)
AngII	angiotensin II
AP	action potential
APD	action potential duration
APS	ammonium persulfate
area dep	area under the curve of the departure phase
area ret	area under the curve of the return phase
AT1R	angiotensin II receptor type 1
ATP	adenosine triphosphate
AUC	area under the curve
AVN	atrioventricular node
β-AR	β-adrenergic receptor
baseline%peak h	peak height as percentage of baseline
BCA	bicinchoninic acid
BK-type K^+ channel	large conductance (Big K^+), Ca^{2+}-activated K^+ channel
Cacna1c	calcium channel gene, voltage-dependent, L type, alpha 1C subunit
Cacna2d1	calcium channel gene, voltage-dependent, alpha2/delta subunit 1
Cacnb2	calcium channel gene, voltage-dependent, beta 2 subunit
cAMP	cyclic adenosine monophosphate
Cav1.2	L-type Ca^{2+} channel pore-forming subunit alpha 1C
Cav1.3	L-type Ca^{2+} channel pore-forming subunit alpha 1D
CCH	carbachol
Chrm2	cholinergic receptor, muscarinic 2, cardiac (gene)
CICR	Ca^{2+}-induced Ca^{2+} release
CM	cardiomyocyte
DAPI	4',6-Diamidino-2-phenylindole
ddPCR	digital droplet PCR
dep v t	time to maximal departure velocity
dep v	departure velocity
DMEM	Dulbecco's Modified Eagle's Medium
ECG	electrocardiogram
EGF	epidermal growth factor
EGFR	epidermal growth factor receptor
ERK1/2	extracellular signal-regulated kinase 1/2
EV	empty vector
F	forward (primer)
F_{340}/F_{380}	ratio of fluorescence intensities at 340 nm and 380 nm excitation wavelengths

FCS	fetal calf serum
FITC	fluorescein isothiocyanate
fps	frames per second
fura-2 AM	fura-2 acetoxymethyl ester
G_i	inhibiting G protein
GIRK1/4	G-protein-coupled inwardly rectifying K^+ channel
G_s	stimulating G protein
h	hour(s)
hAT1R	human AT1R
HB-EGF	heparin-binding EGF-like growth factor
HBSS	Hank's Balanced Salt Solution
HCN	hyperpolarization-activated cyclic nucleotide-gated cation channel
HSP90	heat shock protein 90 kDa
i.p.	intraperitoneal
I_{Ca}	Ca^{2+} current
$I_{Ca,L}$	L-type Ca^{2+} current
$I_{Ca,T}$	T-type Ca^{2+} current
I_f	HCN-mediated funny current
$I_{K,ACh}$	ACh-mediated inwardly rectifying K^+ current through GIRK1/4
$I_{K,ATP}$	ATP-sensitive inwardly rectifying K^+ current
I_{K1}	inwardly rectifying K^+ current
I_{Kr}	rapidly activating delayed rectifying K^+ current
I_{Ks}	slowly activating delayed rectifying K^+ current
I_{Kur}	ultra-rapid delayed rectifying K^+ current
IP3	inositol 1,4,5-trisphosphate
IP3R	IP3 receptor
ISO	isoprenaline
I_{to}	transient outward K^+ current
KCl	potassium chloride
Kcnd2	potassium voltage-gated channel gene, Shal-related family, member 2
Kcnj3	potassium inwardly-rectifying channel gene, subfamily J, member 3
Kcnj5	potassium inwardly-rectifying channel gene, subfamily J, member 5
KO	knockout
LNA	locked nucleic acid
LTCC	L-type Ca^{2+} channel
LVAD	left ventricular assist device
M2R	muscarinergic acetylcholine receptor type 2
mAT1R	mouse AT1R
mc	mimic control
MEM	minimal essential medium
min	minute(s)
miR	microRNA
miRNA	microRNA
NA	noradrenaline
NCX	Na^+/Ca^{2+} exchanger
neoCMs	neonatal cardiomyocytes
nonCMs	non-cardiomyocytes
pAKT	phosphorylated AKT

PBS	phosphate buffered saline
PCR	polymerase chain reaction
peak h	peak height
peak t	peak time (time to peak)
pERK1/2	phosphorylated ERK1/2
PKA	protein kinase A
PKC	protein kinase C
PLB	phospholamban
PMCA	plasma membrane Ca^{2+} ATPase
qPCR	quantitative PCR
R	reverse (primer)
ret v t	time to maximal return velocity
ret v	return velocity
RFP	red fluorescent protein
RISC	RNA-induced silencing complex
ROI	region of interest
RyR2	ryanodine receptor 2
S.O.C. medium	Super Optimal Broth (S.O.B.) with 20 mM glucose
SAN	sinoatrial node
SDS	sodium dodecyl sulfate
SEAP	secreted alkaline phosphatase
SERCA2a	sarco/endoplasmic reticulum Ca^{2+} ATPase
SR	sarcoplasmic reticulum
TAC	transverse aortic constriction
TEMED	tetramethylethylenediamine
TGFβ	transforming growth factor beta
Tl^{+}	Thallium ion
TQ	tertiapin q
TTCC	T-type Ca^{2+} channel
WT	wild type

8.2 Overview of movies showing beating neoCMs

Movies from spontaneous contraction recordings under control conditions and after application of ISO or verapamil can be found on the supplemental CD/DVD. Attached images are overviews of manual ROIs used for analysis with the Image J plugin Myocyter. An overview of the file names in each folder is given below. Each file name is used for a movie and for the corresponding ROI overview image.

untransfected neoCMs spontaneous contraction verapamil (for quantification see Fig. 33):
S1_neoCM control
S2_neoCM verapamil 1 and 2

mc-transfected neoCMs spontaneous contraction ISO:
S3_neoCM mc control
S4_neoCM mc ISO 1
S5_neoCM mc ISO 2
(for corresponding tracings of ROI 3 see Fig. 37 A)

miR-222-transfected neoCMs spontaneous contraction ISO:
S6_neoCM miR-222 control
S7_neoCM miR-222 ISO 1
S8_neoCM miR-222 ISO 2
(for corresponding tracings of ROI 1 see Fig. 37 A)

8.3 List of figures and tables

Tables

8.4 Supplemental materials and methods

8.4.1 Buffers and media for isolation of adult mouse cardiomyocytes and cardiac fibroblasts

Buffers were made as described by Liao and Jain (R. Liao & Jain, 2007).

Perfusion buffer:	135 mM NaCl, 4 mM KCl, 1 mM $MgCl_2$, 10 mM HEPES, 0.33 mM NaH_2PO_4, 10 mM glucose, 10 mM 2,3-butanedione monoxime, 5 mM taurine, pH 7.2 at 37°C
Digestion buffer:	0.3 mg/g body weight collagenase D, 0.4 mg/g body weight collagenase B and 0.05 mg/g body weight protease type XIV are dissolved in 25 ml perfusion buffer.
Transfer buffer A:	135 mM NaCl, 4 mM KCl, 1 mM $MgCl_2$, 10 mM HEPES, 0.33 mM NaH_2PO_4, 5.5 mM glucose, 10 mM 2,3-butanedione monoxime, 5 mg/ml FCS, pH 7.4 at 37°C
Transfer buffer B:	137 mM NaCl, 5.4 mM KCl, 1.8 mM $CaCl_2$, 0.5 mM $MgCl_2$, 10 mM HEPES, 5.5 mM glucose, pH 7.4 at 37°C
Transfer solutions with different calcium concentrations:	
	Transfer buffers A and B are mixed to generate different transfer solutions with increasing calcium concentrations as follows: 0.06 mM: 29 parts transfer buffer A, 1 part transfer buffer B; 0.24 mM: 13 parts transfer buffer A, 2 parts transfer buffer B; 0.6 mM: 2 parts transfer buffer A, 1 part transfer buffer B; 1.2 mM: 1 part transfer buffer A, 2 parts transfer buffer B.
Plating medium:	minimal essential medium (MEM), 100 U/ml penicillin–streptomycin, 2 mM L-glutamine, 10 mM 2,3-butanedione monoxime, 5% FCS
Culture medium A (for less than 24 h culture):	
	MEM, 100 U/ml penicillin/streptomycin, 2 mM L-glutamine, 0.1 mg/ml bovine serum albumin.
Culture medium B (for longer than 24 h culture):	
	MEM, 100 U/ml penicillin/streptomycin, 2 mM L-glutamine, 0.1 mg/ml bovine serum albumin, 10 mM 2,3-butanedione monoxime, 10 µg/ml insulin, 5.5 µg/ml transferrin, 5 ng/ml insulin–transferrin–sodium selenite media supplement.

8.4.2 Buffer and medium for neoCM isolation and cultivation

digestion buffer:	HBSS, 0.5 mg/ml trypsin, 20 µg/ml DNase II
neoCM medium:	DMEM 4.5 g/l glucose, 1-5% FCS, 20 µg/ml vitamin B_{12}

8.4.3 Buffers for calcium measurements

Ringer solution 5 mM KCl contained (in mM): NaCl 122.5, KCl 5.4, $MgCl_2$ x 6 H_2O 0.8, $CaCl_2$ x 2 H_2O 1.2, NaH_2PO_4 x H_2O 1.0, glucose 5.5, HEPES 10. pH was adjusted at room temperature (RT) with NaOH.

The pH value of a solution is temperature-dependent and increases with a factor of approximately 0.014 per 1°C temperature difference (ΔT). To obtain a pH of 7.4 at 37°C the corresponding pH at RT was calculated using the following formula: pH(RT) = 7.4 + ($\Delta T \cdot 0.014$); $\Delta T = 37 - RT$.

This solution was used as control or with addition of either 100 nM AngII, 1 µM ionomycin or 10 µM losartan (plus AngII) as test solution. Stock solutions of the substances were prepared with water (AngII, losartan) or DMSO (ionomycin).

Ringer solution 25 mM KCl contained (in mM): NaCl 102.5, KCl 25.4, $MgCl_2$ x 6 H_2O 0.8,

CaCl$_2$ x 2 H$_2$O 1.2, NaH$_2$PO$_4$ x H$_2$O 1.0, glucose 5.5, HEPES 10. pH was adjusted as described above. This solution was used with or without addition of 20 µM verapamil (stock solution prepared in water).

8.4.4 General media and buffers

LB medium:	Bacto tryptone	10 g (Thermo Fisher)
	yeast extract	5 g
	NaCl	10 g
	Solved in 1 l H$_2$O and adjusted to pH 7.0 with 1 N NaOH (1 ml).	

LB agar plates:	Bacto tryptone	10 g
	yeast extract	5 g
	NaCl	10 g

Solved in 1 l H$_2$O and adjusted to pH 7.0 with 1 N NaOH (1 ml). Add 15 g Agar and autoclave 25 min. Let cool down to 50-60°C, add antibiotics, pour into petri dishes. Keep at 4°C.

10xPBS:	NaCl	160 g
	KCl	4 g
	Na$_2$HPO$_4$	28.84 g
	KH$_2$PO$_4$	4 g
	in 2 l H$_2$O	

RIPA buffer (denaturing):

	NaCl	150 mM
	Tris (base)	10 mM
	Nonidet P-40	1% (w/w)
	SDS	0.1%
	Sodium deoxycholate	1% (w/w)
	Triton X-100	0.1%
	Protease inhibitor cocktail	1:500
	EDTA	1 mM
	Sodium orthovanadate	184 mg/l
	pH 7.4	

2xRedmix:	0.5 M Tris-HCl pH 6.8	12.5 ml
	10% SDS	20 ml
	2-mercaptoethanol	5 ml
	glycerol	10 ml
	bromophenol blue	5 mg
	final volume 50 ml	

Stacking gel (5%), volumes for 1 gel [ml]:

	Acrylamide/Bis-acrylamide (26:0.7)	0.425
	APS (10%)	0.025
	SDS (10%)	0.025

0.5 M Tris-HCl (pH 6.8)	0.312
water	1.700
TEMED	0.005

Separating gel (10%), volumes for 1 gel [ml]:

Acrylamide/Bis-acrylamide (29.3:0.53)	2.140
APS (10%)	0.075
SDS (10%)	0.125
1.5 M Tris-HCl (pH 8.8)	1.563
water	2.285
TEMED	0.020

DMEM:	DMEM powder	10.15 g/l (Merck)
	NaHCO$_3$	2 g/l
	Glucose	1 g/l
	5% CO$_2$, pH 7.2	

8.5 Plasmid maps
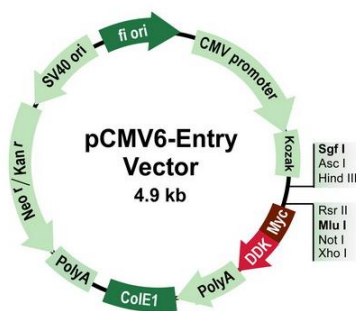
pCMV6-Entry mammalian expression vector with C-terminal Myc-DDK tag. Backbone for GIRK1, GIRK4 and M2R expression vectors.
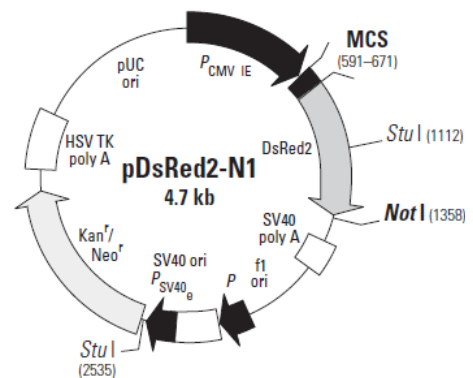
pDsRed2-N1 vector. This vector was used as transfection control for Fluxor experiments.
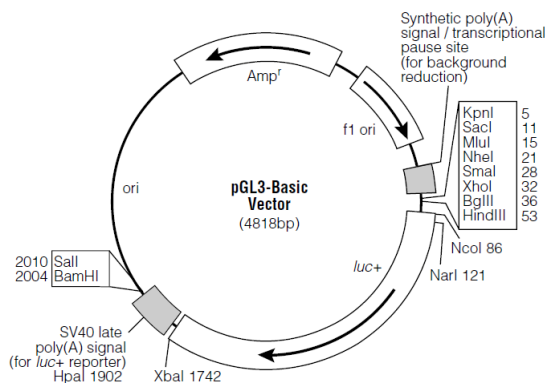
pGL3-Basic vector. Backbone of the pGL3-hmiR-221 vector containing the human miR-221/222 promoter fragment.
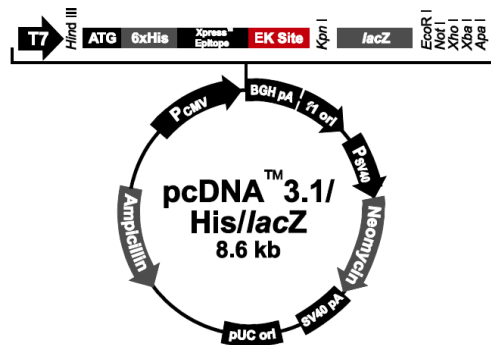
pcDNA3.1/His/*lacZ* vector. Used to normalize luciferase activity to β-galactosidase activity in miR-221/222 promoter luciferase assays.

111
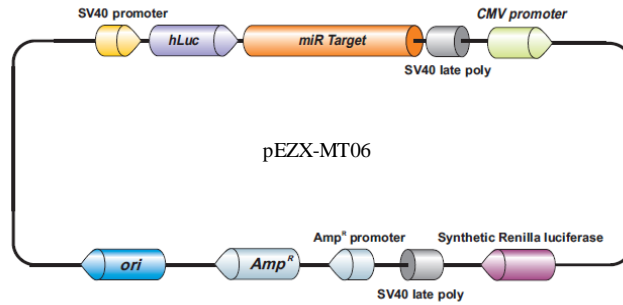
pEZX-MT06 vector. Dual luciferase reporter construct for ion channel 3'-UTR assays.
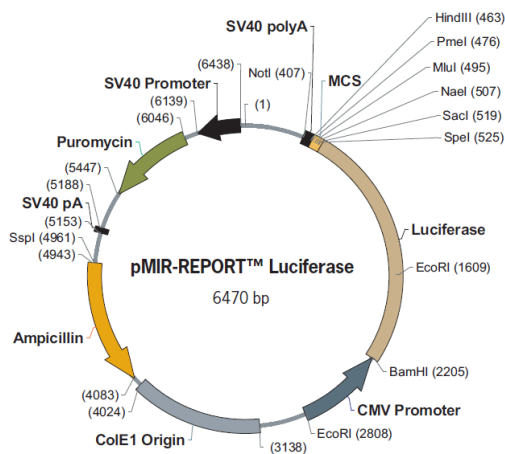
pMIR-REPORT Luciferase vector. Backbone of pMiR-221-3p-luc and pMiR-222-3p-luc. pMiR-221 and pMiR-222 are firefly luciferase reporter constructs containing mature miR-221 or miR-222 sequences and were used as positive controls for miR-221/222 activity in luciferase assays.
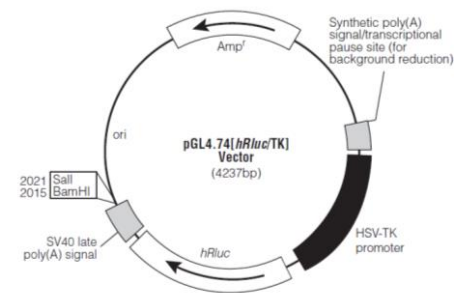
pGL4.74[*hRluc*/TK] vector. Renilla luciferase expression vector was used to normalize firefly luciferase activity of pMiR-221 and pMir-222.
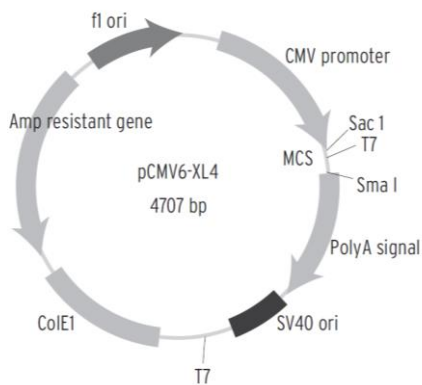
pCMV6-XL4 vector. Backbone of pAT1R expression vector (pCMV6-XL4-AT1R).
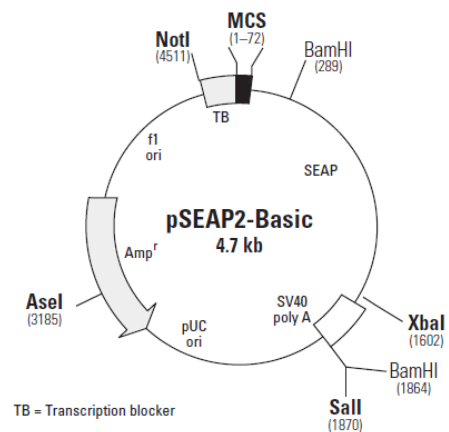
pSEAP2-Basic vector. This vector was used as empty vector control for pAT1R in miR-221/222 promoter experiments.

112

Declaration

I hereby sincerely declare that I have prepared and written this thesis "Influence of miR-221/222 on GIRK1/4 channel function and LTCC-dependent calcium handling in cardiomyocytes" on my own and without external help. I have used only the sources and resources that I specified. All statements and thoughts taken directly or indirectly from external sources have been identified as such in the thesis.

I also declare that this thesis does not exist in the same or similar form in another examination procedure. I declare that I have not undertaken any previous doctorate attempt, and that no doctorate attempt is initiated at another scientific institution.

Maria Knyrim
Leipzig, 22.10.2021

Curriculum vitae

Personal details:

Name:	Maria Knyrim
Date of birth:	31.03.1990
Place of birth:	Erfurt
ORCID:	0000-0003-4211-2361

Academic studies:

10/2008 – 09/2011	**Bachelor programme in biochemistry/molecular biology** Friedrich-Schiller-University Jena
11/2010 – 08/2011	Bachelor thesis **"Physiological responses of *Nicotiana attenuata* after herbivory mediated by cytokinins"** Max Planck Institute for Chemical Ecology Jena, department for Molecular Ecology (Dr. S. Meldau, Prof. I. T. Baldwin)
10/2011 – 04/2014	**Master programme in molecular medicine** Friedrich-Schiller-University Jena
10/2012 – 02/2014	Master thesis **"Influence of age and enriched environment on adult neurogenesis in the murine hippocampus – Phenotypic analysis of neuronal vs. glial cell fate in newborn cells"** University hospital Jena, Hans Berger Clinic for Neurology, Department of Experimental Neurology, Group Ageing and plasticity (Dr. Ch. Frahm)

Work experience:

28.08.2012 - 31.10.2012	**Research assistant in the group of Dr. S. Meldau** Max Planck Institute for Chemical Ecology Jena, Department of Molecular Ecology
01.01.2014 - 30.11.2014	**Research assistant in the group of Prof. M. Wartenberg** University Hospital Jena, Department of Internal Medicine I, Molecular cardiology and stem cell research
01.12.2014 - 31.08.2016	**Research associate in the group of Dr. S. Schwind** University Hospital Leipzig, Department of Hematology and internal Oncology
01.09.2016 – 31.03.2019	**PhD student in the GRK1591** (Project B2; group of PD Dr. Barbara Schreier and Prof. Dr. Claudia Großmann) Martin Luther University Halle/Wittenberg, Medical Faculty, Julius Bernstein Institute of Physiology Topic: **miR-221/222 in cardiac electrical remodelling**
Since 01.04.2019	**PhD student** in the group of PD Dr. Barbara Schreier and Prof. Dr. Claudia Großmann Martin Luther University Halle/Wittenberg, Medical Faculty, Julius Bernstein Institute of Physiology Topic: **miR-221/222 in cardiac electrical remodeling**

Publications and Presentations:

Research articles:

- Stephanie Binas*, **Maria Knyrim***, Julia Hupfeld, Udo Kloeckner, Sindy Rabe, Sigrid Mildenberger, Katja Quarch, Nicole Strätz, Danny Misiak, Michael Gekle, Claudia Grossmann, Barbara Schreier: **miR-221 and -222 target CACNA1C and KCNJ5 leading to altered cardiac ion channel expression and current density** Cellular and Molecular Life Sciences 2019, https://doi.org/10.1007/s00018-019-03217-y
  * contributed equally

- Julia Hupfeld*, Maximilian Ernst*, **Maria Knyrim***, Stephanie Binas, Udo Kloeckner, Sindy Rabe, Katja Quarch, Danny Misiak, Matthew Fuszard, Claudia Großmann, Michael Gekle, Barbara Schreier: **miR-208b reduces the expression of Kcnj5 in a cardiomyocyte cell line** Biomedicines 2021
  https://doi.org/10.3390/biomedicines9070719
  * contributed equally

- **Maria Knyrim**, Sindy Rabe, Claudia Grossmann, Michael Gekle, Barbara Schreier: **Influence of miR-221/222 on cardiomyocyte calcium handling and function** Cell & Bioscience 2021, https://doi.org/10.1186/s13578-021-00676-4

Poster and oral presentations:

- 96th annual meeting of the German Physiological Society 16.03.-18.03.2017 (Greifswald): poster presentation
- Congress for doctoral students of the MLU medical faculty 2017 (Halle/Saale): poster presentation
- Europhysiology 14.09.-16.09.2018 (London): poster presentation
- 98th meeting of the German Physiological Society 30.09.-02.10.2019 (Ulm): poster presentation
- Research Day and Congress for doctoral students of the MLU medical faculty 2019 (Halle/Saale): talk "miR-221/222 in cardiac electrical remodeling"

Maria Knyrim

Leipzig, 22.10.2021

Acknowledgements